ECMWF COPERNICUS REPORT

Copernicus Atmosphere Monitoring Service

Upgrade verification note for the CAMS near-real time global atmospheric composition service

Evaluation of the e-suite for the CAMS 47R1 upgrade of October 2020

Issued by: KNMI

Date: 2-10-2020

Ref: CAMS84_2018SC1_D3.2.1-202009_esuite

IMPLEMENTED BY ECMWF

Upgrade verification note for the CAMS near-real time global atmospheric composition service

Evaluation of the e-suite for the CAMS 47R1 upgrade of October 2020

AUTHORS:
H. J. Eskes (KNMI), S. Basart (BSC), A. Benedictow (MetNo), Y. Bennouna (CNRS-LA), A.-M. Blechschmidt (IUP-UB), S. Chabrillat (BIRA-IASB), Y. Christophe (BIRA-IASB), K. M. Hansen (AU), J. Kapsomenakis (AA), B. Langerock (BIRA-IASB), M. Pitkänen (FMI), M. Ramonet (LSCE), A. Richter (IUP-UB), N. Sudarchikova (MPG), M. Schulz (METNO), A. Wagner (MPG), T. Warneke (UBC), C. Zerefos (AA)

REPORT OF THE COPERNICUS ATMOSPHERE MONITORING SERVICE, VALIDATION SUBPROJECT.

CITATION:
Eskes, H. J., S. Basart, A. Benedictow, Y. Bennouna, A.-M. Blechschmidt, S. Chabrillat, Y. Christophe, K. M. Hansen, J. Kapsomenakis, B. Langerock, M. Pitkänen, M. Ramonet, A. Richter, N. Sudarchikova, M. Schulz, A. Wagner, T. Warneke (UBC), C. Zerefos, Upgrade verification note for the CAMS near-real time global atmospheric composition service: Evaluation of the e-suite for the CAMS 47R1 upgrade of October 2020, Copernicus Atmosphere Monitoring Service (CAMS) report, CAMS84_2018SC2_D3.2.1-202009_esuite.pdf, 2 October 2020, doi:10.24380/fzdx-j890.

STATUS:
Version 1, final

DATE:
2 October 2020

Executive Summary

The Copernicus Atmosphere Monitoring Service (CAMS, http://atmosphere.copernicus.eu) is a component of the European Earth Observation programme Copernicus. The CAMS global near-real time (NRT) service provides daily analyses and forecasts of reactive trace gases, greenhouse gases and aerosol concentrations.

The CAMS service includes an activity (CAMS-84) dedicated to the validation of the service products. The latest validation results for the CAMS-global near-real time service (the o-suite) products can be found in Schulz et al. (2020) and the activity is described in Eskes et al. (2015). The observational datasets used for this validation are described in Eskes et al. (2019). These validation reports and the verification websites can be found at http://atmosphere.copernicus.eu/user-support/validation/verification-global-services.

Before each upgrade, the new model and assimilation configuration is operated in parallel (the e-suite) to the operational NRT service (the o-suite, CY46R1) for about half a year. For the October 2020 upgrade (ECMWF CY47R1) the e-suite run has experiment id "0074", with class=mc, and is available from 1 October 2019 onwards. The corresponding control run, without the assimilation of the atmospheric composition satellite data, has experiment id "hdir". New this year is that also the GHG delayed mode analysis and forecast runs are upgraded to the same 47R1 model version. The e-suite run ids are “hd7v” for the analysis, “he9e” for the control, and “he9h” for the high-resolution forecast. These greenhouse gas runs are available from 1 January 2020.

Below a set of quick-look validation results are presented from a comparison of the performance of the e-suite runs with the operational run (o-suite) and independent observations. The main conclusions are listed below, and the evidence for these findings is presented in section 2 in the form of a series of plots comparing e-suite, o-suite and independent observations. The o-suite and e-suite system changes are discussed in section 1.

Main conclusions on the performance of the e-suite

The upgrade of the CAMS global system of October 2020 involves model changes (listed in section 1) which are reflected in the validation results presented. Overall, the quality of the e-suite is comparable to the o-suite, with many examples where the performance has improved or where the performance has degraded. The scorecard below summarises the results.

In the lower and middle stratosphere (25-32 km altitude) the stratospheric ozone profiles in the new model version (e-suite) shows clear improvements over the o-suite, operational between July 2019 and September 2020. There are significant changes in the simulated and analysed aerosol distribution. The simulation of dust over Northern Africa, and the Mediterranean has improved considerably, with reduced biases in AOD, PM10 and PM2.5. PM10 over North America and Europe has improved. On the other hand, the e-suite shows increases in sulphate and changes in the Ångstrøm exponent which results in larger biases. For the tropospheric trace gases the differences are more modest, with generally small improvements, such as in surface ozone over Europe.

Property	***Rel. score***	***Property***	***Rel. score***
Global AOD	-	CO surface	**n**
Ångstrøm exponent	- -	CO profiles (aircraft)	**n**
Dust AOD	++	CO columns (satellite, FTIR)	**n**
Dust PM10 Mediterranean	++	Tropospheric NO_2 column	+
Surface PM10, Europe and US	++	Fire-produced NO2 and HCHO	+
Surface PM2.5, Europe and US	+	HCHO column	**n**
Ozone, free troposphere (ozone sonde)	**n**	Ozone stratospheric profile	++
Ozone tropospheric profile (aircraft)	**n**	UV radiation (UV-index)	-
Surface ozone, Arctic	**n**	Surface methane	-
Surface ozone, Midlatitude	+	Methane column	-
Surface ozone, Antarctic	-	Surface CO_2	**n**
Surface ozone, Europe	+	CO_2 column	**n**
Ozone column	**n**		

Table S1. Scorecard for the relative performance of the e-suite versus the performance of the o-suite against independent observations. Meaning of the "relative score" symbols:
++ *e-suite performs significantly better than the o-suite;*
+ *e-suite shows small improvements;*
n *(neutral) no significant difference between o-suite and e-suite;*
- *score is somewhat degraded in the e-suite;*
- - *e-suite performs significantly worse than the o-suite.*

Global Aerosol

The comparison between o-suite and e-suite and the respective control simulations show an increase in sulphate OD (+45%), associated with compensating reductions of dust (-40%) and sea salt ODs (-20%), so that total AOD remains similar (see figure 2.1.1 and table 2.1.1). The control experiment comparison, along with the assimilation experiments, shows that a change in the assimilation step is responsible for most of the sulphate OD increase. Dust and sea salt OD

reductions are similar in the assimilation and control experiments. Sulphate is now also spreading in the assimilation step to high Northern latitudes. Note by contrast the similarity of the o-suite and e-suite control experiments. The increase in sulphate seems to come from issues with the AOD assimilation on top of changes in the aerosol speciation due to model changes (under investigation). Reported dust and sea salt emission function changes are likely responsible for the downward shift for those two components.

The size shift of sea salt during emission to smaller particles is likely to have increased the lifetime and surface concentrations of PM25 and PM10 in the global mean (+80% and +30% respectively) (see figure 2.1.1 and table 2.1.1). This is less visible at inner-continental sites, which are used for the PM concentration evaluation, see figure 2.1.3.

As a result of a shift to more sulphate - and possibly also the smaller sea salt - the Ångstrøm exponent (wavelength dependent AOD) at globally 340 Aeronet sites is less well simulated (Fig. 2.1.2). The FGE increases from +16% to +27%, the MNMB bias increases from+10% to +26% (see scatterplots in figure 2.1.2 and further scores in tables 2.1.2). Also, the total AOD MNMB increases in the period from +24% to +31%, despite reductions in overall dust and sea salt OD, thus reflecting the increase in sulphate OD, in particular in Northern latitudes.

Evaluation using PM10 concentrations (climatological means) at continental European and North American sites (Fig. 2.1.3) indicate that the very high PM10 concentrations in the o-suite have disappeared, and correlation increases from 0.55 to 0.83 in the e-suite. Similarly, PM25 at these sites improved slightly in the e-suite, see table 2.1.2.

Dust and aerosol evaluation over North Africa, the Middle East and Europe

The comparison for December 2019 – May 2020 shows that the e-suite (0074) has smaller dust concentrations in comparison with the current o-suite (0001), for both the column-load and the surface concentrations, see Figure 2.2.1 and Figure 2.2.3. In comparison with MODIS Collection 6.1 Level 3 Daily, the e-suite (0074) reduces the DOD in desert dust sources in the Sahara in comparison with the current o-suite (0001). In particular, the extreme PM10 concentrations (> 75 $\mu g/m^3$ in average for the whole period) that the current o-suite predicted over Southern Europe are strongly reduced in the e-suite. Apart from sea-salt, AOD is reduced in the e-suite in particular over the North Atlantic. At the surface over oceans and seas, the e-suite shows enhanced PM10 and PM2.5 background levels, up to 50 $\mu g/m^3$ and 25 $\mu g/m^3$ respectively for PM10 and PM2.5. In contrast, the o-suite shows surface concentrations up to 25 and 10 $\mu g/m^3$ respectively for PM10 and PM2.5 over oceans and seas.

The comparison with dust-filtered AERONET Level 1.5 3-hourly observations (Figure 2.2.2 and Figure 2.2.4) shows that the mean bias for the current o-suite (-0.04 and 0.00 respectively for winter and spring) is reduced in the e-suite (-0.06 and -0.05 respectively for winter and spring), which is lower than the results of the WMO Sand and Dust Storm Warning Advisory and Assessment system (SDS-WAS) Multi-model ensemble (-0.04 and -0.03 respectively for winter and spring). In terms of correlation, the e-suite presents slightly higher results (0.55 and 0.75 respectively for winter and spring) in comparison with the current o-suite (0.59 and 0.73 respectively for winter and spring), but

is still lower than the results of the SDS-WAS Multi-model (0.79 and 0.82 respectively for winter and spring).

The e-suite reduces the strong overestimations observed in the o-suite in PM10 in Central Europe (Figure 2.2.5 and Figure 2.2.6). Furthermore, the e-suite enhances the PM2.5 levels reducing the general underestimation observed over Europe.

Tropospheric ozone (O_3)

The o-suite and e-suite experiments were compared with ozone sondes (Fig. 2.3.1). Over the Arctic, all four runs show biases in the range of ±10%. The e-suite bias is within 0-7%. Over the Northern midlatitudes, biases remain within 1-14%, again, the e-suite shows somewhat smaller biases. For Antarctica, biases range between -20% and 15%. The o-suite shows the largest positive biases in December, e-suite and e-control show larger negative biases, especially during February (up to -18.8%).

Ozone in-situ surface concentrations have been compared with WMO Global Atmosphere Watch observations, NOAA ESRL stations and European Airbase observations. For Europe and Asia, the e-suite and o-suite and the respective control runs show nearly identical biases. For stations located in the Southern Hemisphere (CPT, USH, NEU) the e-suite and control run show larger negative biases than the o-suite, especially during DJF, see Figs. 2.4.1 and 2.4.3 (DJF: o-suite: -9% to 4%, e-suite:-30% to -7%, MAM: o-suite: -17% to 0%, e-suite:-20% to -3%). Correlation coefficients are similar, but the e-suite control run has improved somewhat compared to the o-suite control run.

The comparison with the ESRL observations shows that for Arctic, USA and Tropics, e-suite and o-suite and the respective control runs show nearly identical biases (Fig. 2.4.4.to 2.4.9). Nevertheless, there is a small improvement in both bias and correlations for the e-suite and also the e-suite control run compared to the o-suite and control over USA stations and Lauder New Zealand station (NH and SH mid-latitudes). For stations located in Antarctica (SPO and ARH) the e-suite corrects the o-suite positive bias during the October-February period over Arrival Heights (ARH) but shows a larger negative bias over South Pole station (SPO) during the same period.

For ozone profile comparisons against IAGOS aircraft measurements (October 2019 – July 2020), results from e-suite (0074) and o-suite (0001) are very similar for the most regions sampled with often a slightly smaller bias for the e-suite than for the o-suite. This can be seen on the time series of the daily bias at Frankfurt (Fig. 2.5.1) as well as on the time series of the monthly MNMB calculated for different atmospheric layers (Surface Layer, Boundary Layer, Free troposphere, Upper Stratosphere and Lower Stratosphere) and regions (Fig. 2.5.2, 2.5.3 and 2.5.4). Over South Africa, the e-suite and o-suite differ more than over the other regions in the Free Troposphere where MNMB from the two models present different signs. However, it should be noted that sampling is poor over this region for the considered period. The comparison between the e-suite analysis and associated control run in the lowest layers and Free Troposphere shows that the assimilated run always presents better or similar performance to those of the run without assimilation. Over Europe in the Free Troposphere, the bias of the e-suite remains mostly stable over the evaluation period while the bias from control run appear to increase slightly at the beginning of Spring 2020, and consequently the differences between the two runs are larger in the second half of the period. This

is also shown on the plots of the MNMB as a function of altitude calculated over different sub-periods (Fig. 2.5.5).

Ozone total columns from the o-suite, e-suite and control experiments have been compared to IASI Metop-A version v20151001/v20191122 daytime only satellite observations (see section 2.8). The four model configurations are in overall good agreement with the observations. There is a change in the biases from slightly positive in the o-suite to slightly negative in the e-suite over the low- and mid-latitudes.

Tropospheric ozone (O_3) in Europe

The e-suite, o-suite, e-suite control run and o-suite control run were validated with European EEA-AirBase ozone surface observations during the time period 01/10/2019 - 31/05/2020 (Fig. 2.6.1. t0 2.6.4). The e-suite reduces the positive offset observed in the o-suite over central European stations, down to 10% during Oct-Nov 2019 and down to 6% during DJF 2019/2020. It reproduces also better the day to day ozone variability mainly over the MAM 2020 period (up to 15% more explained variance than o-suite), as well as for the whole period 1 October 2019 – 31 May 2020 (up to 10% more explained variance than o-suite).

Tropospheric ozone (O_3) in the Arctic

Surface ozone mixing ratios predicted with the pre-e-suite were evaluated against measurements from three Arctic sites. There is no major difference in performance between the 47R1 e-suite and the o-suite in predicted surface ozone (Fig. 2.7.1).

Tropospheric Carbon Monoxide (CO)

Carbon monoxide surface concentrations have been compared with WMO Global Atmosphere Watch observations (Fig. 2.9.1, 2.9.2). The o-suite and e-suite show very similar biases for European and Asian stations. For CPT and USH in the Southern Hemisphere, the e-suite shows MNMBs closer to zero (DJF: o-suite: -2 to -6%, e-suite -2% to 2%, MAM: o-suite: -20% to 6%, e-suite: -18% to 9%), whereas the e-suite control run has larger negative MNMBs in all regions (DJF: o-control: -25 to 6%, e-control -20% to -3%, MAM: o-control: -22% to 20%, e-control: -29% to 12%).

From the comparison with IAGOS aircraft CO profiles (October 2019 – July 2020), no notable difference is found between the e-suite and o-suite performances for CO. This is shown on the time series of the daily bias at Frankfurt (Fig. 2.10.1) as well as on the time series of the monthly MNMB calculated for different atmospheric layers (Surface Layer, Boundary Layer, Free troposphere, Upper Stratosphere and Lower Stratosphere) and regions (Fig. 2.10.2, 2.10.3 and 2.10.4). Over Europe the differences between the e-suite and its control run appear more pronounced starting from March until the end of the evaluation period. This effect is found in all layers, in particular in the Free Troposphere and to a minor extent in the other layers. The bias from the e-suite remains roughly stable while the bias from control run increases largely in the Free Troposphere. A similar behaviour is also found over East Asia for CO, but the differences vanish at the end of the evaluation period. These differences are also clearly shown on the plots of the MNMB as a function of altitude calculated over different sub-periods (Fig. 2.10.5, 2.10.6 and 2.10.7). These differences between the

e-suite and associated control run might be explained by the impact of the lockdowns on the emissions during the COVID-19 pandemic.

CO total columns from the o-suite, e-suite and control experiments have been compared to MOPITT v8 (thermal infrared radiances) daytime satellite retrievals (section 2.11). Verification with the satellite observations shows that the o-suite and e-suite runs are in very good agreement with observations, showing bias less than 10%, and are very similar to each other. Some discrepancies between two model runs have a regional and/or temporal character. The control run shows higher negative bias over the SH during autumn/winter (up to 30%) and over the NH during spring (up to 40%) (except for the South African region).

Comparisons against TCCON FTIR (Section 2.12) indicate that the e-suite performs slightly better in that the overall bias of CO total columns is reduced from -3.6 ppb (o-suite analysis) to -3.4 ppb (e-suite analysis) and that the overall correlation increased from 0.92 to 0.94. From the comparison with the NDACC data (tropospheric and stratospheric partial columns), the e-suite perform significantly better in stratosphere: the overall bias reduces from -11.6% (o-suite analysis) to -8.9% (e-suite analysis), which is comparable to the NDACC uncertainty on stratospheric partial columns. Comparison against NDACC tropospheric columns shows a slight improvement in terms of overall bias and correlation. These conclusions also hold for the 1d forecasts. The 47R1 control run performs significantly worse in the troposphere compared to the current control run.

Tropospheric Nitrogen dioxide (NO_2)

Tropospheric columns of NO_2 have been compared with GOME-2 satellite observations. Time series comparisons (Figure 2.13.1) show that the e-suite compares better than the o-suite to GOME-2 retrievals over East-Asia and North-Africa, but slightly worse for Europe. Map based comparisons (See Figure 2.13.2 to 2.13.4 for some example months) show similar issues for the e-suite compared to the o-suite (underestimation over Central Europe in winter, overestimation over several emission hotspots). However, the e-suite shows an improved performance compared to the o-suite over emission hotspots in East-Asia and over regions of fire activity in South-Eastern Australia and Siberia. There are only small differences in general between e-suite and e-suite control.

Comparisons against NDACC MAXDOAS data (Section 2.14) indicates that the baseline value for the e-suite has changed. At Bremen and Uccle this leads to an increased bias for the e-suite. Not all high pollution events are captured in both the e-suite and o-suite.

Formaldehyde (HCHO)

Total columns of HCHO have been compared with GOME-2 satellite observations. The time series comparisons (Figure 2.15.1) show only small differences between the e-suite and o-suite. However, global maps (Figures 2.15.2 to 2.15.4) show that the e-suite performs better over regions of fire activity in South-Eastern Australia and Siberia, while differences are small over other regions. There is basically no difference between e-suite and e-suite control.

Comparisons against NDACC MAXDOAS data confirm that there is little difference between the o- and e-suite performance (Fig. 2.15.5).

Stratospheric ozone

Model profiles of the CAMS runs were compared to balloon sonde measurements (Fig. 2.16.1 to 2.16.4). For the Antarctic, Arctic and Northern midlatitudes, o-suite and e-suite show very similar results for the integrated columns. The profile comparisons show a large improvement of the e-suite control compared to the o-suite control, related to the improved parameterized chemistry. The e-suite and o-suite differences are much smaller, and both agree well with the sonde observations. Profile shape improvements in the e-suite relative to the o-suite are found in the range around 20-30 hPa and 200-300 hPa (Fig. 2.16.2 to 2.16.4).

The comparison against six NDACC LIDAR stations (Sec. 2.18) shows a clear improvement in the profile shape of the e-suite compared to the o-suite at all sites. Comparison against the UVVIS stratospheric columns confirms this: the overall bias reduces from 4% (o-suite) to 3% (e-suite).

Ozone concentration profiles in the stratosphere of the e-suite and the o-suite were compared with satellite observations from ACE-FTS v3.6, SAGE III-ISS v5.1 and MLS V4.2 offline. The e-suite performs generally better in the mid-stratosphere for the analyses as well as for the 4th day forecasts. Bias oscillations observed for the o-suite are removed in the e-suite in this height range. In the upper stratosphere, while the abnormal bias in the winter polar region is also corrected, the biases against the observations are better or worse depending on the altitude and latitude band. Apart from ozone we also compared the stratospheric temperature profiles and find differences less than 1K in the range 300hPa to about 7 hPa. Above, a latitude-dependent positive difference of up to more than 15K is present.

UV radiation

Comparisons with ground-based reference UV-index measurements show that, on average, the e-suite (47R1) performs equally well as the current o-suite (46R1) (Fig. 2.20.1). However, a major reduction in the e-suite UVI performance is found at Davis, Antarctic, where the relative bias is reduced from 0.23 to -0.19 (from o-suite to e-suite), which brings down the correlation coefficient from 0.92 to 0.88 and increases the relative RMSE from 0.41 to 0.46, respectively (Fig. 2.20.2). This indicates that some local and noticeable feature in the e-suite degrades the CAMS UVI performance in the Antarctic summer.

Greenhouse gases: Methane (CH_4)

The NDACC FTIR profiles (section 3.1) indicate that the e-suite differs from the o-suite in the troposphere. The e-suite tropospheric column bias increased from -1.7% (o-suite high-resolution) to -2.1% (e-suite high-resolution). A similar change is observed for the analysis. The stratospheric partial columns performance did not change significantly.

Comparison against TCCON xCH_4 (section 3.2) also shows an increased underestimation for the e-suite runs compared to the o-suite runs. The same behavior is observed at the ICOS surface stations

(section 3.4), where we see that the biases of both o-suite and e-suite are similar in early 2020, but the o-suite only shows a decrease of this bias in spring.

Greenhouse gases: Carbon dioxide (CO_2)

For TCCON xCO_2 and ICOS surface site the e-suite and the o-suite runs are very similar (sections 3.3 and 3.5). The conclusions for the comparisons with surface and total column observations are very consistent.

Table of Contents

1. Description of the o-suite and e-suite

Below a short model description is given on both the CAMS o-suite operational data-assimilation and forecast run and the new e-suite.

1.1 o-suite: model and data assimilation aspects

This section provides information on the CAMS global data-assimilation and forecast operational configuration (the CAMS o-suite). The dates of the last upgrade are listed in Table 1.1. Table 1.2 provides information on the satellite data used in the o-suite. Further details on the model runs and their data usage can be found at http://atmosphere.copernicus.eu/documentation-global-systems.

The o-suite consists of the IFS-CB05 chemistry combined with the CAMS bulk aerosol model. The chemistry is described in Flemming et al. (2015) and Flemming et al. (2017), aerosol is described in Morcrette et al. (2009). The forecast length is 120 h. The o-suite data is stored under **expver '0001'** of **class 'MC'**. On 21 June 2016 the model horizontal resolution has seen an upgrade from T255 to T511, and forecasts are produced twice per day.

A short summary of the main model specifications:

- The modified CB05 tropospheric chemistry is used (Williams et al., 2013), originally taken from the TM5 chemistry transport model (Huijnen et al., 2010)
- Stratospheric ozone during the forecast is computed from the Cariolle scheme (Cariolle and Teyssèdre, 2007) as already available in IFS, while stratospheric NOx is constrained through a climatological ratio of HNO_3/O_3 at 10 hPa.
- Monthly mean dry deposition velocities are based on the SUMO model provided by the MOCAGE team.
- Data assimilation is described in Inness et al. (2015) and Benedetti et al. (2009) for chemical trace gases and aerosol, respectively. Satellite data assimilated is listed in Table 2.2 and Fig. 2.1.
- Anthropogenic emissions changed to CAMS_GLOB v2.1 with the July 2019 update (46R1). Previous versions used MACCity (Granier et al., 2011) and a climatology of the MEGAN-MACC emission inventories (Sindelarova et al., 2014).
- NRT fire emissions are taken from GFASv1.2 (Kaiser et al. 2012).

Table 1.1: Overview of the operational model runs used as reference in this validation report.

Forecast system	Exp. ID	Brief description	Upgrades (e-suite ID)	Cycle
O-suite	0001	Operational CAMS DA/FC run	20190709-present	46R1
Control	h7c4	control FC run without DA	20190709-present	46R1
GHG run	h72g	Tco399L137 NRT CO_2, CH_4 analyses (~25km)	20191201-present	46R1
	h9sp	High resolution Tco1279 (~9km) NRT CO_2, CH_4 forecast	20191201-present	46R1

Table 1.2: Satellite retrievals of reactive gases and aerosol optical depth that are actively assimilated in the o-suite.

Instrument	Satellite	Provider	Version	Type	Status
MLS	AURA	NASA	V4	O3 Profiles	20130107 -
OMI	AURA	NASA	V883	O3 Total column	20090901 -
GOME-2	Metop-A	Eumetsat	GDP 4.8	O3 Total column	20131007 - 20181231
GOME-2	Metop-B	Eumetsat	GDP 4.8	O3 Total column	20140512 -
GOME-2	Metop-C	Eumetsat	GDP 4.9	O3 Total column	20200505 -
SBUV-2	NOAA-19	NOAA	V8	O3 21 layer profiles	20121007 -
OMPS	Suomi-NPP	NOAA / EUMETSAT		O3 Profiles	20170124 - 20190409
TROPOMI	Sentinel-5P	ESA		O3 column	20181204-
IASI	MetOp-A	LATMOS/ULB Eumetsat	-	CO Total column	20090901 - 20180621 20180622 - 20191118
IASI	MetOp-B	LATMOS/ULB Eumetsat	-	CO Total column	20140918 - 20180621 20180622 -
IASI	MetOp-C	Eumetsat		CO total column	20191119 -
MOPITT	TERRA	NCAR	V5-TIR V7-TIR V7-TIR Lance V8-TIR	CO Total column	20130129 - 20160124 - 20180626 20180626 20190702
OMI	AURA	KNMI	DOMINO V2.0	NO2 Tropospheric column	20120705 -
GOME-2	MetOp-A	Eumetsat	GDP 4.8	NO2 Tropospheric column	20180626 - 20200504
GOME-2	MetOp-B	Eumetsat	GDP 4.8	NO2 Tropospheric column	20180626 -
GOME-2	MetOp-C	Eumetsat	GDP 4.9	NO2 Tropospheric column	20200505-
GOME-2	MetOp-A	Eumetsat	GDP 4.8	SO2 Total column	20150902 -
GOME-2	MetOp-B	Eumetsat	GDP 4.8	SO2 Total column	20150902-
GOME-2	MetOp-C	Eumetsat	GDP 4.9	SO2 Total column	20200505-
MODIS	AQUA / TERRA	NASA	Col. 5 Deep Blue Col. 6, 6.1	Aerosol total optical depth, fire radiative power	20090901 - 20150902 - 20170124 -
PMAp	METOP-A METOP-B	EUMETSAT		AOD	20170124 - 20170926 -

The aerosol model includes 14 prognostic variables (Remy et al., 2019).

- 3 size bins each for sea-salt and desert dust
- 2 bins (hydrophibic and hydrophobic) each for organic matter and black carbon

Figure 1.1: Satellite observation usage in the real-time analysis, for ozone, CO, aerosol AOD and NO2, from October 2014 onwards. Top rows (in green): products assimilated using averaging kernels. Sentinel-5P TROPOMI ozone is assimilated since Dec. 2018 (5079=O3) and other products from TROPOMI are monitored (35016=NO2, 35015=CO, 5081=SO2).

- 1 bin for sulphate
- 2 bins (fine and coarse) for nitrate (New since 46R1)
- 1 bin for ammonium (New since 46R1)

The SO_2 precursor for sulphate aerosol no longer exists as a separate prognostic in the aerosol scheme, which since 46R1 couples directly to the SO_2 in the chemistry scheme instead. Likewise, the precursors for the new nitrate and ammonium aerosol (nitric acid and ammonia) are also part of the chemistry scheme rather than the aerosol scheme.

Aerosol total mass is constrained by the assimilation of MODIS and PMAp AOD (Benedetti et al. 2009). A variational bias correction is currently applied for the PMAp AOD based on the approach used also elsewhere in the IFS (Dee and Uppala, 2009).

A history of updates of the o-suite is documented in earlier MACC-VAL and CAMS reports and can be found at https://atmosphere.copernicus.eu/node/326. This includes a list with changes concerning the assimilation system. The CAMS o-suite system is upgraded regularly, following updates to the ECMWF meteorological model as well as CAMS-specific updates such as changes in chemical data assimilation.

The latest upgrade of the system took place on 9 July 2019 and is based on IFS version cy46r1_CAMS and involves the move from 60 to 137 vertical levels, see https://atmosphere.copernicus.eu/cycle-46r1 or https://confluence.ecmwf.int/display/COPSRV/Current+global+production+suites.

The validation report for this 46r1 upgrade is described in Basart et al. 2019: https://atmosphere.copernicus.eu/sites/default/files/2019-07/CAMS84_2018SC1_D3.2.1-201907_esuite_v1.pdf

The meteorological changes can be found on the ECMWF-IFS CY46R1 page, https://confluence.ecmwf.int/display/FCST/Implementation+of+IFS+cycle+46R1.

1.2 o-suite control

The control run (relevant expver = **h7c4** since 09/07/2019) applies the same model settings as the o-suite cy46r1, except that data assimilation is not switched on. The meteorology in the control run is initialized with the meteorological fields from the o-suite.

1.3 High-resolution CO_2 and CH_4 forecasts and delayed-mode analyses

The pre-operational forecasts of CO_2 and CH_4 use an independent setup of the IFS at a resolution of TL1279, i.e. ~16 km horizontal, and with 137 levels. This system runs in real time and does not apply data assimilation for the greenhouse gases.

The land vegetation fluxes for CO_2 are modelled on-line by the CTESSEL carbon module (Boussetta et al., 2013). A biogenic flux adjustment scheme is used in order to reduce large-scale biases in the net ecosystem fluxes (Agusti-Panareda, 2015). The anthropogenic fluxes are based on the annual mean EDGARv4.2 inventory using the most recent year available (i.e. 2008) with estimated and climatological trends to extrapolate to the current year. The fire fluxes are from GFAS (Kaiser et al., 2012). Methane fluxes are prescribed in the IFS using inventory and climatological data sets, consistent with those used as prior information in the CH_4 flux inversions from Bergamaschi et al. (2009). The anthropogenic fluxes are from the EDGAR 4.2 database (Janssens-Maenhout et al, 2012) valid for the year 2008. The biomass burning emissions are from GFAS v1.2 (Kaiser et al., 2012). The high-resolution forecast experiments also included a linear CO scheme (Massart et al., 2015).

The experiments analysed in this report are:

- "**h72g**" NRT CO_2, CH_4 analyses from 1 December 2019, with a resolution Tco399 (~25km) and 137 vertical levels. Cycle 46R1.
- "**h9sp**" NRT CO_2, CH_4 forecasts from 1 December 2019, with high resolution Tco1279 (~9km) and 137 vertical levels. Cycle 46R1.

1.4 e-suite

The change of the CAMS system to cycle 47R1 is planned to be implemented on **6 October 2020** for the aerosol and reactive trace gas components. For the greenhouse gases the upgrade to 47R1 is planned for **1 November 2020**. See also https://confluence.ecmwf.int/display/CUSF/CAMS+Model+CY47R1+upgrade+on+6+October+2020.

Details of the upgrade are provided on: https://confluence.ecmwf.int/display/COPSRV/Implementation+of+IFS+cycle+47r1.

The e-suite data is available from ECMWF MARS under class=mc, **expver=0074**, and is evaluated from 1 October 2019, and is compared with the 2019/2020 o-suite described above.

The e-suite control run data is available from ECMWF MARS under class=rd, **expver=hdir**, and is evaluated from 1 October 2019, and is compared with the 2019/2020 o-suite described above.

The greenhouse gas Cy47R1 experiment consist of three runs, starting from 1-1-2020:

- Analysis: **expver = hd7v**, class=rd (resolution tco399))
- Control: **expver = he9e**, class=rd (also resolution tco399)
- High resolution forecast: **expver = he9h**, class=rd (resolution tco1279).

Meteorological content of the new cycle:

The meteorological changes can be found on the ECMWF-IFS CY47R1 page, https://confluence.ecmwf.int/display/FCST/Implementation+of+IFS+cycle+47R1.

Atmospheric composition content of the new cycle:

Assimilation:

- No changes compared to 46R1

Observations:

- TROPOMI volcanic SO2:
  - 20191211: Activation
  - 20200714-20200804: volcanic TROPOMI SO2 blacklisted because of ESA algorithm update
  - 20200805 onwards: volcanic TROPOMI SO2 re-activated, but with modified blacklist, only assimilating SO2>5DU, thus blacklisting data from outgasing volcanoes
- OMPS O3 layers from NOAA-20 and NPP activated on 20200806
- SBUV/2 NOAA-19 O3 layers retired on 20200806
- No other changes compared to the observations used in 46R1.

Emissions:

- Updated emissions inventories: CAMS_GLOB_ANT v4.2 (anthropogenic) and volcanic outgassing (based on Carn et al., 2017).
- Updated to GFASv1.4 biomass-burning emissions.
- Excluded agricultural waste burning from CAMS_GLOB_ANT, avoiding double-counting with GFAS.
- Improved diurnal cycle (CO, NO, SO2, NH3) and vertical profile for anthropogenic emissions (SO2, all over sea).

Other model changes:

- Hybrid Linear Ozone (HLO) scheme (a Cariolle-type linear parameterisation of stratospheric ozone chemistry using the multi-year mean of the CAMS reanalysis as mean state).
- New sea-salt emission scheme based on Albert et al. (2016), providing better agreement with measured sea-salt size distribution.
- Updated dust source function, reducing excess dust in the Sahara, Middle East and other regions, and restoring missing dust over Australia.
- Revised coefficients in UV processor, based on ATLAS3 spectrum.

2. Upgrade evaluation results: e-suite versus o-suite

2.1 Global aerosol evaluation

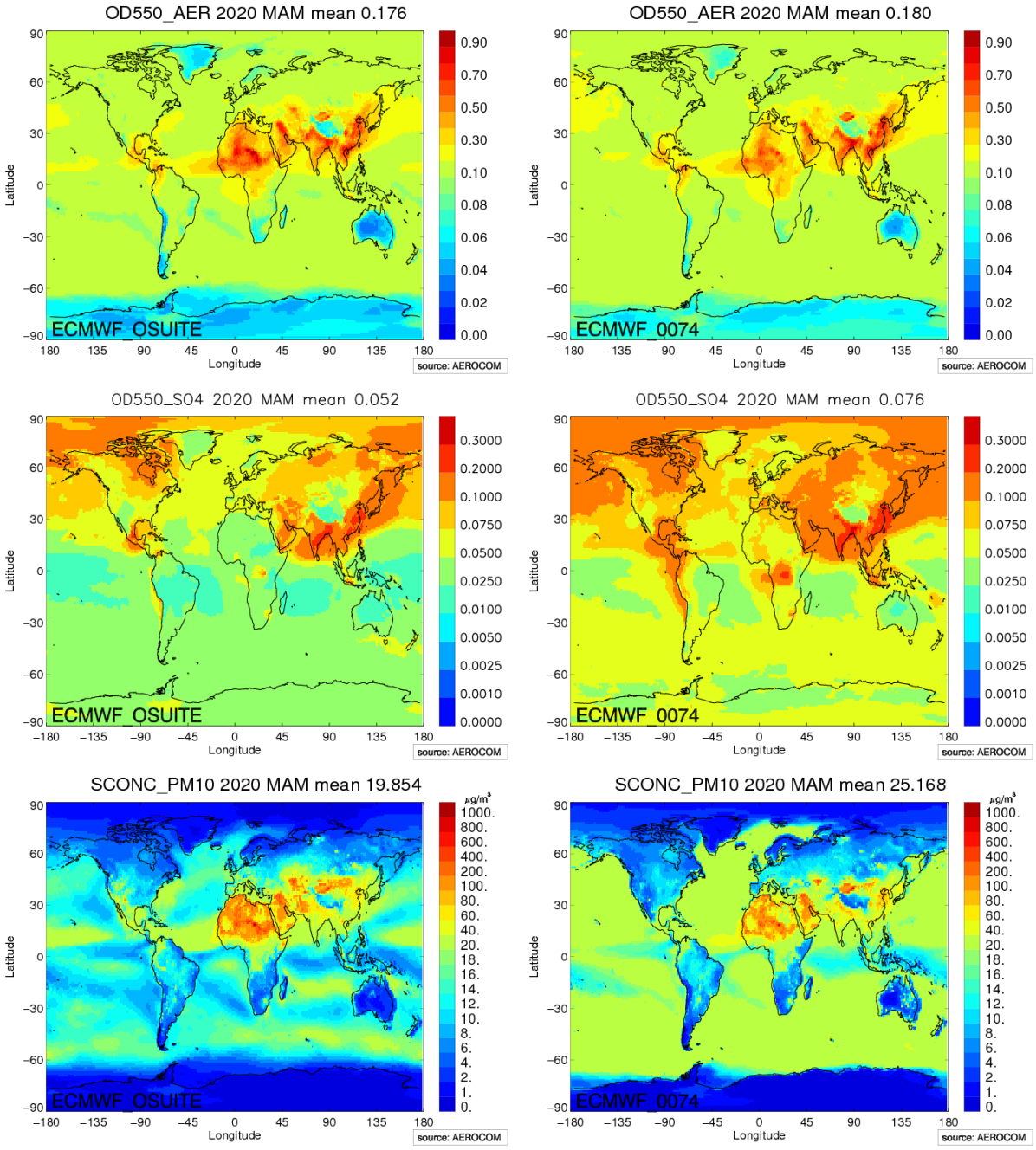

Figure 2.1.1 (a): March-May 2020 average fields of AOD (upper row), sulphate optical depth (middle row) and PM10 surface concentration (lowest row) for o-suite (left) and e-suite (experiment 0074, right). Even though total AOD has not changed much, a significant increase in sulphate AOD and surface sea salt is observed. Overall, the increase in sulphate AOD is compensated by decreases in dust and sea salt AOD.

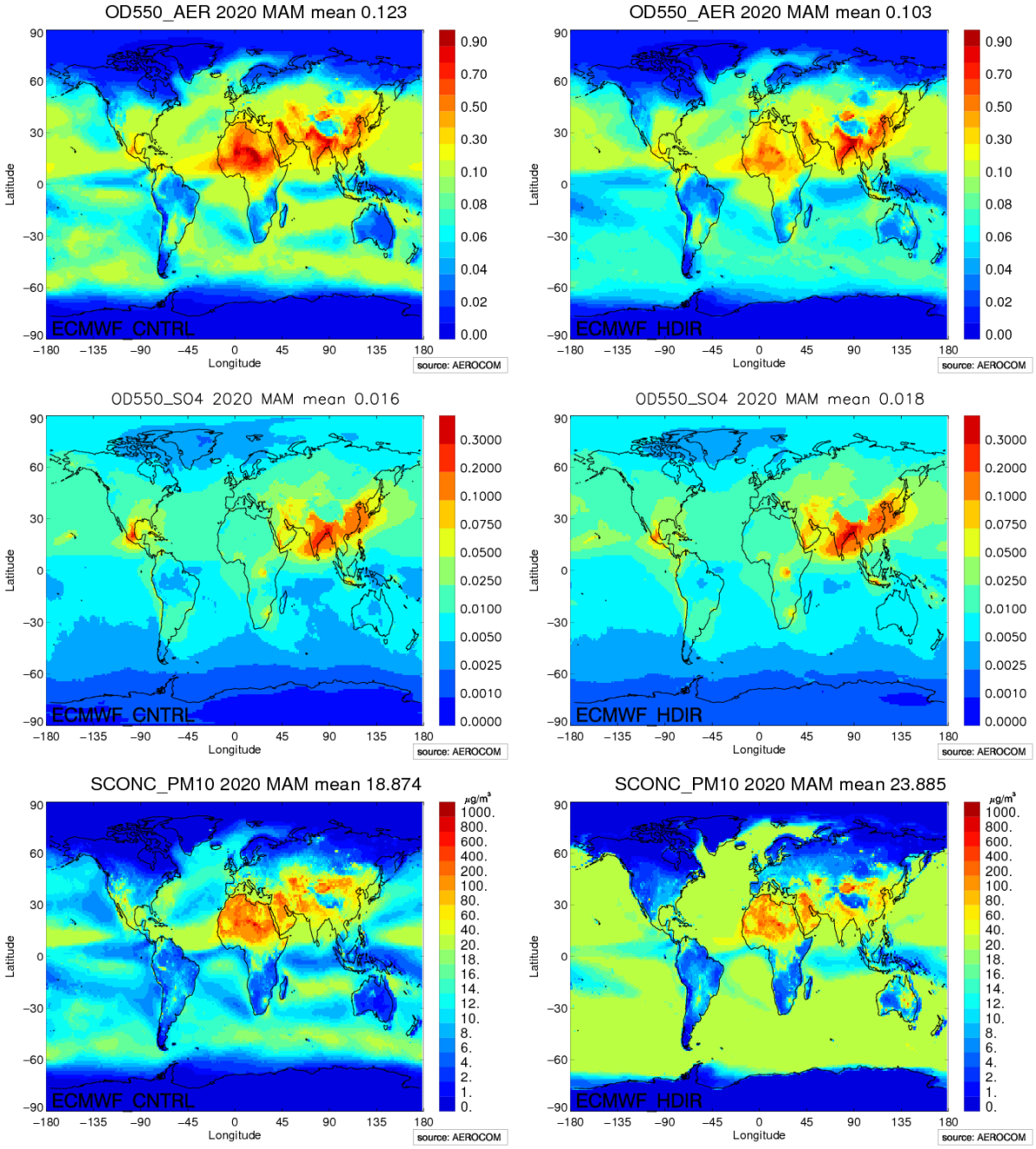

Figure 2.1.1 (b): March-May 2020 average fields of AOD (upper row), sulphate optical depth (middle row) and PM10 surface concentration (lowest row) for o-suite control (CNTRL) and e-suite control (E-CNTRL, experiment HDIR). Even though total AOD has not changed much, a significant increase in sulphate AOD and surface sea salt is observed. Overall, the increase in sulphate AOD is compensated by decreases in dust and sea salt AOD.

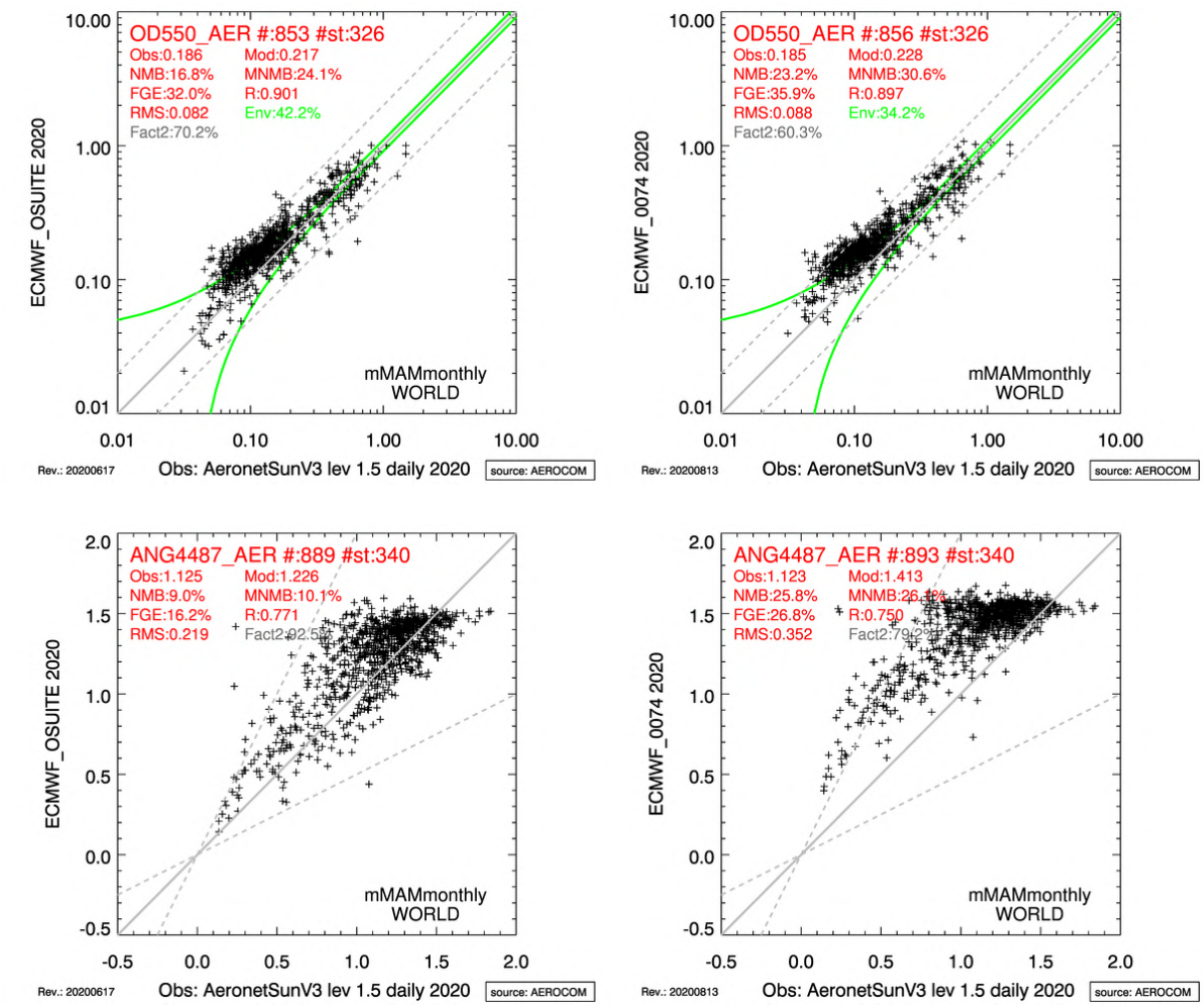

Figure 2.1.2: March-May 2020 evaluation for global Aeronet v3 level1.5 AOD (OD550_AER, upper row), for o-suite (left) and e-suite (experiment 0074; right) and Angstrøm exponent (ANG4487_AER, lower row). The scores (bias, RMS, correlation, fraction within factor 2) for AOD have degraded a bit. As a result of the shift to more sulphate, the Ångstrøm exponent is less well simulated and shows a clear positive bias.

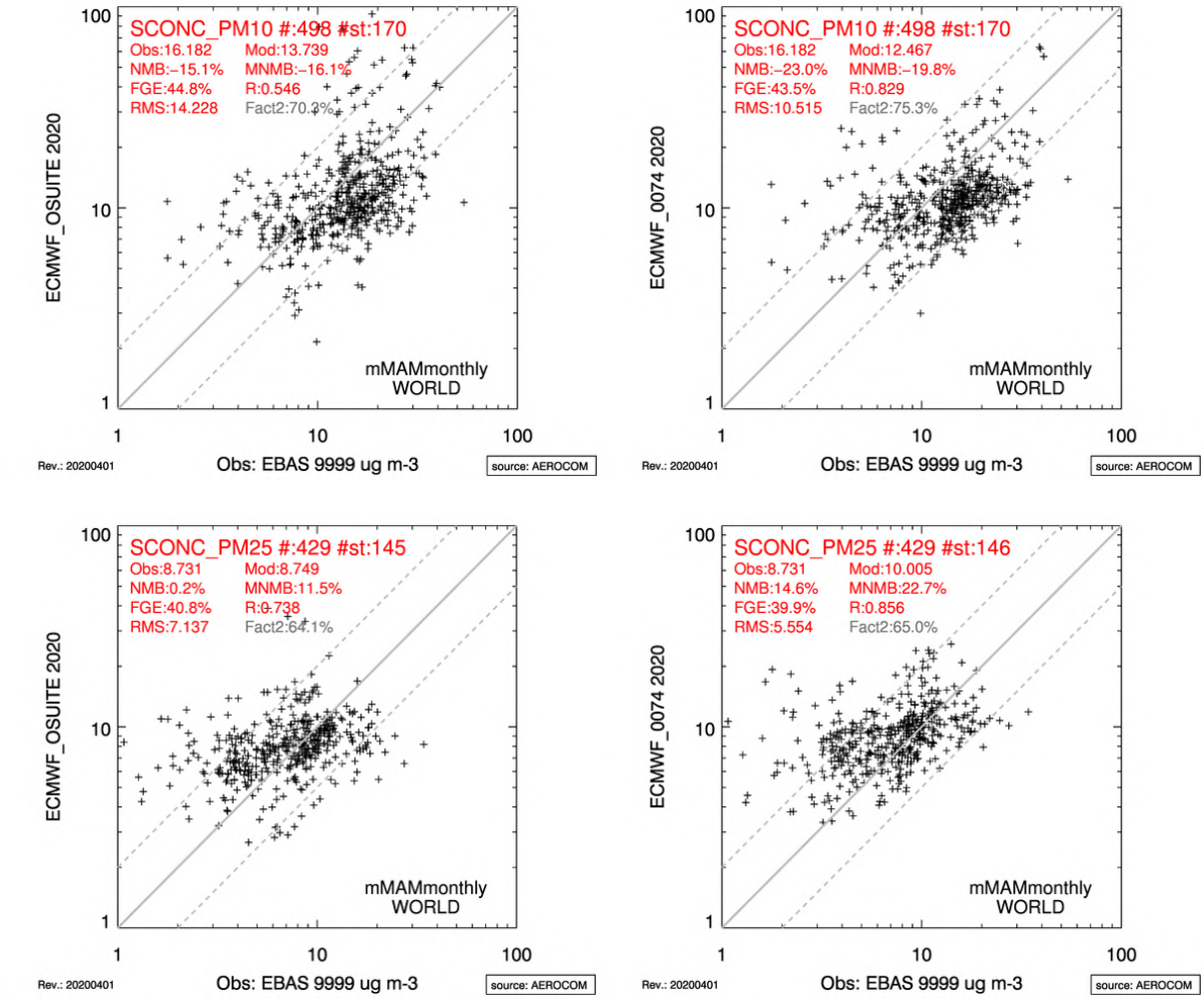

Figure 2.1.3: March-May 2020 evaluation for o-suite (left) and e-suite (experiment 0074; right) of the European plus North American climatological PM10 surface concentration (top figures), and PM25 surface concentration (bottom figures). The very high PM10 concentrations in the o-suite have disappeared, and correlation increases from 0.55 to 0.83 in the e-suite. Similarly, PM25 at these sites improved slightly in the e-suite.

Table 2.1.1. Mean global total and speciated AOD and surface PM10 and PM2.5 concentrations [μg m-3] in the o-suite, o-suite control (CNTRL), e-suite (experiment 0074) and e-suite control (E-CNTRL, experiment HDIR) for the latest March, April and May 2020 period. The right columns show the relative change between o-suite and e-suite and the respective control simulations.

	O-SUITE	E-SUITE	CNTRL	E-CNTRL	E-SUITE/ O-SUITE	E-CNTRL/ CNTRL
AOD@550	0.176	0.180	0.123	0.103	+2%	-16%
BC-OD@550	0.0070	0.0051	0.0022	0.0021	-27%	-5%
Dust-OD@550	0.026	0.015	0.031	0.017	-40%	-45%
NO3-OD@550	0.0047	0.0047	0.0068	0.0074	+0%	+9%
OA-OD@550	0.038	0.039	0.020	0.020	+3%	+0%
SO4-OD@550	0.052	0.076	0.016	0.018	+47%	+14%
SS-OD@550	0.047	0.038	0.045	0.036	-19%	-21%
PM2.5	8.30	15.3	7.20	13.9	+84%	+93%
PM10	19.6	25.2	18.9	23.9	+29%	+26%

Table 2.1.2. MNMB and spatial correlation R of AOD and surface PM10 and PM2.5 concentrations [μg m-3] in the o-suite, o-suite control (CNTRL), e-suite (experiment 0074) and e-suite control (E-CNTRL, experiment HDIR) for the latest March, April and May 2020 period. The values correspond to figure 2.1.2. Data are collocated on daily basis and then averaged per month, before statistics are calculated.

MNMB [%]	O-SUITE	E-SUITE	CNTRL	E-CNTRL
AOD@550	+24.1	+30.6	-21.9	-31.1
ANG4487	+10.1	+26.1	-9.7	+11.3
PM2.5	+11.5	+22.7	-23.4	-14.0
PM10	-16.1	-19.8	-43.4	-52.2

R	O-SUITE	E-SUITE	CNTRL	E-CNTRL
AOD@550	0.90	0.90	0.83	0.84
ANG4487	0.77	0.75	0.74	0.76
PM2.5	0.74	0.86	0.81	0.91
PM10	0.55	0.83	0.63	0.88

2.2 Dust and aerosol evaluation over North Africa, the Middle East and Europe

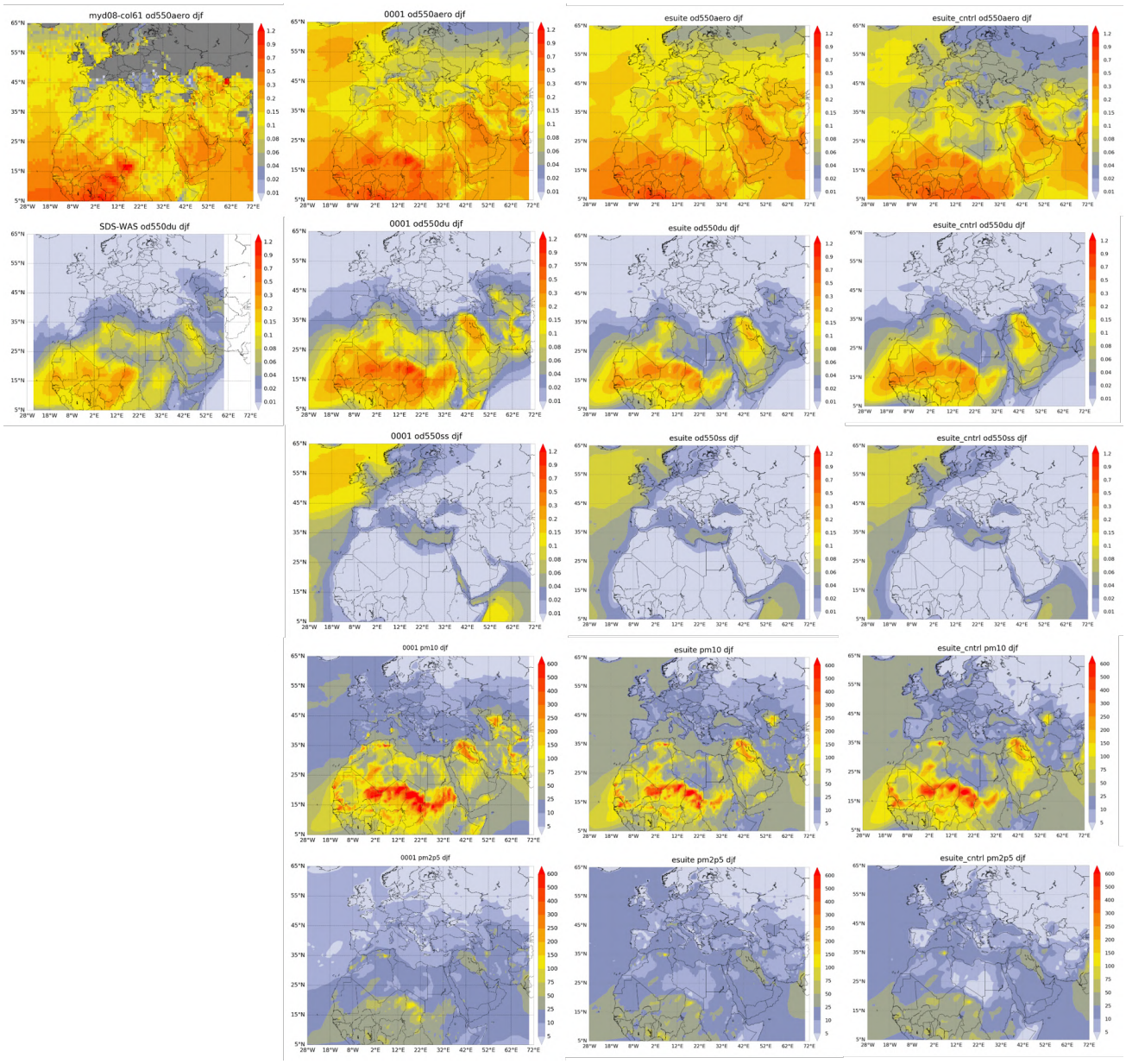

Figure 2.2.1. Seasonal averaged aerosol optical depth (od550aero; top row), dust optical depth (od550du; second row) and sea-salt (od550ss; third row), PM10 (pm10, in µg/m3; row 4) and PM2.5 (pm2p5, in µg/m3; last row) from current o-suite (expid 0001, second column), e-suite (expid 0074, third column) and e-suite control run (expid hdir, fourth column) from December 2019 to February 2020. CAMS outputs are compared with MODIS Collection 6.1 Level 3 aerosol optical depth (top-left) and the SDS-WAS multi-model product (second row, left panel). The e-suite shows a reduced desert dust source over the Sahara compared to the o-suite in better agreement with SDS-WAS. The extreme PM10 concentrations over Southern Europe in the o-suite have improved in the e-suite.

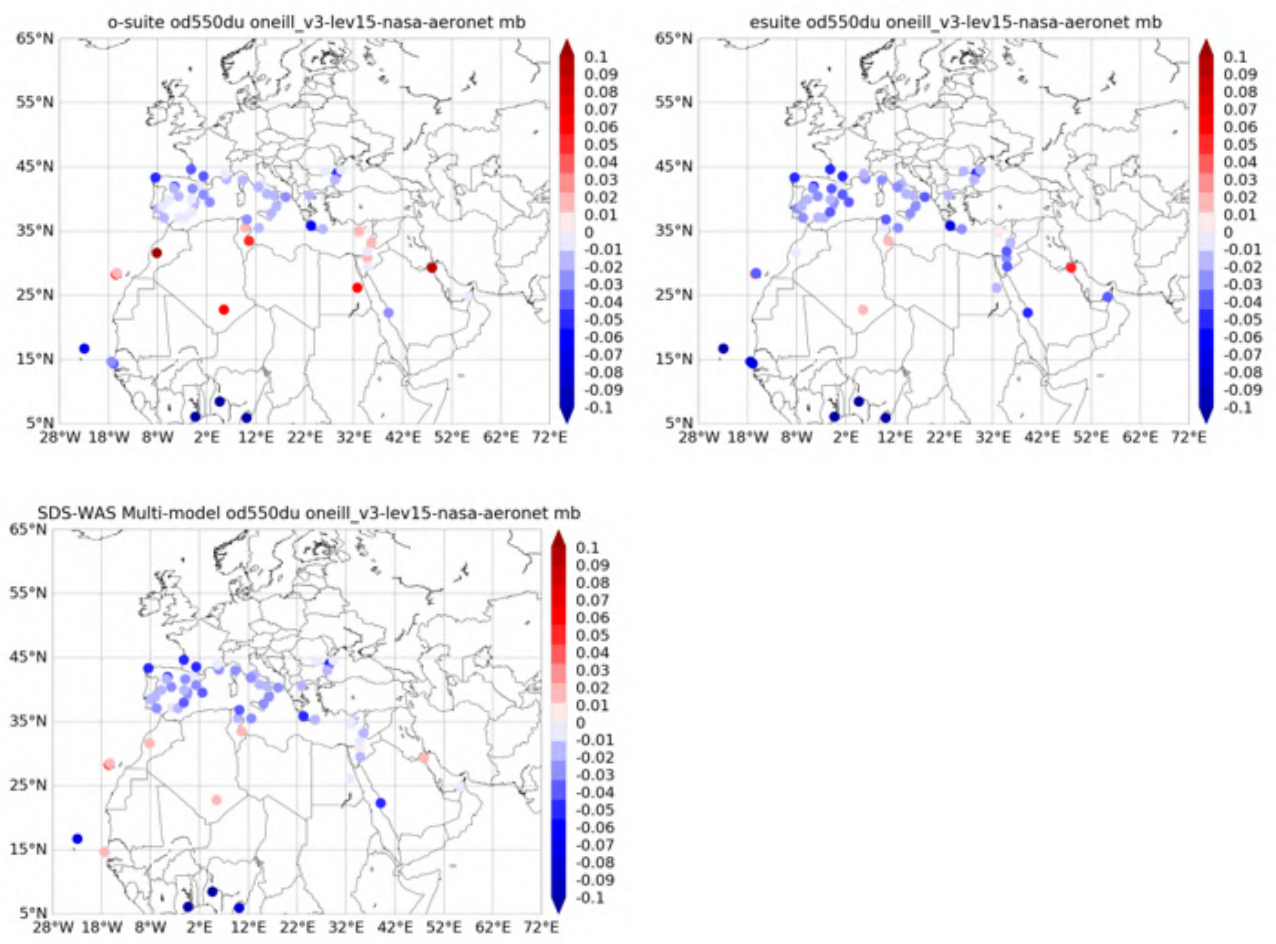

Figure 2.2.2. Skill scores (mean bias) for 24-hour forecasts of the CAMS o-suite (left column), e-suite (central column) and DOD Multi-model SDS-WAS Median (right column) from December 2019 to February 2020. Coarse AOD from AERONET is the reference. The mean bias for the current o-suite is reduced in the e-suite.

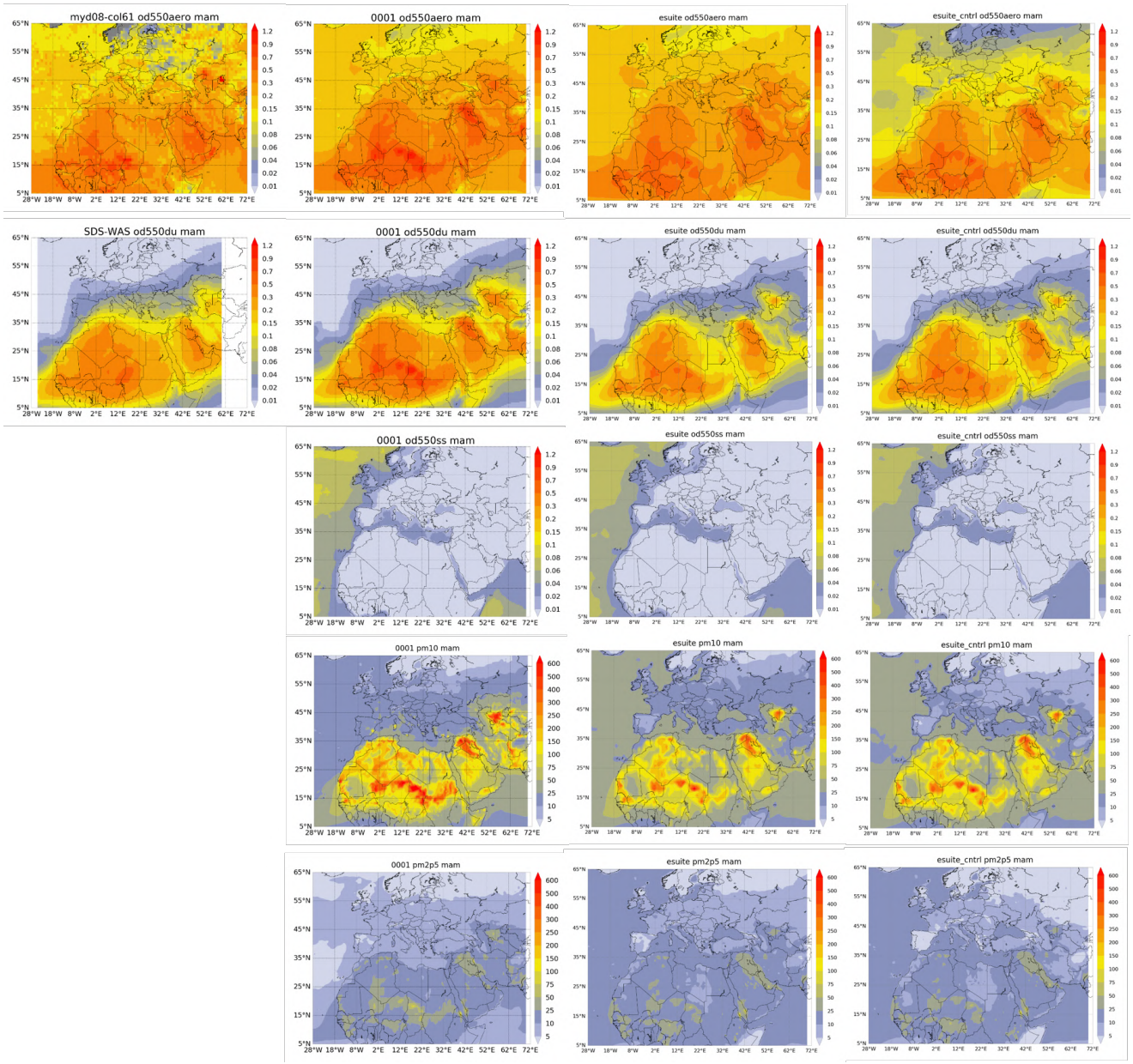

Figure 2.2.3. Seasonal averaged aerosol optical depth (od550aero; first row), dust optical depth (od550du; second row) and sea-salt (od550ss; third row), PM10 (pm10, in µg/m3; row 4) and PM2.5 (pm2p5, in µg/m3; last row) from the current o-suite (expid 0001, second column), the e-suite (expid 0074, third column) and e-suite control run (expid hdir, fourth column) from March 2020 to May 2020. CAMS outputs are compared with MODIS Collection 6.1 Level 3 aerosol optical depth (top left) and the SDS-WAS multi-model product (second row, left). The e-suite shows a reduced desert dust source over the Sahara compared to the o-suite in better agreement with SDS-WAS. The extreme PM10 concentrations over Southern Europe in the o-suite have improved in the e-suite.

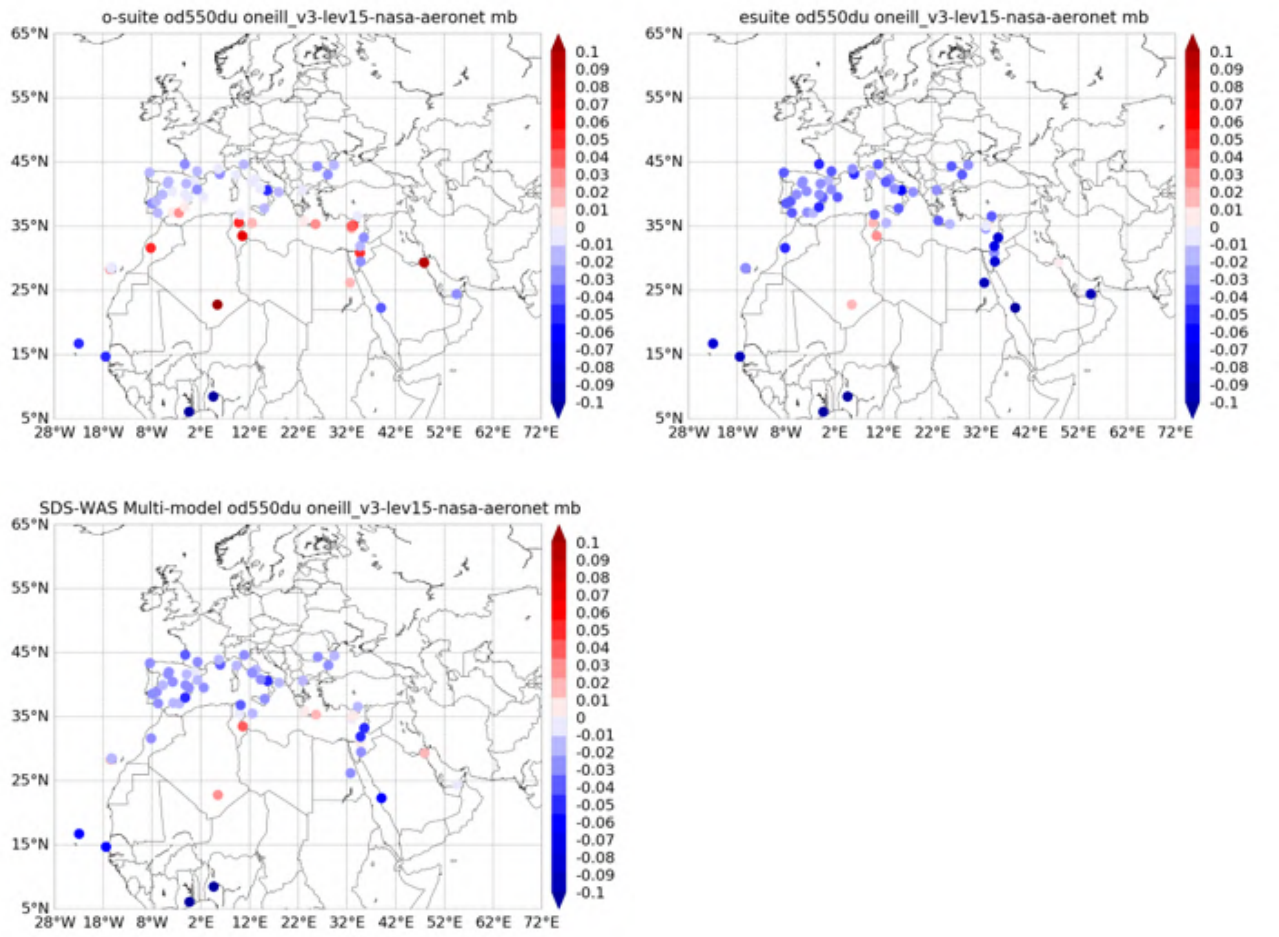

Figure 2.2.4. Skill scores (MB) for 24-hour forecasts of CAMS o-suite (left column), e-suite (central column) and DOD Multi-model SDS-WAS Median (right column) from March 2020 to May 2020. Coarse AOD from AERONET is the reference. The e-suite shows smaller AOD values in the Mediterranean than the o-suite, removing the large overestimations of the o-suite, but also leading to underestimations in Southern European countries.

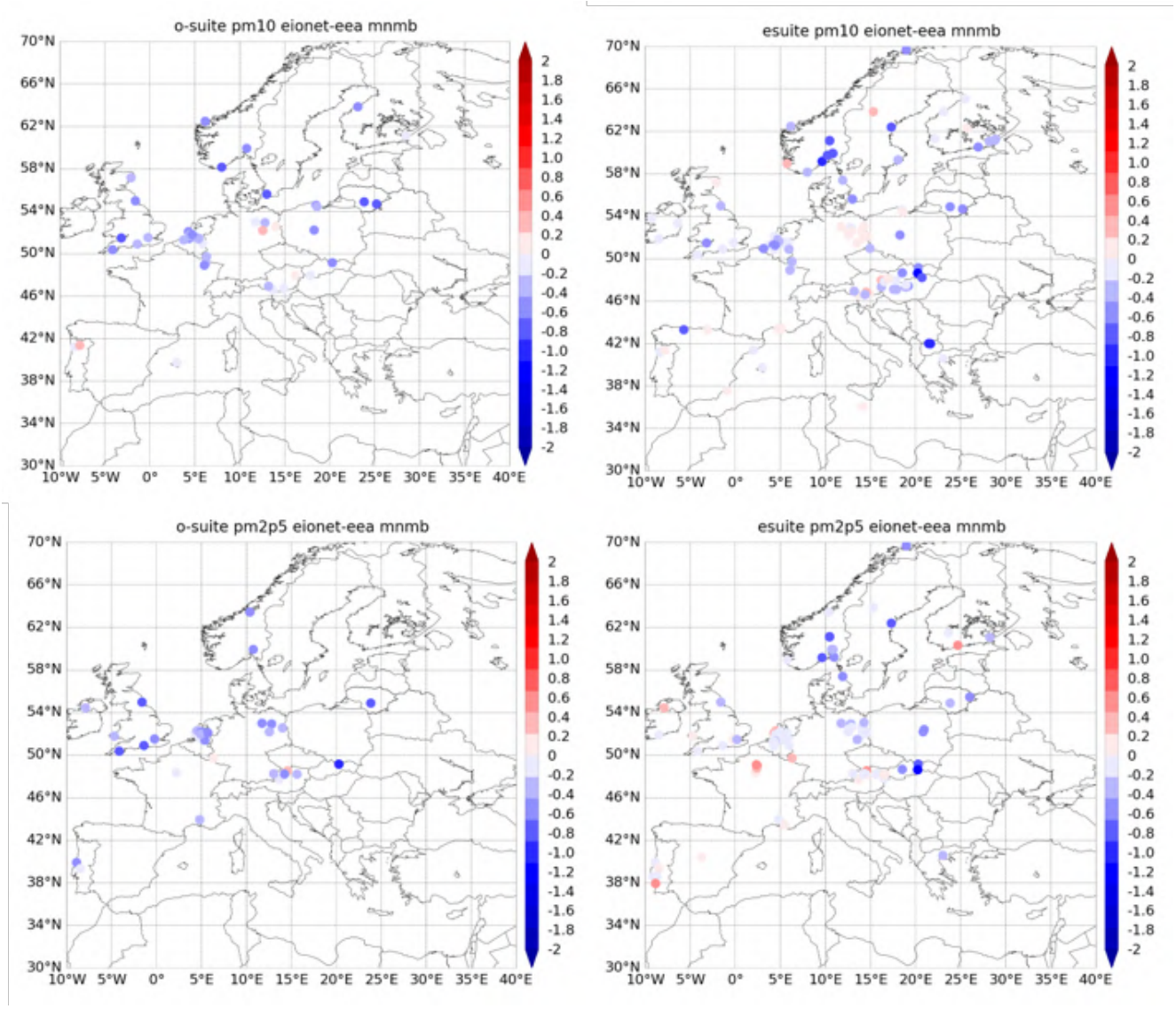

Figure 2.2.5. Skill scores (MNMB) for the 24-hour forecasts (at 3hourly basis) of CAMS o-suite and e-suite, from December 2019 to February 2020. Three-hourly PM10 from EIONET is the reference. Only global scale representative available stations are displayed. The e-suite enhances the PM2.5 levels reducing the general underestimation observed over Europe.

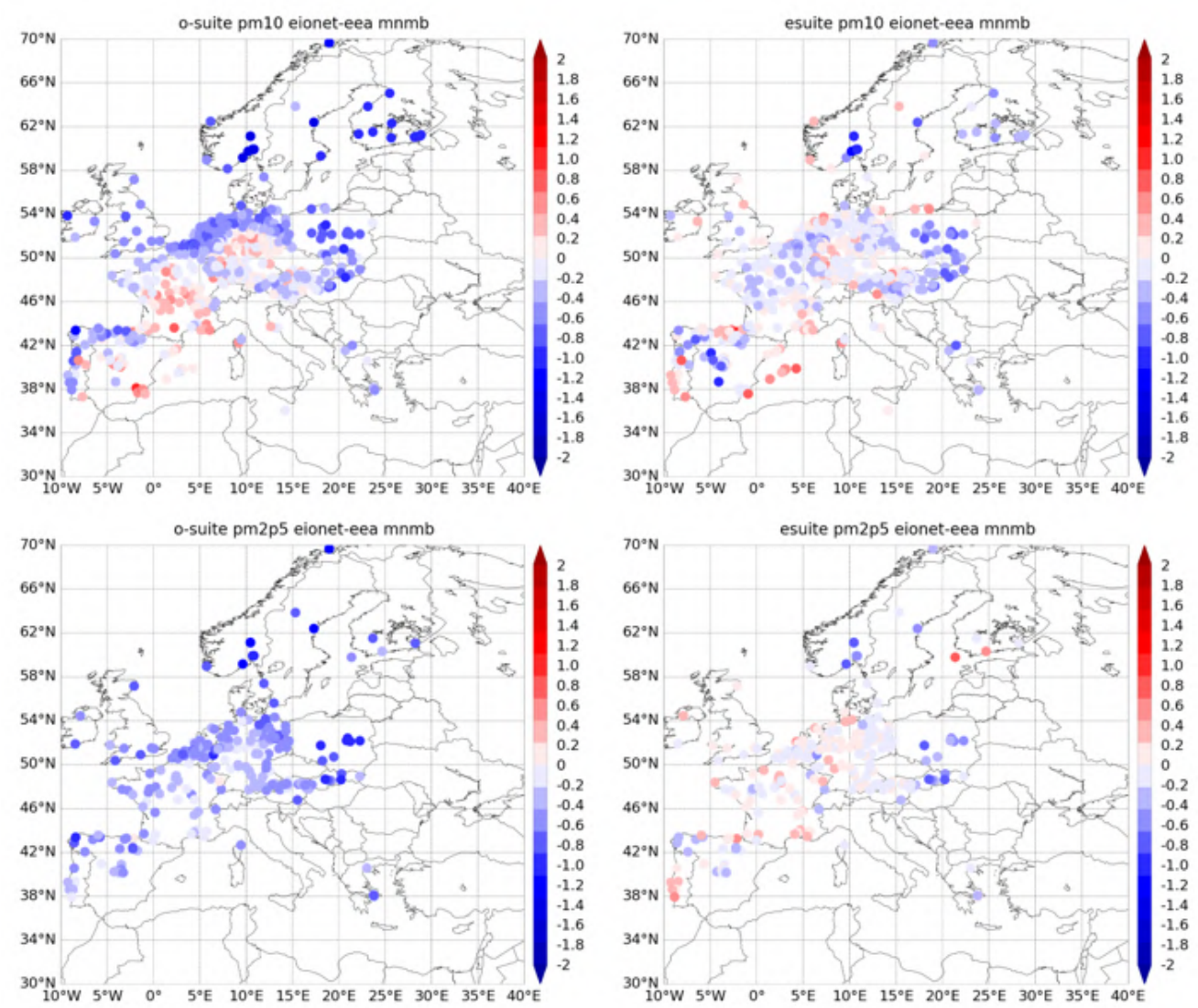

Figure 2.2.6. Skill scores (MNMB) for 24-hour forecasts (at 3hourly basis) of CAMS o-suite and e-suite, from March 2020 to May 2020. Three-hourly PM10 from EIONET is the reference. Only global scale representative available stations are displayed. The e-suite reduces the strong overestimations observed in the o-suite in PM10 in Central Europe, and the e-suite enhances the PM2.5 levels reducing the general underestimation observed over Europe.

2.3 Verification with ozone sonde data in the free troposphere

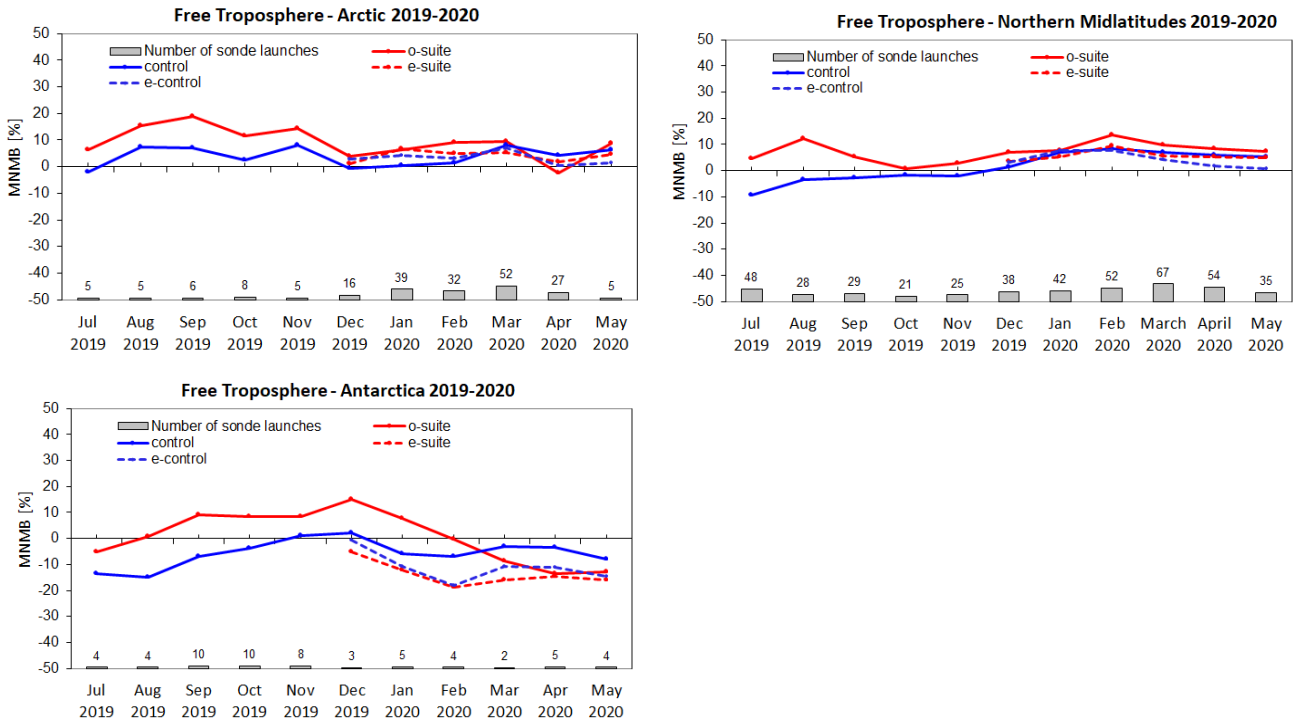

Fig. 2.3.1. Modified normalised mean bias (MNMB) for the o-suite (red, solid), e-suite (red, dashed) and control runs (blue). The control runs are plotted for the period December 2019 to May 2020. The free troposphere is defined as the altitude range between 300 and 750 hPa. Differences between the o-suite and e-suite are small.

2.4 Verification with GAW and ESRL-GMD surface ozone observations

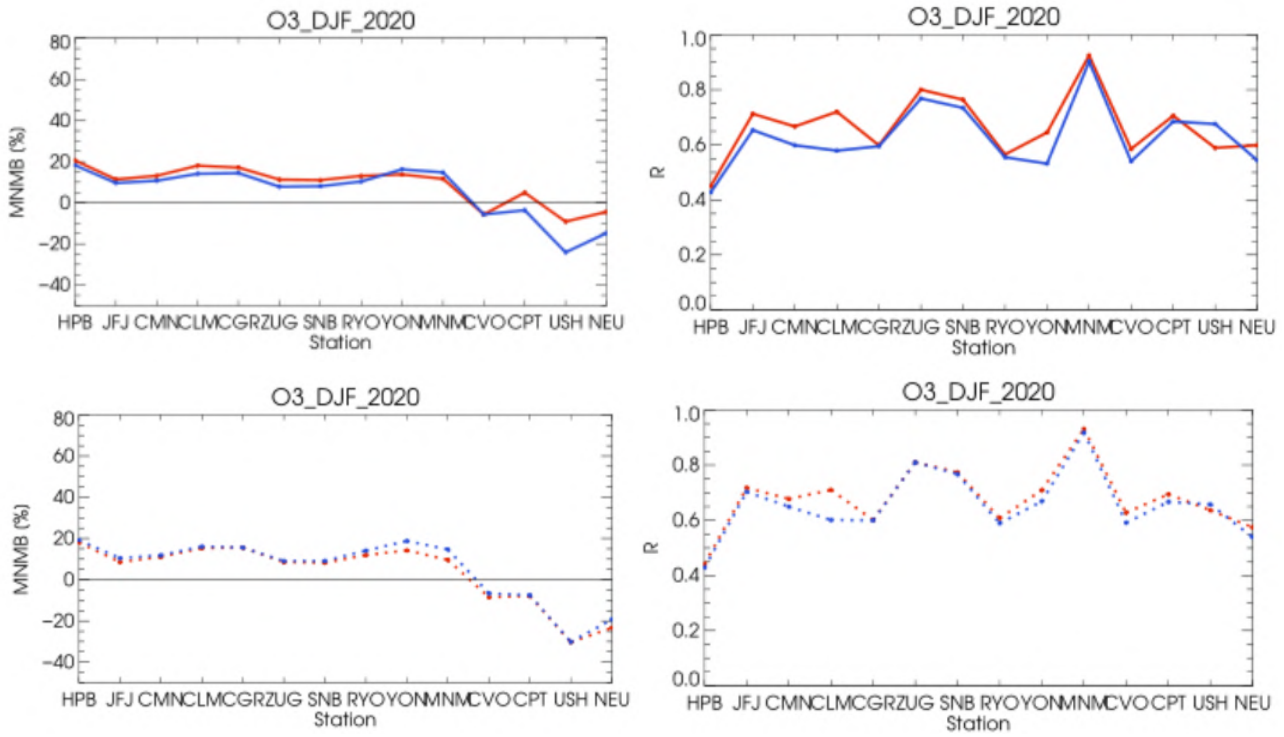

Fig. 2.4.1. Comparison with surface ozone at GAW stations: MNMB (left) and correlation coefficient (right) of o-suite and control for the period DJF 2019/2020. Upper panel are for the o-suite (red) and control (blue), lower panel e-suite and e-control. Period: December 2019 to February 2020. The e-suite and o-suite show similar biases, except for a negative e-suite bias over Antarctica.

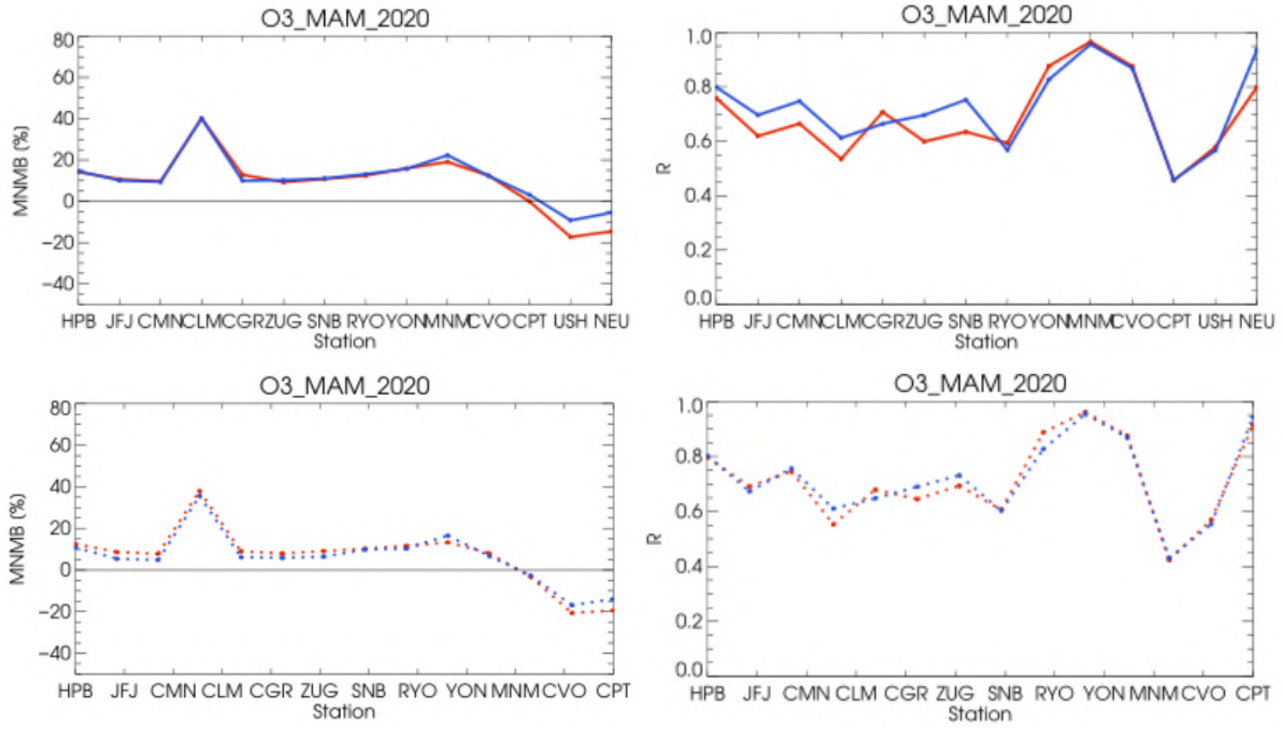

Fig. 2.4.2. Same as Fig. 2.4.1, for March-May 2020.

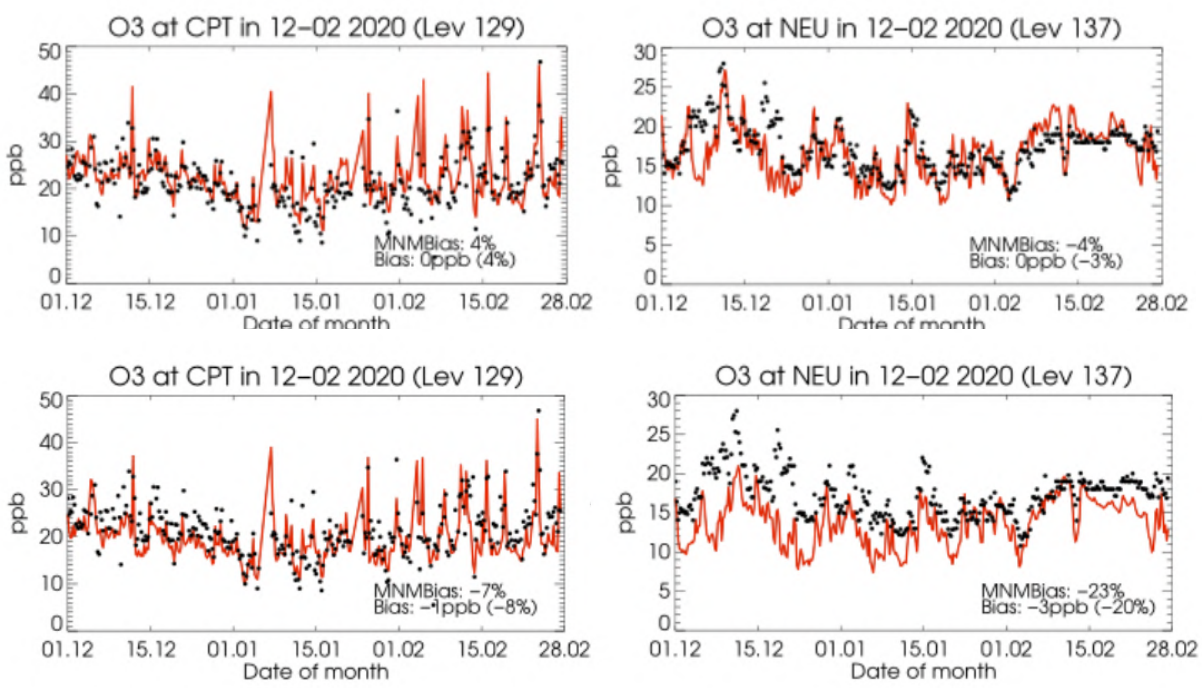

Fig. 2.4.3. Timeseries for Cape Point (CPT) and Neumayer (NEU) in the southern hemisphere. Upper panel: o-suite, lower panel: e-suite. Black: observations, red: o-suite and e-suite, respectively. At Cape Point the two configurations are very similar. In Neumayer (Antarctica) the e-suite develops a negative bias compared to the o-suite.

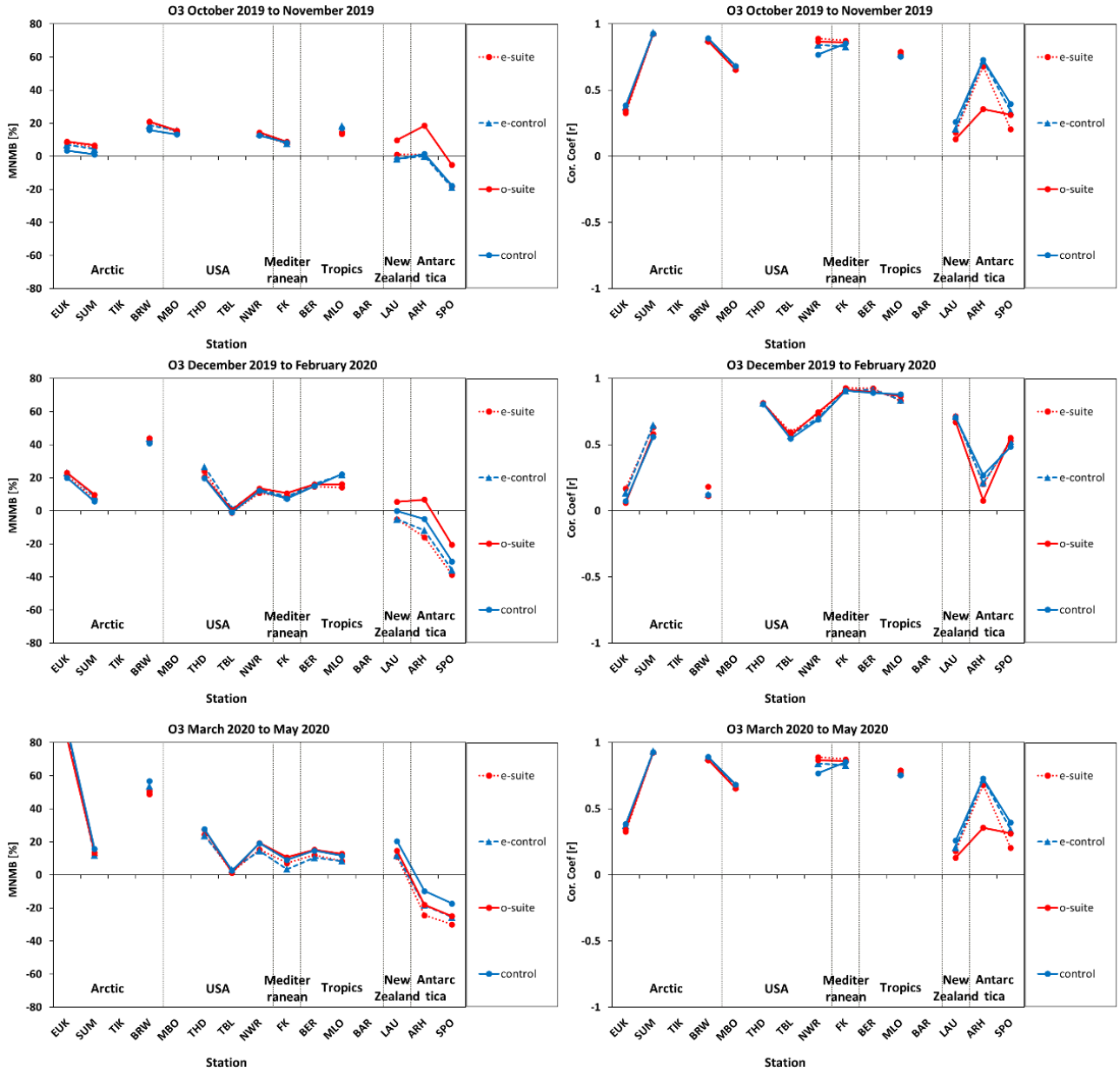

Fig. 2.4.4. Comparisons with ESRL surface observations: Bias (MNMB, left) and correlation coefficient (right) of o-suite (red, solid), e-suite (red, dashed) and control (blue, solid) and e-control (blue, dashed) for the period October-November 2019 (upper panel), DJF 2019/2020 (middle panel), MAM 2020 (bottom panel). Overall e-suite ad o-suite behave similarly, with a small indication of improvements over midlatitudes and a more negative bias over Antarctica.

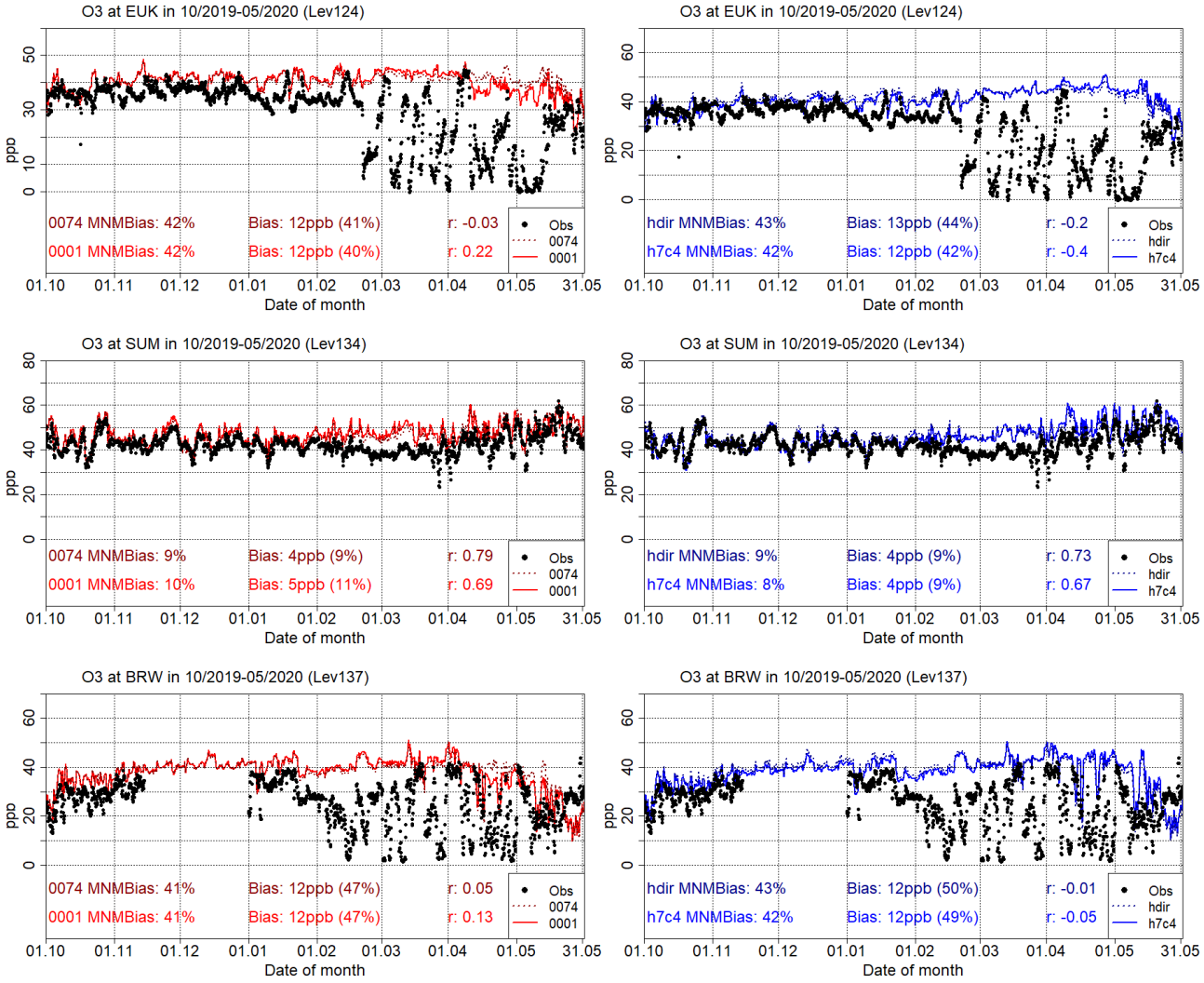

Fig. 2.4.5. Comparisons with ESRL surface observations: Time series for the Arctic ESRL stations. Red: o-suite; red-dash: e-suite; blue: o-suite control run; blue-dash: e-suite control run.

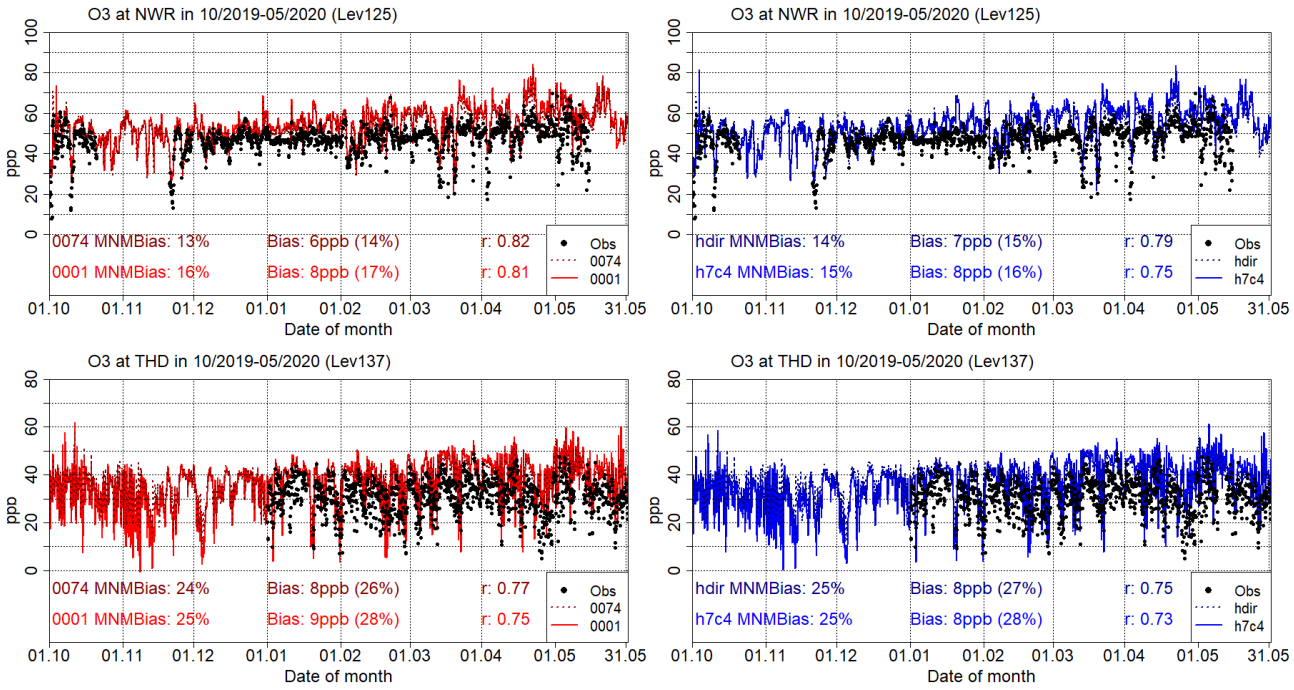

Fig. 2.4.6. Comparisons with ESRL surface observations: Time series for the USA ESRL stations. Red: o-suite; red-dash: e-suite; blue: o-suite control run; blue-dash: e-suite control run.

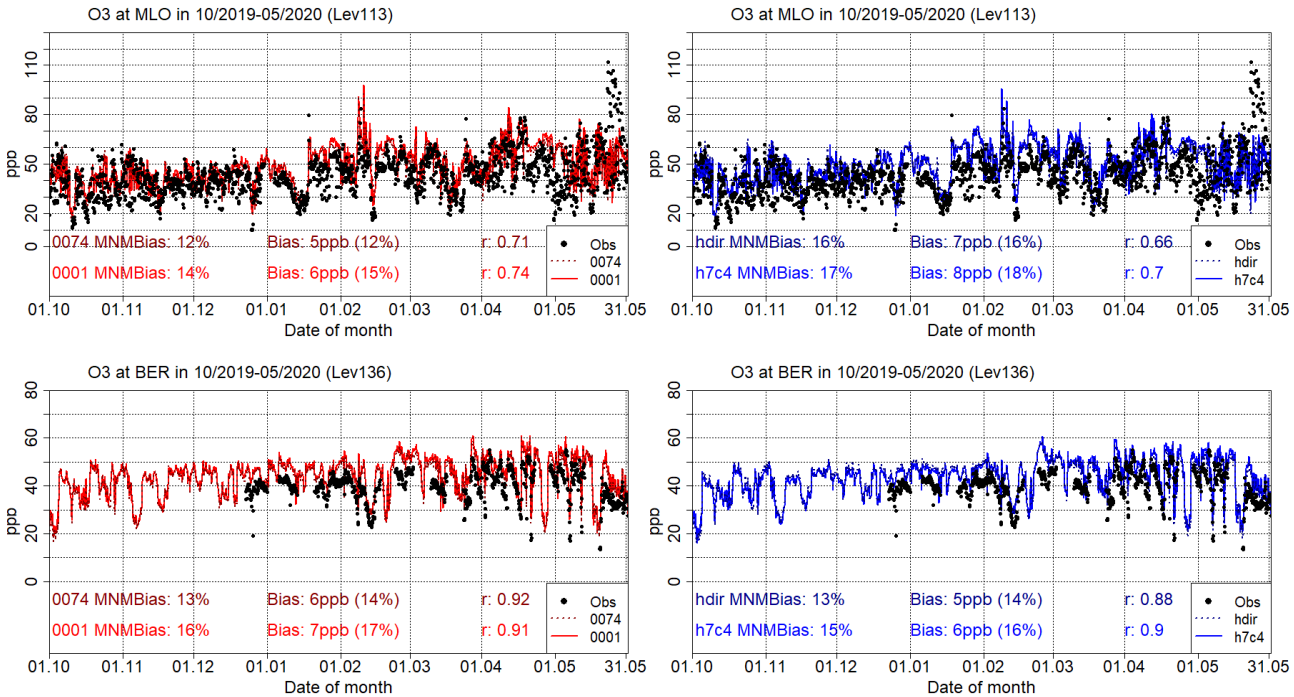

Fig. 2.4.7. Comparisons with ESRL surface observations: Time series for the tropical ESRL stations. Red: o-suite; red-dash: e-suite; blue: o-suite control run; blue-dash: e-suite control run.

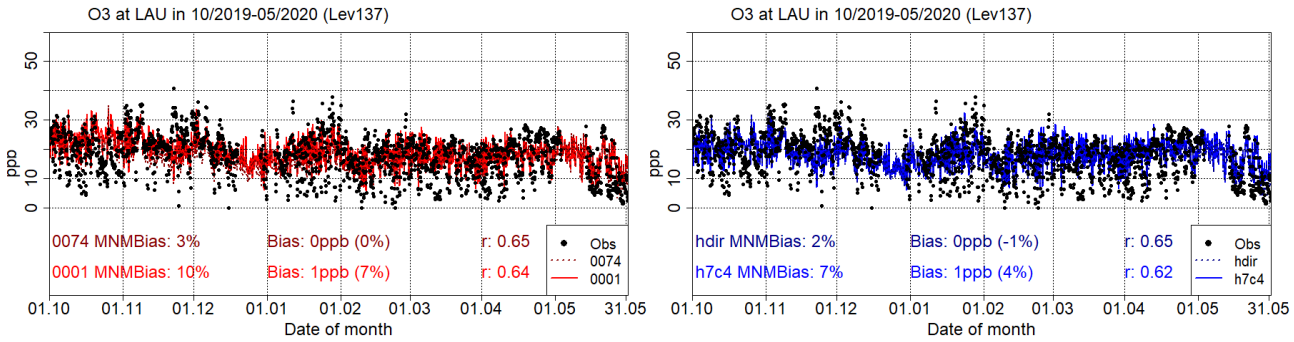

Fig. 2.4.8. Comparisons with ESRL surface observations: Time series for the Lauder ESRL stations. Red: o-suite; red-dash: e-suite; blue: o-suite control run; blue-dash: e-suite control run.

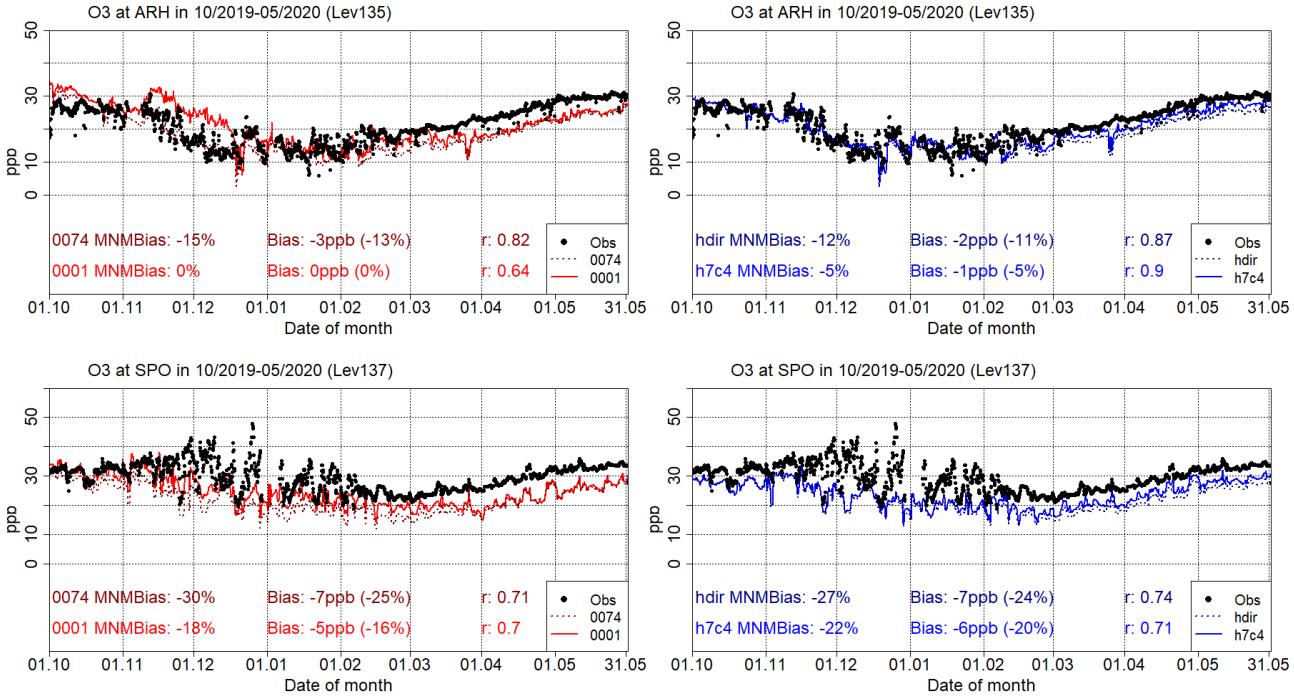

Fig. 2.4.9. Comparisons with ESRL surface observations: Time series for the Antarctic ESRL stations. Red: o-suite; red-dash: e-suite; blue: o-suite control run; blue-dash: e-suite control run.

2.5 Verification with IAGOS ozone and CO observations

For the verifications with IAGOS, Level-1 data was used for comparisons during the entire period between October 2019 and July 2020. Nearly continuous observations are available only at Frankfurt, with some gaps during the period of the COVID-19 pandemic as shown on the time series of ozone (see also CO section).

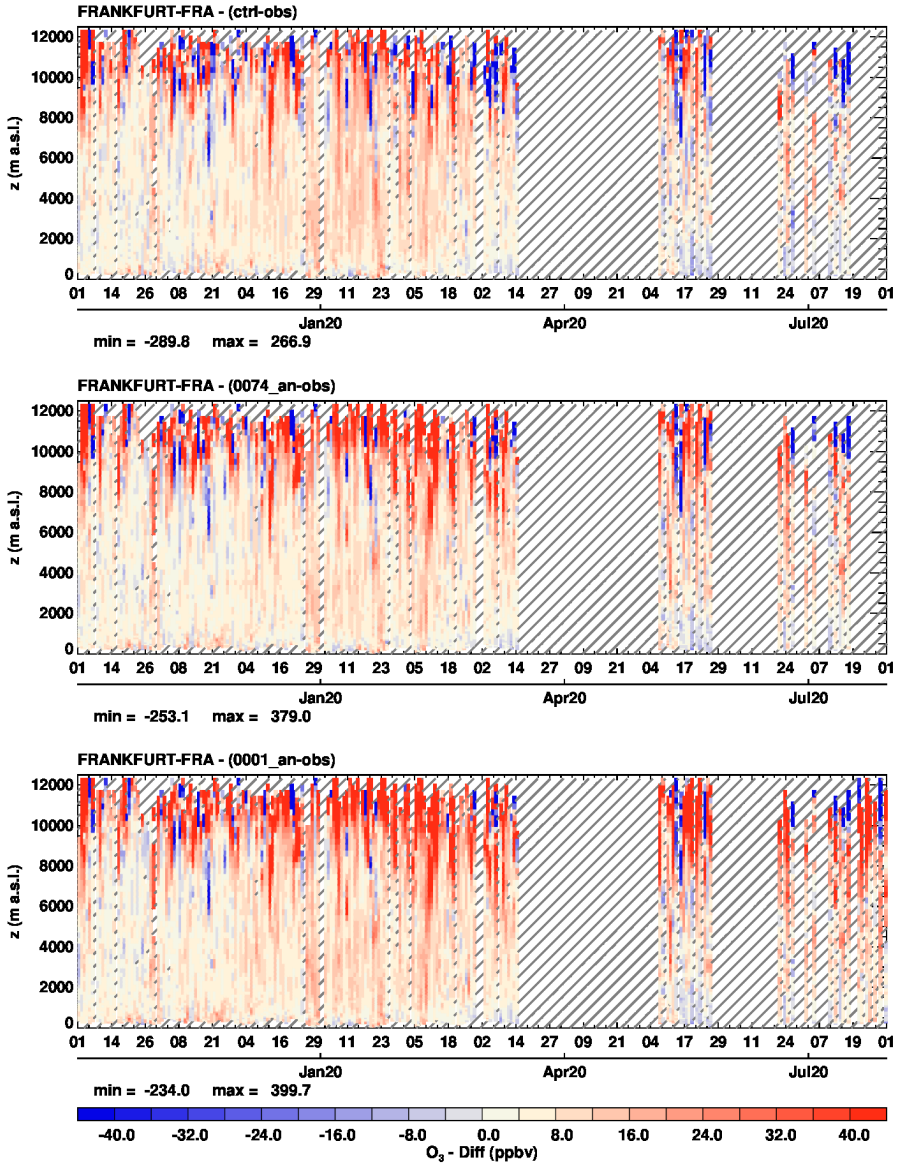

Fig. 2.5.1: Time series of the differences (model analysis minus IAGOS) in the daily profiles of ozone at Frankfurt during October 2019 -July 2020. The top and centre panel are for the e-suite (0074) control run and analysis respectively and the bottom panel is for the o-suite (0001) analysis. The e-suite behaviour for both analysis and control run is very similar to that of the o-suite analysis, and the bias from the e-suite appears in general smaller than that of the o-suite. The time series for the e-suite forecast are not shown here but are very similar to the results for the e-suite analysis (see also Fig. 2.5.2 and 2.5.3).

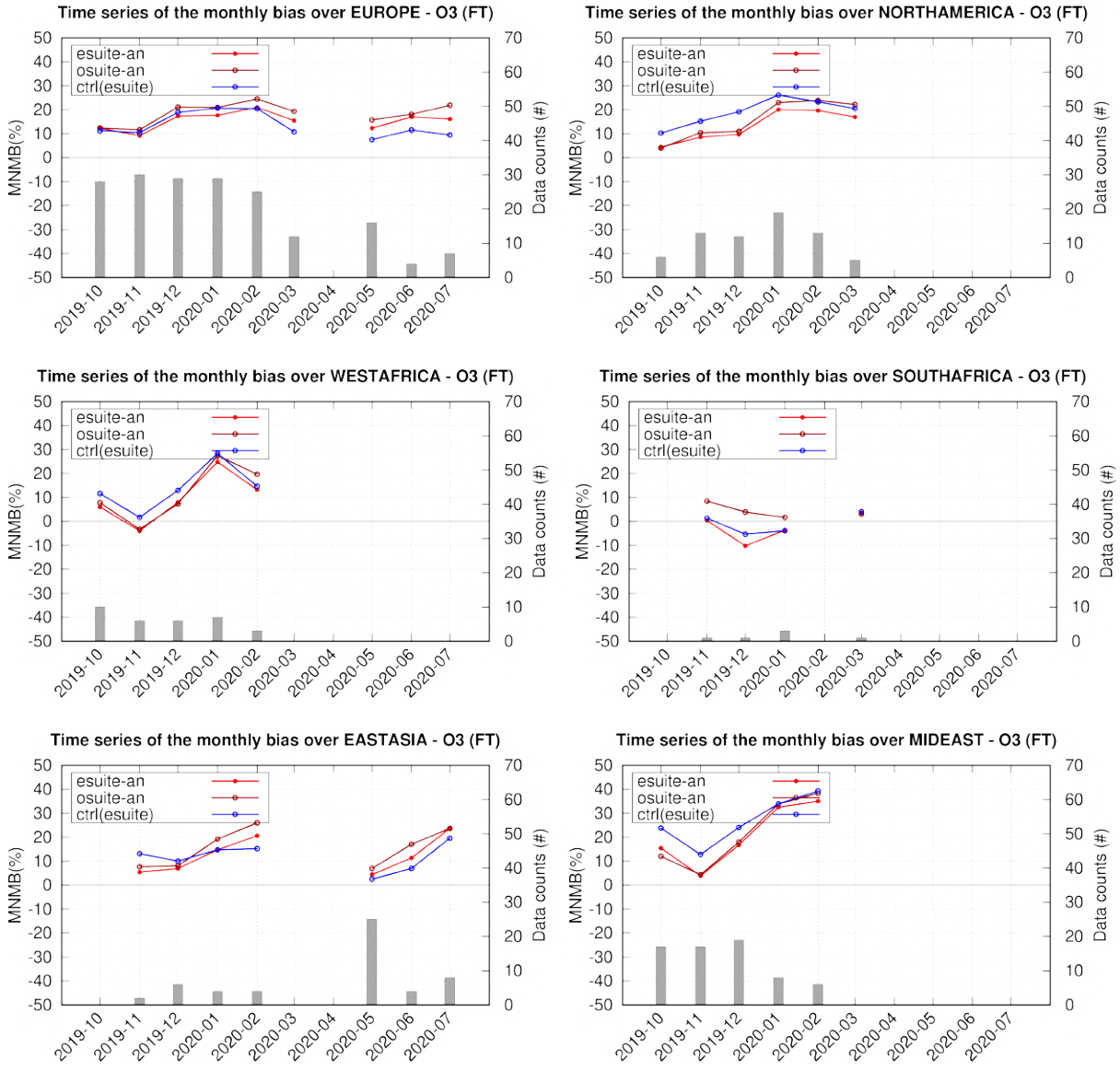

Fig. 2.5.2: Time series of monthly bias (MNMB) from e-suite 0074 (light red, empty circles) and o-suite 0001 (dark red, filled circle) for ozone in the Free troposphere (FT) between October 2019 and July 2020 in 6 regions (Top left: Europe, top right: North America, middle left: Western Africa, middle right: Southern Africa, bottom left: Eastern Asia, bottom right: Middle East). The histogram bars indicate the number of profiles (i.e. layer values) based on available observations. Over all regions with the exception of South Africa, the value of the bias from the e-suite is slightly smaller or close to that of the o-suite. Over South Africa, the absolute value of the bias is smaller than 10% but positive for the o-suite and negative for the e-suite. The assimilation of the e-suite often presents values of the bias smaller or close to those obtained with associated control run. However, the differences in the e-suite runs with and without assimilation appear slightly more pronounced starting from March until the end of the period over Europe (see also Fig. 2.5.5), where the bias become notably smaller for control run. Over East Asia, where IAGOS observations are also available from May to July, no difference is noted between the e-suite and associated control which present similar bias.

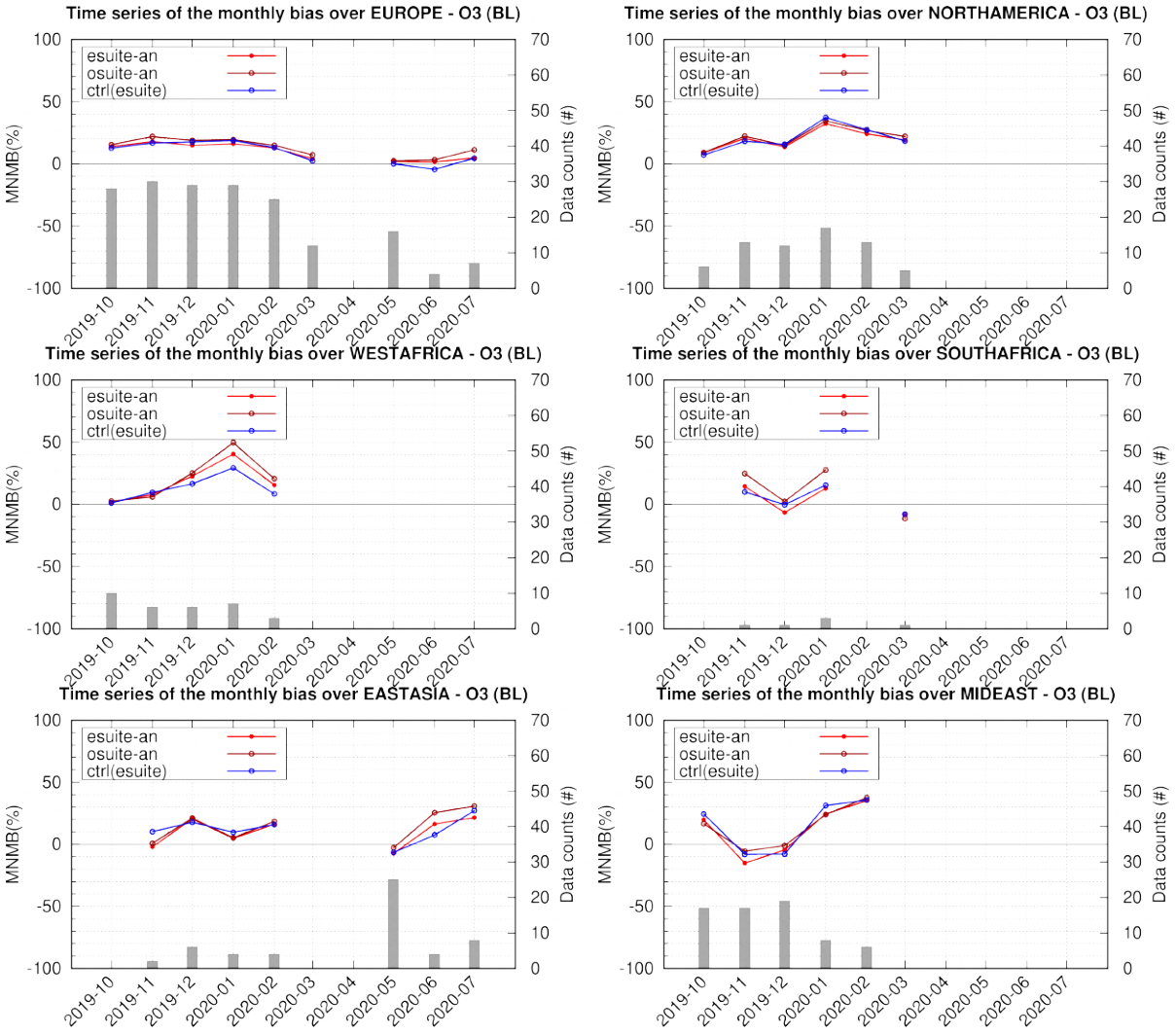

Fig. 2.5.3: Time series of monthly bias (MNMB) from e-suite 0074 (light red, empty circles) and o-suite 0001 (dark red, filled circle) for ozone in the Boundary Layer (BL) between October 2019 and July 2020 in 6 regions (Top left: Europe, top right: North America, middle left: Western Africa, middle right: Southern Africa, bottom left: Eastern Asia, bottom right: Middle East). The histogram bars indicate the number of profiles (i.e. layer values) based on available observations. In general, the behaviour of the models in the boundary layer is similar to what is found for the free troposphere (Fig. 2.5.2), but with less differences in bias values between all models including control run. The control run presents results very similar to those of the e-suite analysis for the full evaluation period and over all regions.

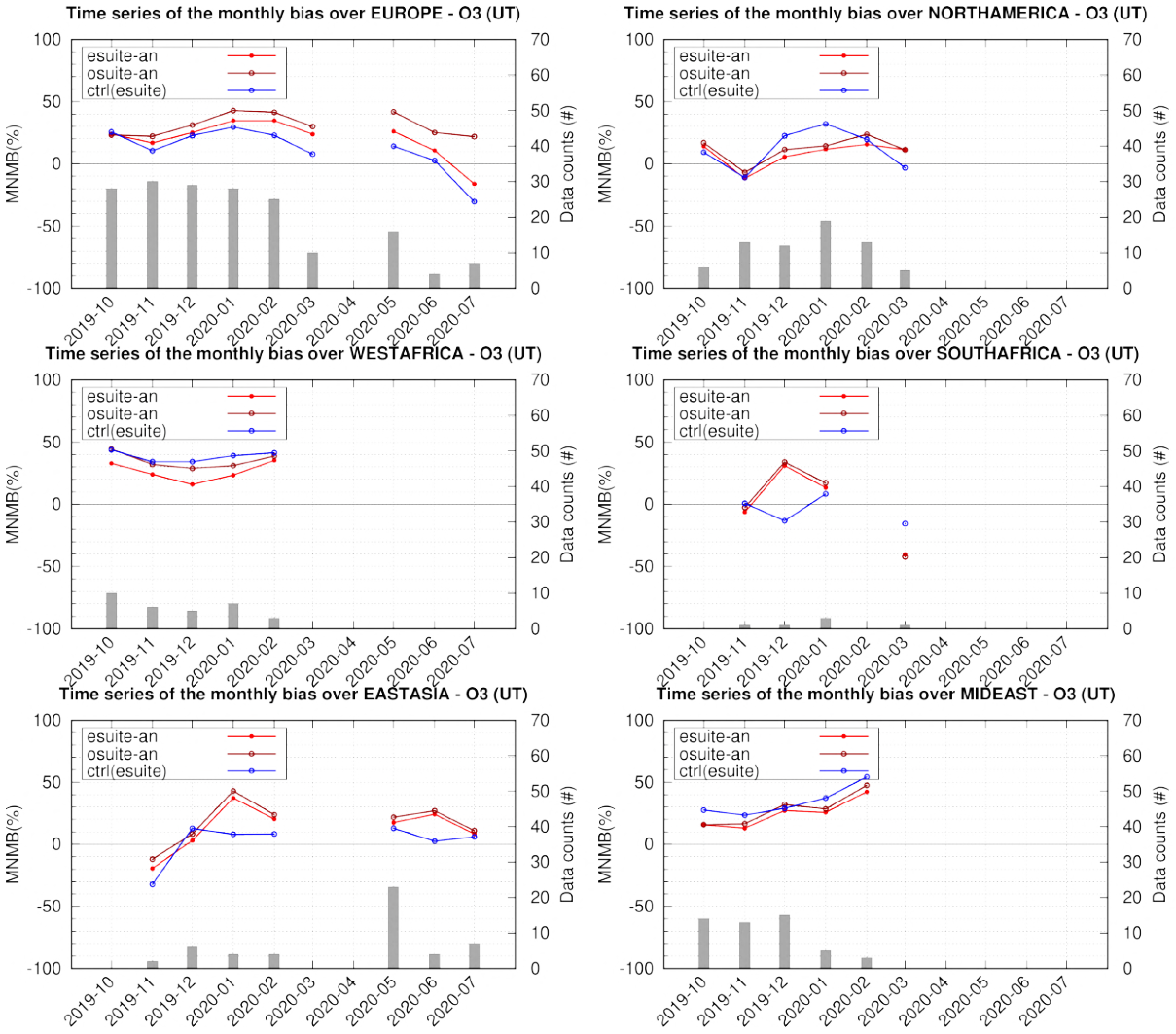

Fig. 2.5.4: Time series of monthly bias (MNMB) from e-suite 0074 (light red, empty circles) and o-suite 0001 (dark red, filled circle) for ozone in the Upper Troposphere (UT) between October 2019 and July 2020 in 6 regions (Top left: Europe, top right: North America, middle left: Western Africa, middle right: Southern Africa, bottom left: Eastern Asia, bottom right: Middle East). The histogram bars indicate the number of profiles (i.e. layer values) based on available observations. The results from the e-suite and o-suite analysis are very similar with a slightly smaller bias from the e-suite. Over Europe, for the last three months of the evaluation period the two models appear to differ slightly more, always with a smaller bias from the e-suite. Moreover, the bias changes from positive to negative in the last month for the e-suite and control run. Overall, the control run mostly present smaller bias than the e-suite analysis over Europe, South Africa and East Asia, while over North America, West Africa and the Middle East, these two runs present either similar results or a slightly larger bias from control run as compared to the e-suite analysis is found.

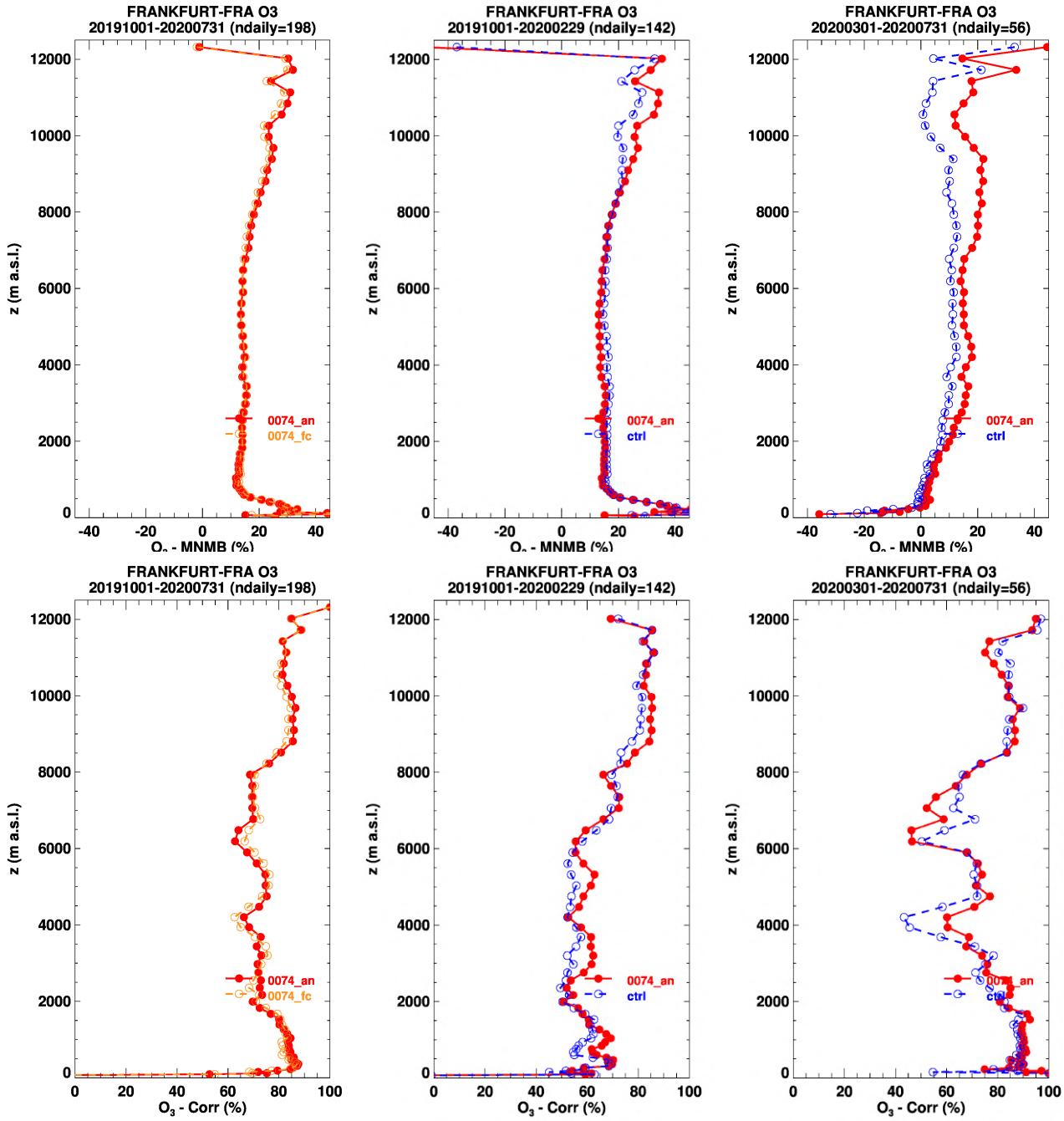

Fig. 2.5.5: Profile of MNMB and Correlation coefficient for ozone at Frankfurt. Results are presented for the full period October 2019 - July 2020 (left) and two sub-periods: October 2019 - February 2020 (middle) and March 2019 - July 2020 (right). Left panels show the e-suite analysis and forecast, the middle and right panels show the e-suite and associated control run. The e-suite analysis and forecast show very similar bias and correlation results. The middle and right top panels show that the bias in the low troposphere is mostly smaller in the second sub-period as compared to the first sub-period for both the e-suite analysis and control run. The MNMB is smaller for the control run than for the e-suite analysis at all levels for the second sub-period, and in particular from the mid to upper troposphere. The e-suite analysis and control run present rather similar correlation coefficients, with significantly better results in the low troposphere for the second sub-period.

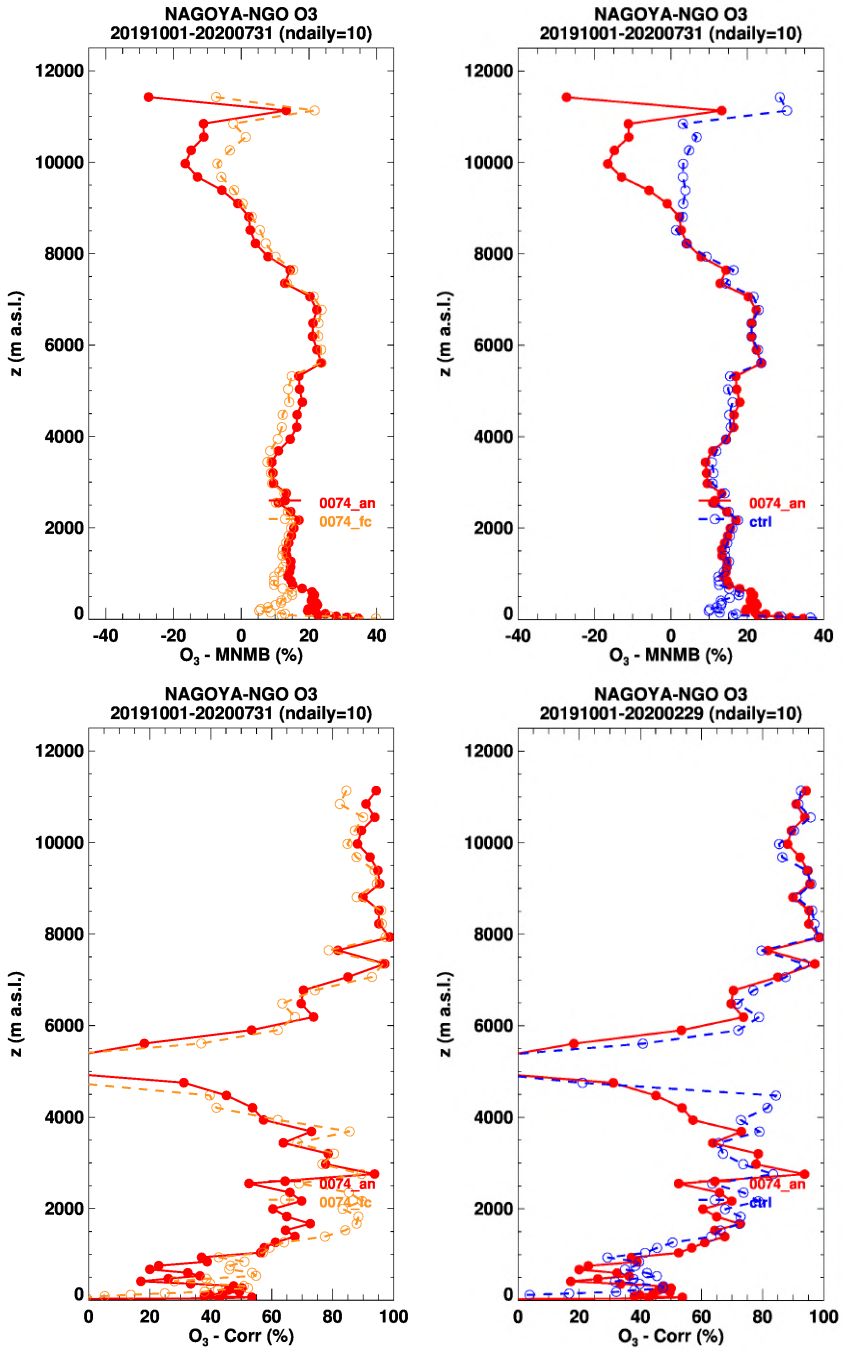

Fig. 2.5.6: Profile of MNMB and Correlation coefficient for ozone at Nagoya where observations are available only until February 2020. Left panels show the e-suite analysis and forecast, the middle and right panels show the e-suite and associated control run. The MNMB and correlation coefficient are similar for all configurations. The same is found at Shanghai (Fig. 2.5.7) where observations are available during the second sub-period as defined in Fig. 2.5.5.

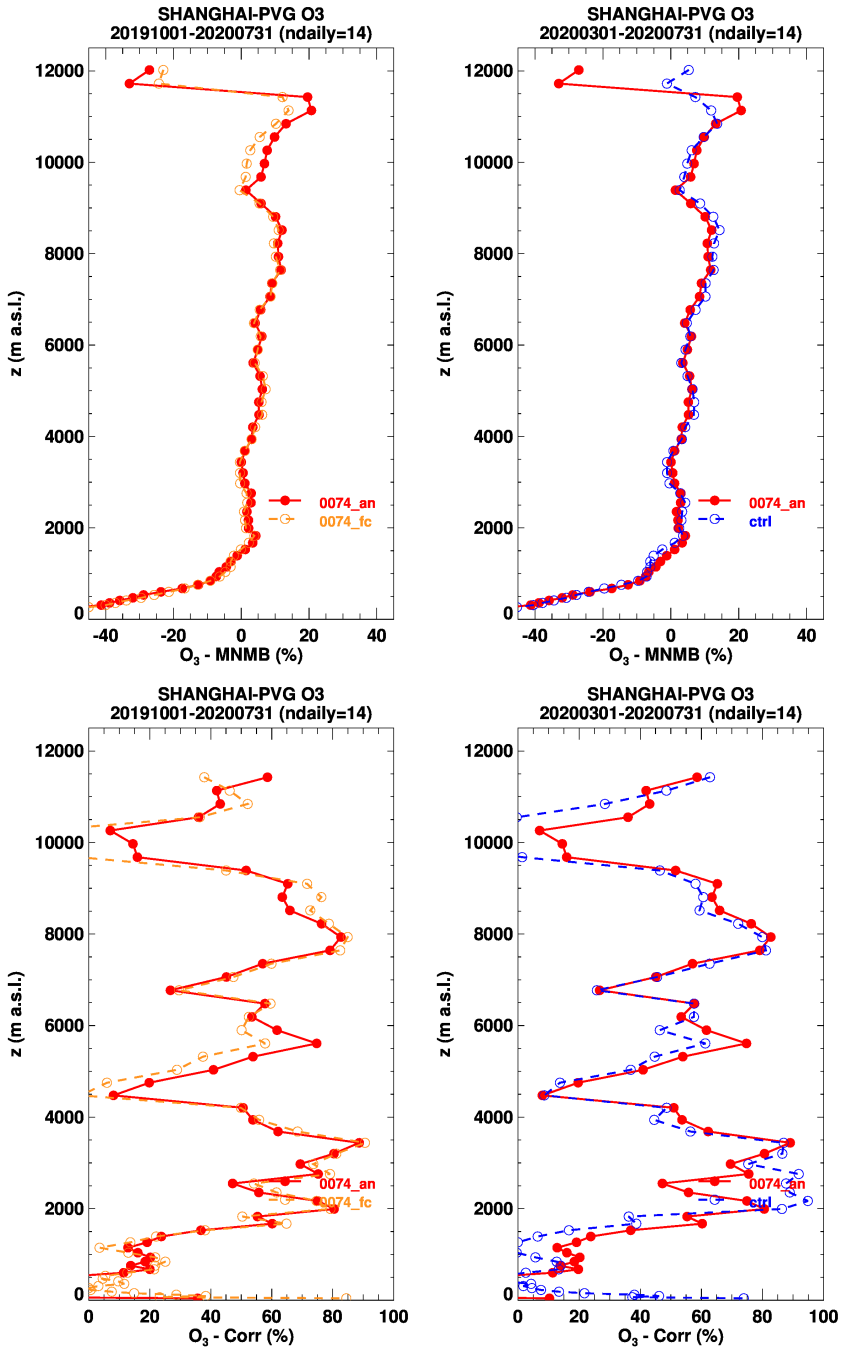

Fig. 2.5.7: Profile of MNMB and Correlation coefficient for ozone at Shanghai where ozone observations are available only starting from May 2020. Left panels show the e-suite analysis and forecast, the middle and right panels show the e-suite and associated control run. MNMB and correlation coefficient present similar results for all models (see also Fig. 2.5.2 for East Asia). The same is found at Nagoya where observations are available during the first sub-period as defined in Fig. 2.5.5 (see Fig. 2.5.6).

2.6 Verification of surface ozone in Europe

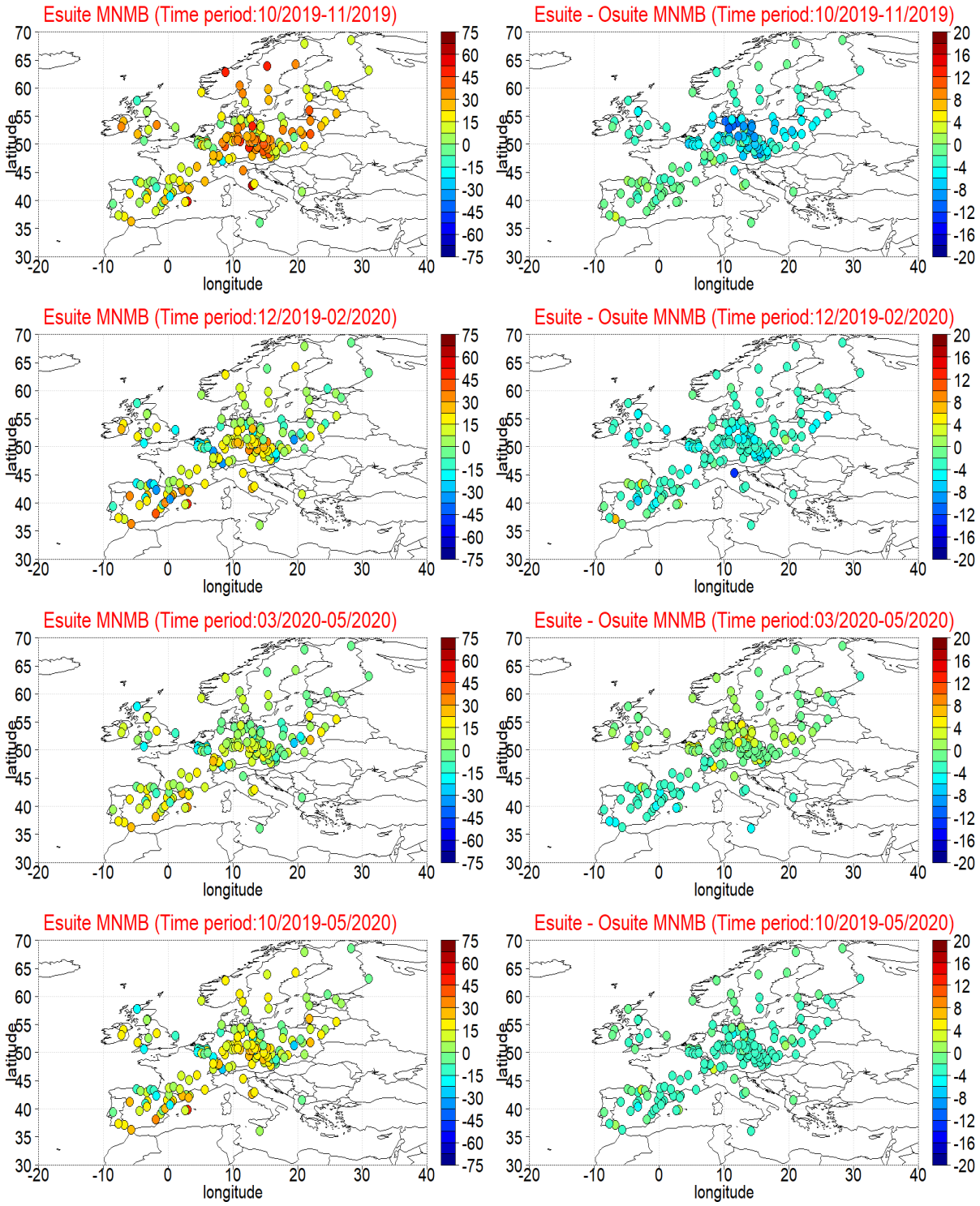

Fig. 2.6.1. Comparisons with Airbase surface ozone. Spatial distribution of e-suite relative bias (MNMB) in % (left) and the difference between e-suite and o-suite MNMB (right), during the periods: October-November 2019 (1st row), DJF 2019/2020 (2nd row), MAM 2020 (3rd row) and the whole period 1st October 2019-31 May 2020.The e-suite reduces the positive offset observed in the o-suite over central European stations.

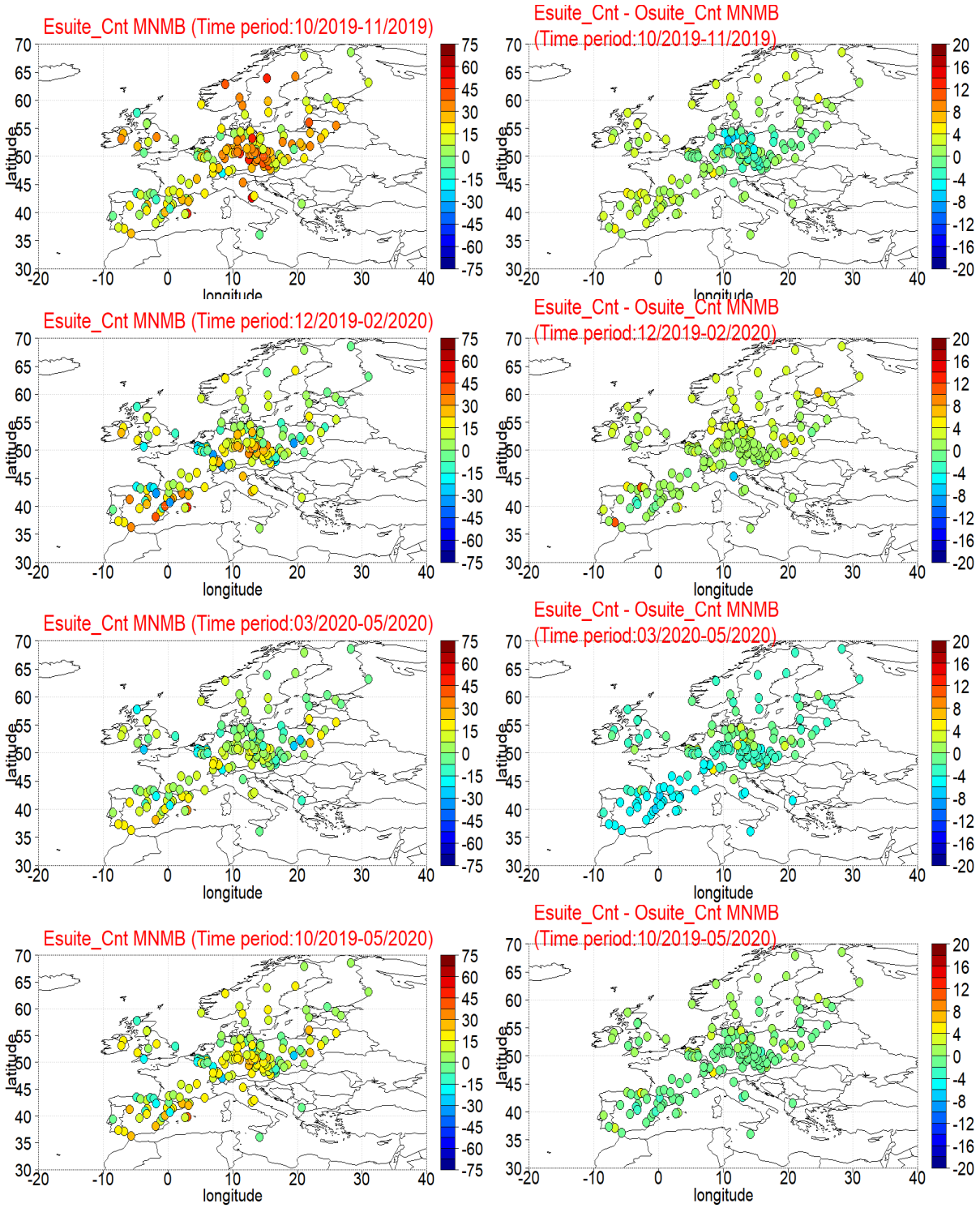

Fig. 2.6.2. Comparisons with Airbase surface ozone. Spatial distribution of e-control MNMB in % (left) and the difference between e-control and control MNMB (right) data during the periods: ON 2019 (1st row), DJF 2019/2020 (2nd row), MAM 2020 (3rd row) and the whole period 1st October 2019-31 May 2020.

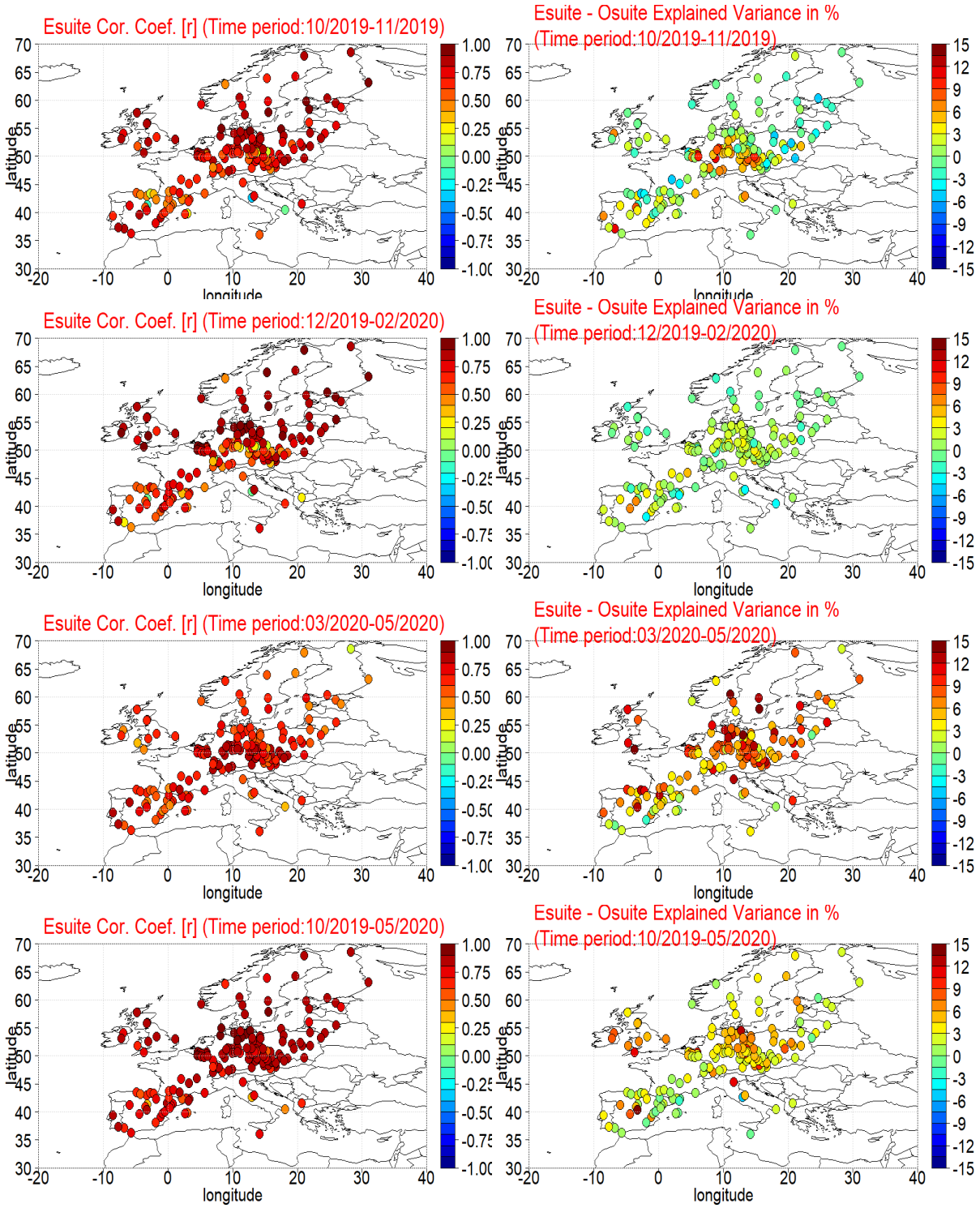

Fig. 2.6.3. Comparisons with Airbase surface ozone. Spatial distribution of e-suite correlation coefficient [r] (left) and the difference between e-suite and o-suite explained variance [%] (right) data during the periods: ON 2019 (1st row), DJF 2019/2020 (2nd row), MAM 2020 (3rd row) and the whole period 1st October 2019-31 May 2020. The e-suite reproduces better the day to day ozone variability, especially over the MAM 2020 period

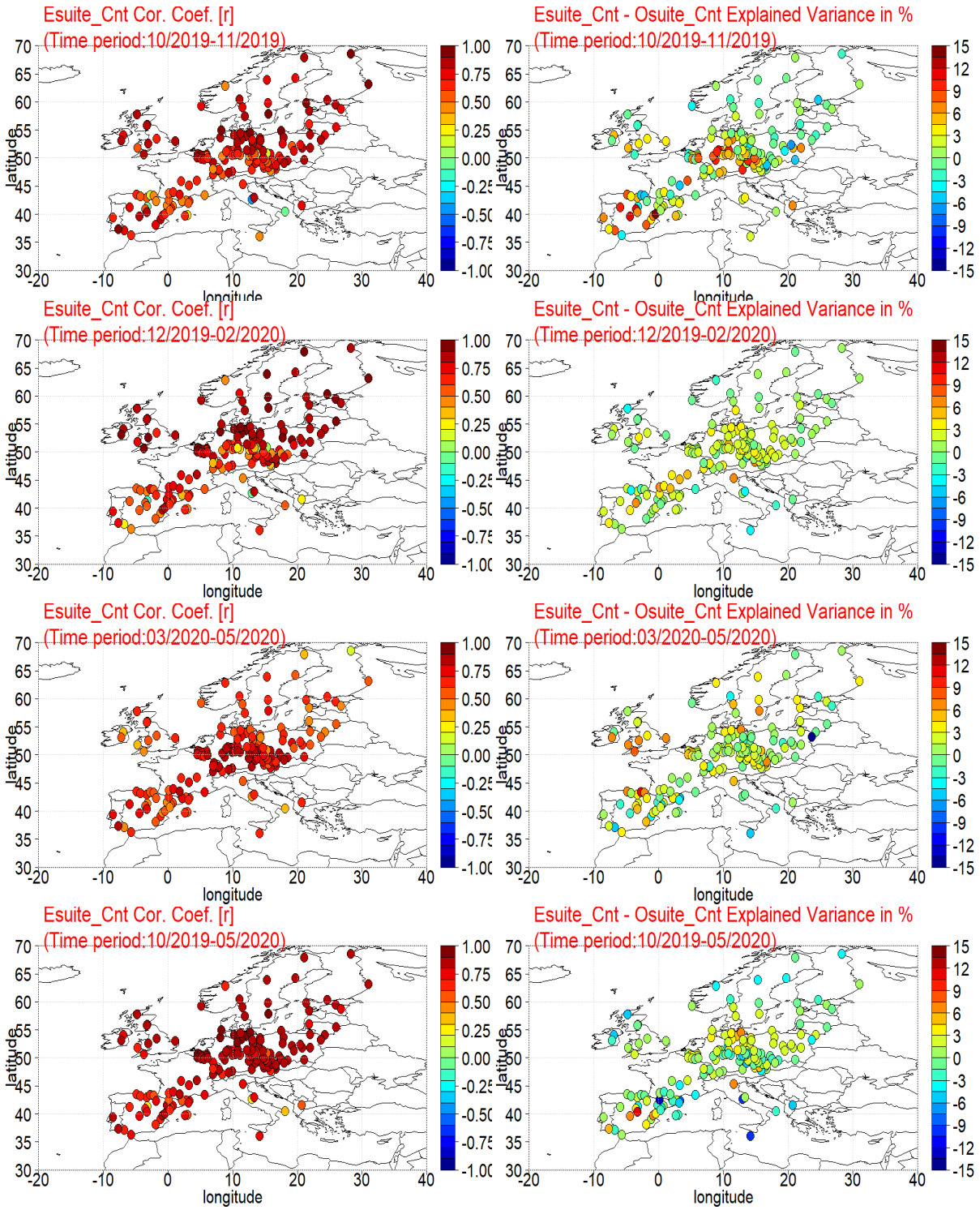

Fig. 2.6.4. Comparisons with Airbase surface ozone. Spatial distribution of e-control correlation coefficient [r] (left) and the difference between e-control and control explained variance [%] (right) data during the periods: ON 2019 (1st row), DJF 2019/2020 (2nd row), MAM 2020 (3rd row) and the whole period 1st October 2019-31 May 2020.

2.7 Verification with ozone surface data in the Arctic

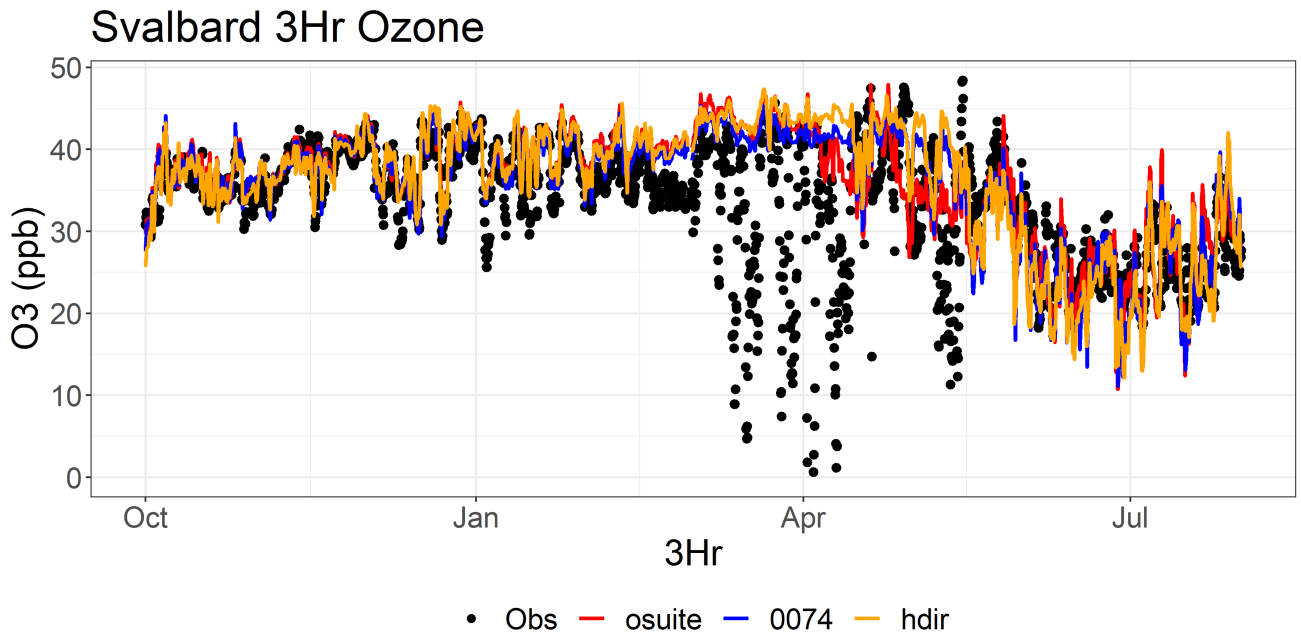

Fig. 2.7.1: Surface ozone concentrations at Zeppelin mountain, Svalbard (78.9oN 11.9oE). Low observed concentrations in March – May are due to halogen chemistry reactions not presently implemented in the CAMS simulations. The e-suite (blue) shows very similar results as the o-suite (red) and the control run (orange).

2.8 Ozone validation with IASI satellite observations

Note that the IASI sensitivity is the lowest over the cold surfaces of Antarctica and Greenland (especially during March-April-May season) where IASI O_3 values are positively biased up to 20%. The highest IASI sensitivity is in the northern mid-latitudes during summer (Boynard et al., 2018). Overall, the IASI ozone total column global mean bias is within 2 %.

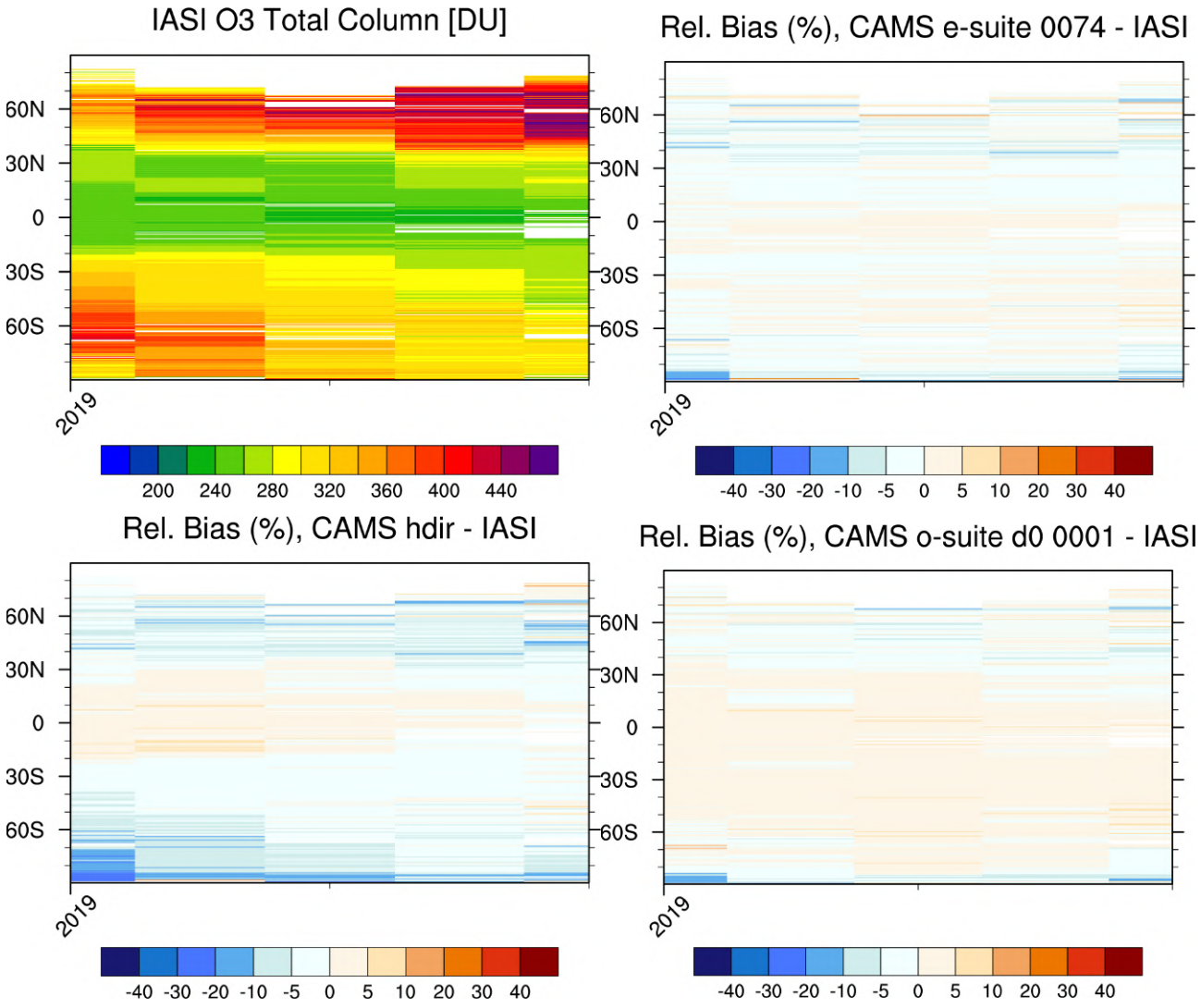

Fig. 2.8.1: IASI Metop-A ozone total column (daytime), in Dobson units (DU), as a function of latitude and time (top) from October 2019 – February 2020. Relative difference (in %) with CAMS e-suite d0 0074 (top-right), CAMS o-suite d0 0001 (bottom-right) and ctrl d0 hdir (bottom-left). In comparison with IASI ozone, the new e-suite performs equally well as the CAMS o-suite in early 2020.

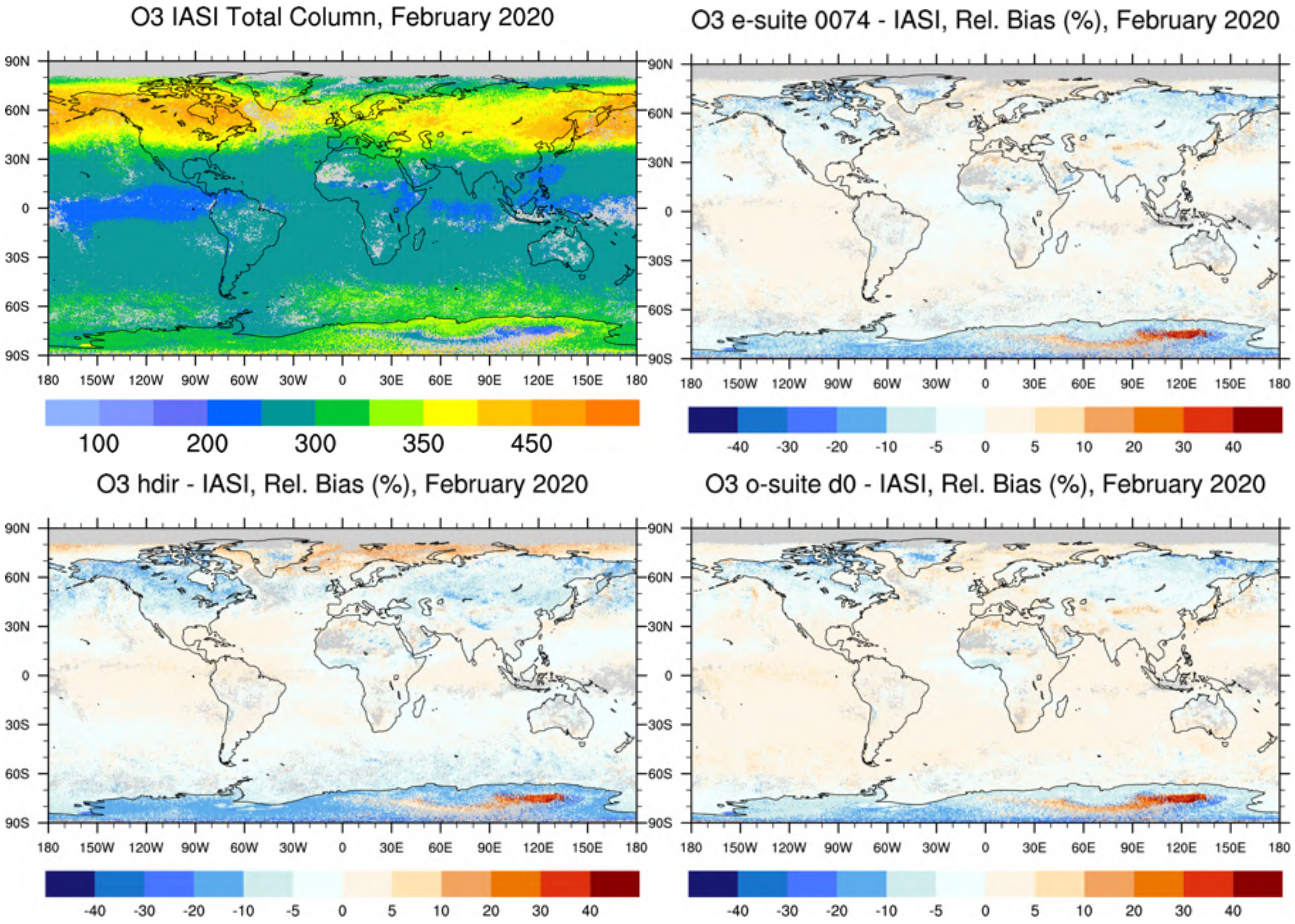

Fig. 2.8.2: Ozone total column for IASI Metop-A daytime satellite observations (top-left) and relative difference with CAMS e-suite d0 (top-right), CAMS o-suite d0 0001 (bottom-right) and ctrl d0 hdir (bottom-left) for February 2020.

2.9 CO validation with Global Atmosphere Watch (GAW) Surface Observations

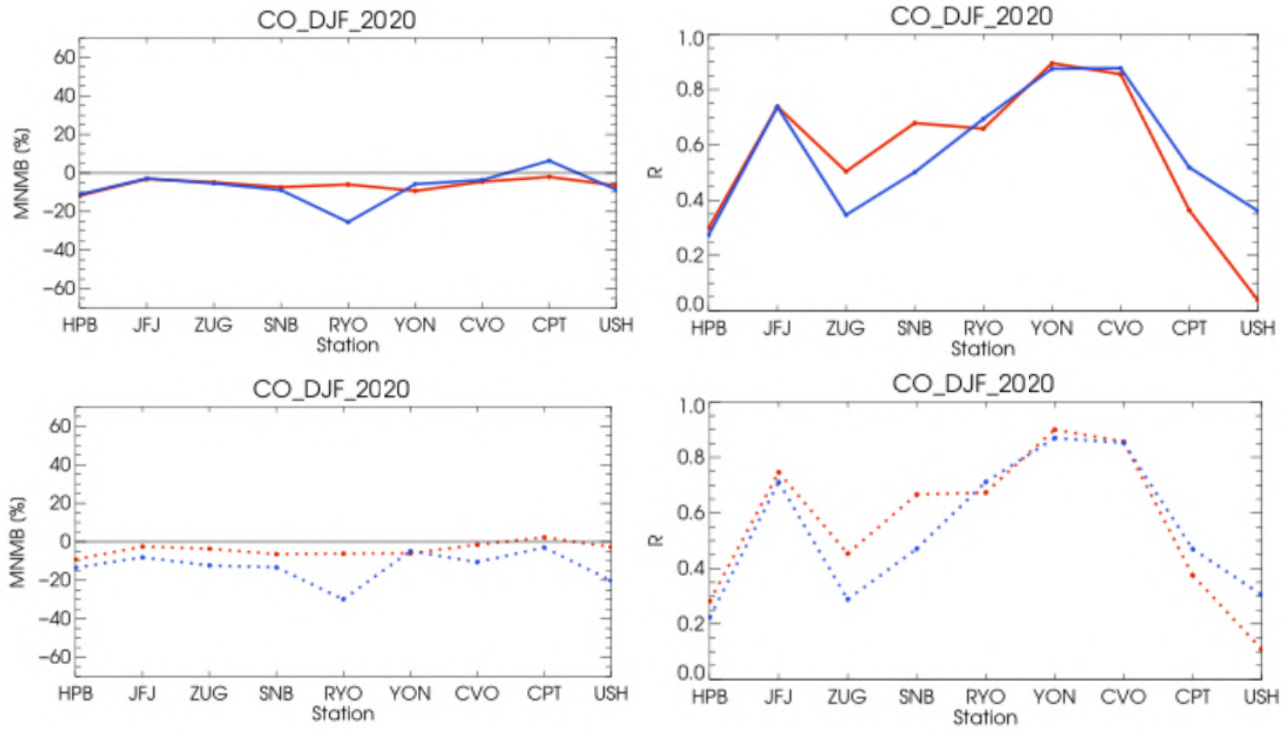

Fig. 2.9.1: Comparison against surface CO in-situ observations at GAW stations: MNMB (left) and correlation coefficient (right) of e-suite and o-suite for the period December 2019 / February 2020. Upper panel are for the o-suite and control, lower panel e-suite and e-control. The e-suite performs very similar to the o-suite.

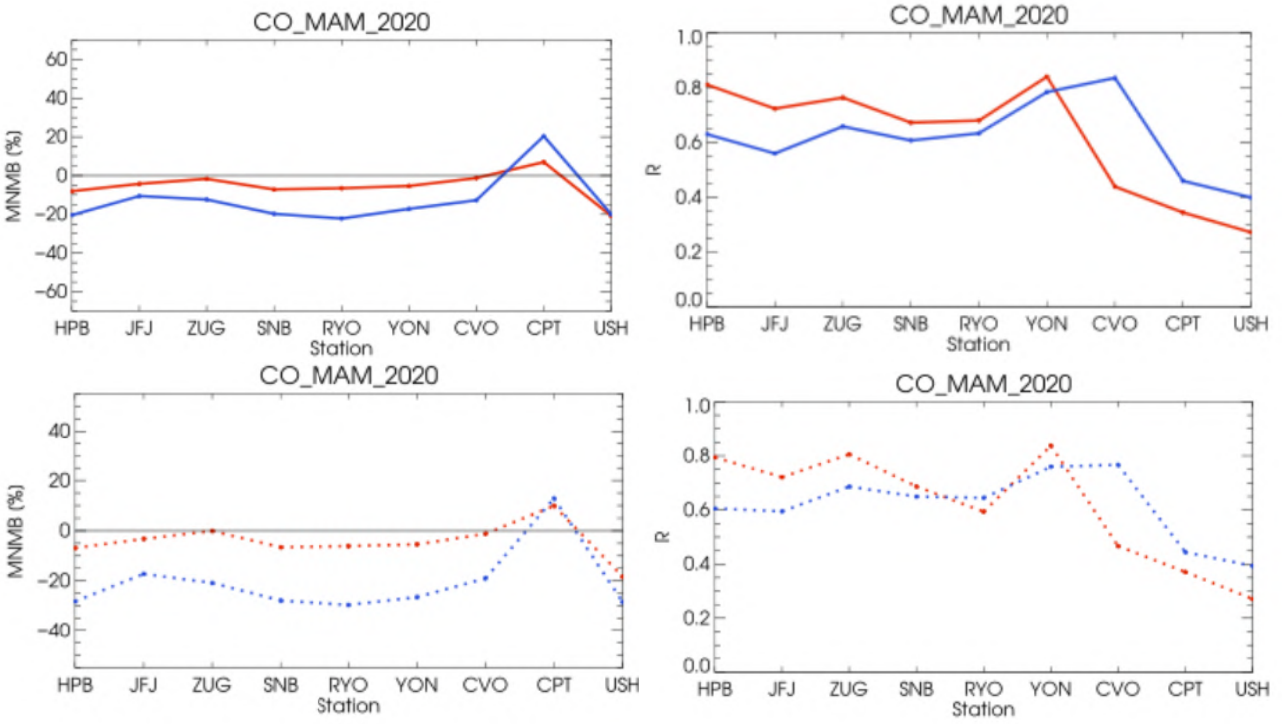

Fig. 2.9.2: Same as Fig. 2.9.1, but for the period March-May 2020.

2.10 CO validation with IAGOS Aircraft observations

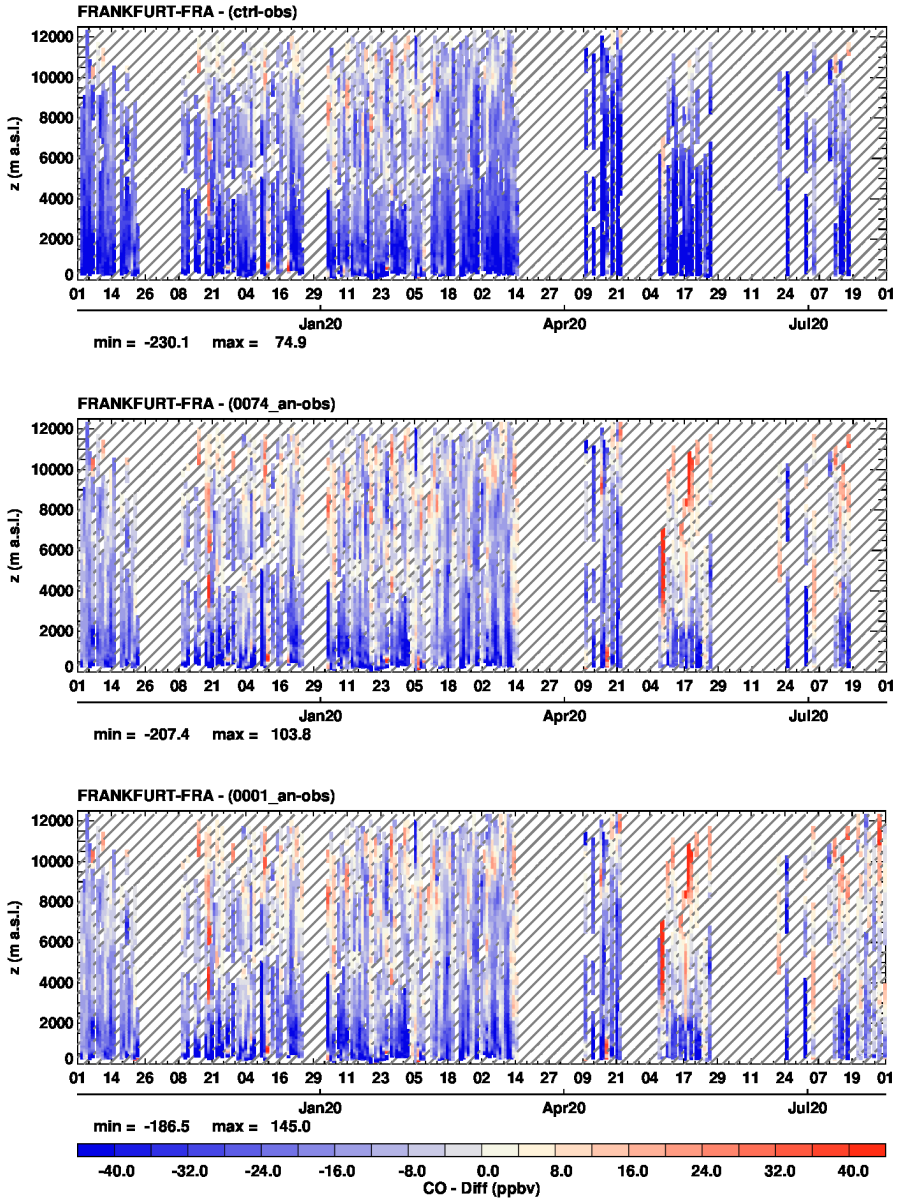

Fig. 2.10.1: Time series of the differences (model analysis minus IAGOS) in the daily profiles of CO at Frankfurt during October 2019 -July 2020. The top and centre panel are for the e-suite (0074) control run and analysis respectively and the bottom panel is for the o-suite (0001) analysis. The e-suite behaviour is very similar to that of the o-suite. Large differences are found between the assimilated run of the e-suite and associated control run which present much larger bias in the low to mid-troposphere. The time series for the e-suite forecast are not shown here but are very similar to the results for the e-suite analysis (see also Fig. 2.10.2 and 2.10.3).

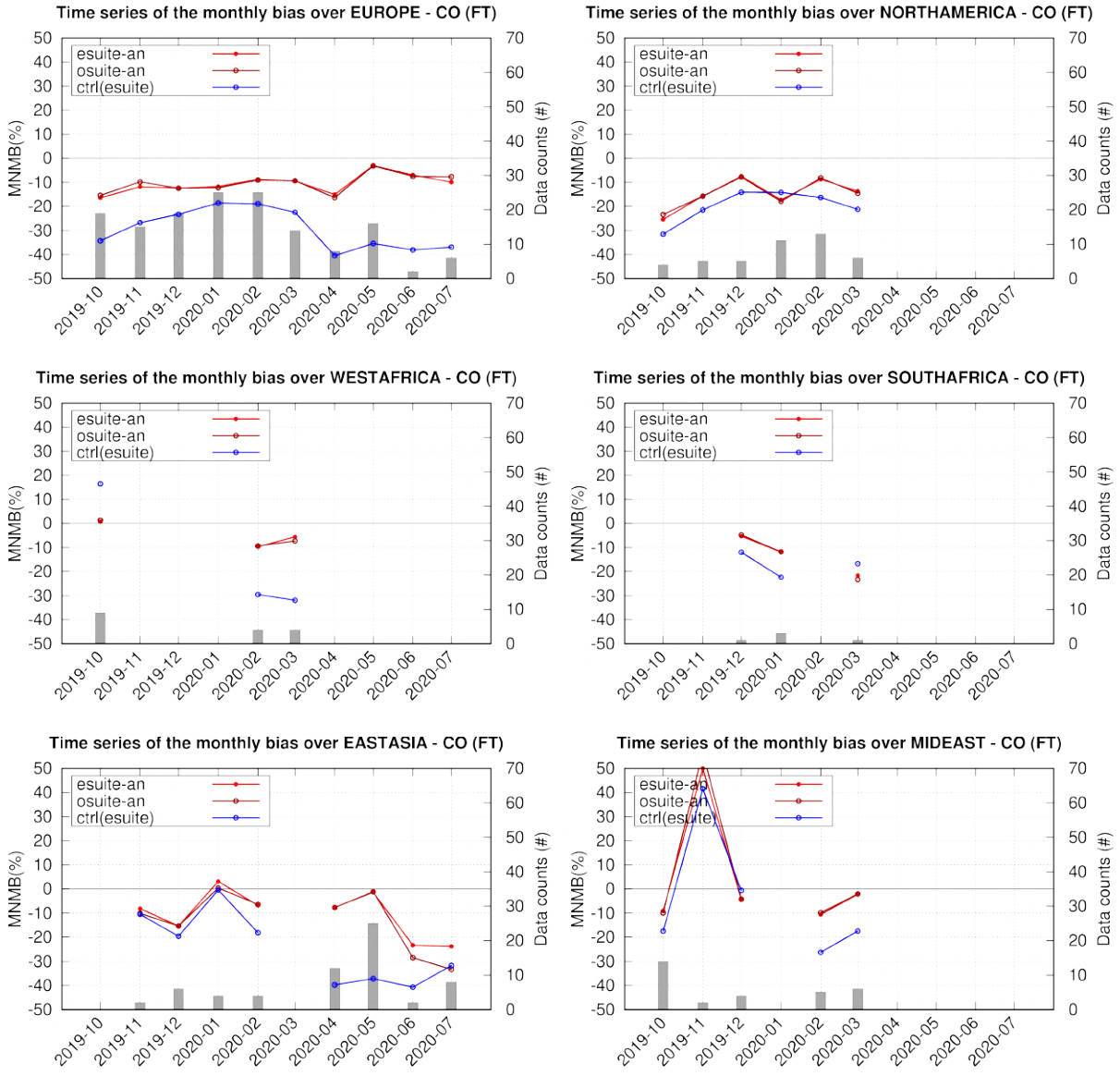

Fig. 2.10.2: Time series of monthly MNMB from e-suite 0074 (light red, empty circles) and o-suite 0001 (dark red, filled circle) for CO in the free troposphere (FT) between October 2019 and July 2020 in 6 regions (Top left: Europe, top right: North America, middle left: Western Africa, middle right: Southern Africa, bottom left: Eastern Asia, bottom right: Middle East). The histogram bars indicate the number of profiles (i.e. layer values) based on available observations. The results from the e-suite and o-suite are very similar except over East Asia in the last two months of the evaluation period where the e-suite performs better than the o-suite. The e-suite run always presents a smaller bias than the associated control run except for some months with very poor sampling. For CO over Europe the differences in the e-suite runs and e-suite control appear more pronounced starting from March until the end of the evaluation period (see also Fig. 2.10.5). The bias from the assimilated run remains roughly stable while the bias from control run increases largely. A similar behaviour is also found over East Asia for CO (see also Fig. 2.10.6 and 2.10.7), but the differences vanish at the end of the period. Over West and South Africa and the Middle East no conclusions can be drawn on these differences between the e-suite runs with and without assimilation due to poor sampling throughout the evaluation period.

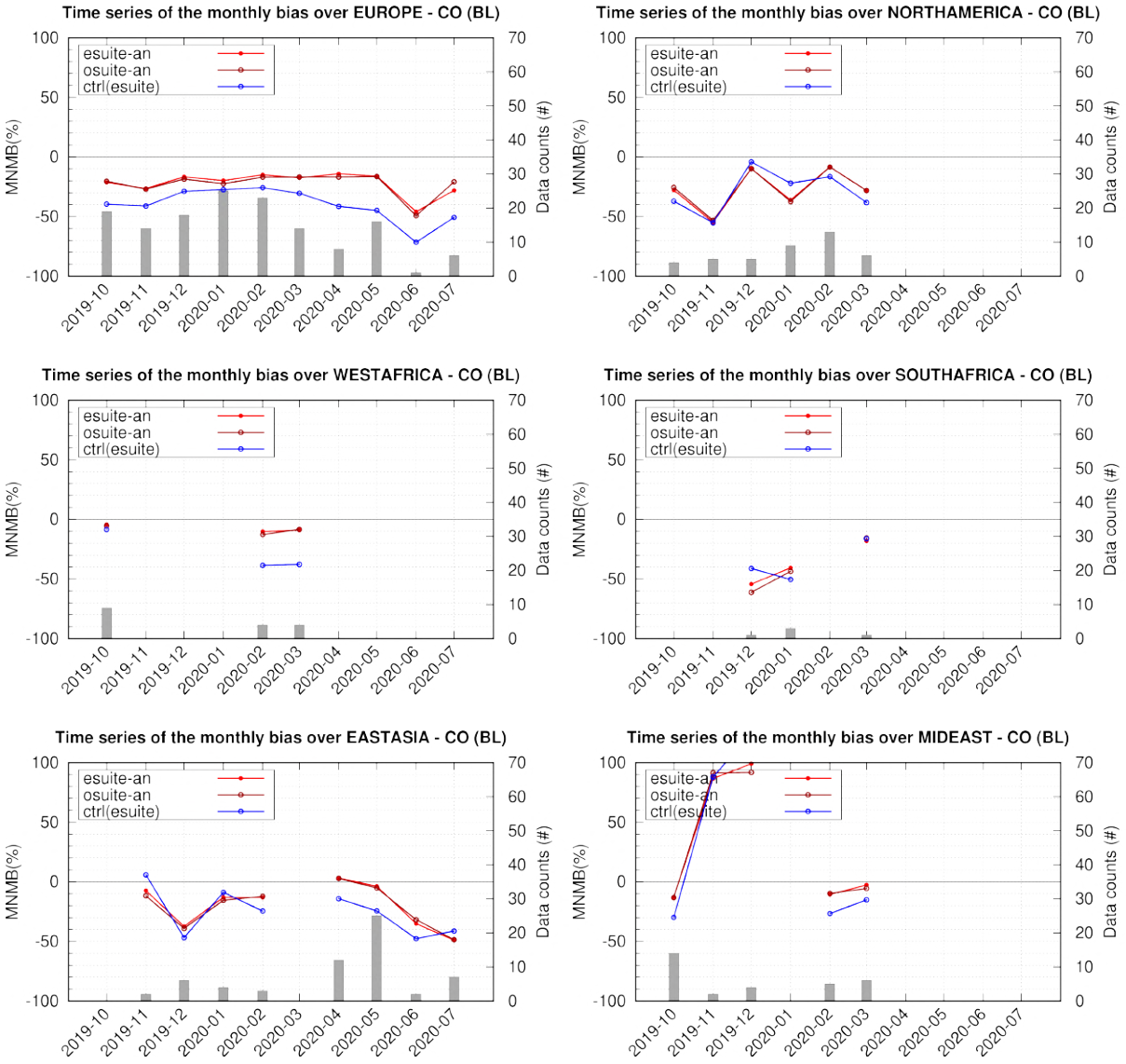

Fig. 2.10.3: Time series of monthly MNMB from e-suite 0074 (light red, empty circles) and o-suite 0001 (dark red, filled circle) for CO in the Boundary Layer (BL) between October 2019 and July 2020 in 6 regions (Top left: Europe, top right: North America, middle left: Western Africa, middle right: Southern Africa, bottom left: Eastern Asia, bottom right: Middle East). The histogram bars indicate the number of profiles (i.e. layer values) based on available observations. In general, the differences between the models in the boundary layer are similar to what is found for the Free Troposphere (Fig. 2.10.2), however the degradation of the bias from control run starting in March observed for Europe and East Asia is less pronounced than in the Free Troposphere.

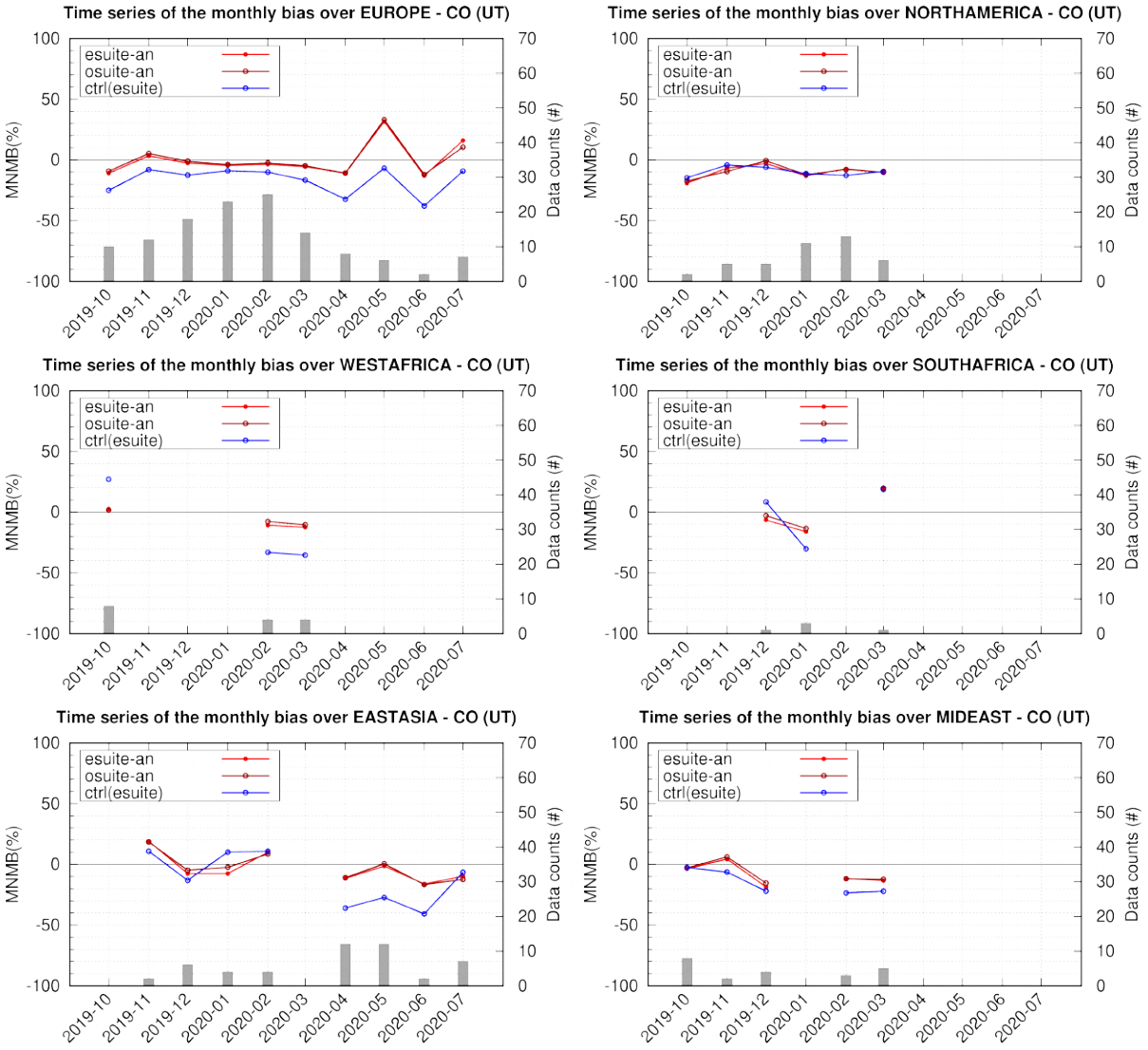

Fig. 2.10.4: Time series of monthly MNMB from e-suite 0074 (light red, empty circles) and o-suite 0001 (dark red, filled circle) for CO in the Upper Troposphere (UT) between October 2019 and July 2020 in 6 regions (Top left: Europe, top right: North America, middle left: Western Africa, middle right: Southern Africa, bottom left: Eastern Asia, bottom right: Middle East). The histogram bars indicate the number of profiles (i.e. layer values) based on available observations. Like for the Boundary Layer, the differences between the models are similar to what is found for the Free Troposphere (Fig. 2.10.2 and 2.10.3), again with less pronounced degradation of the bias than in the Free Troposphere over Europe and East Asia from March on.

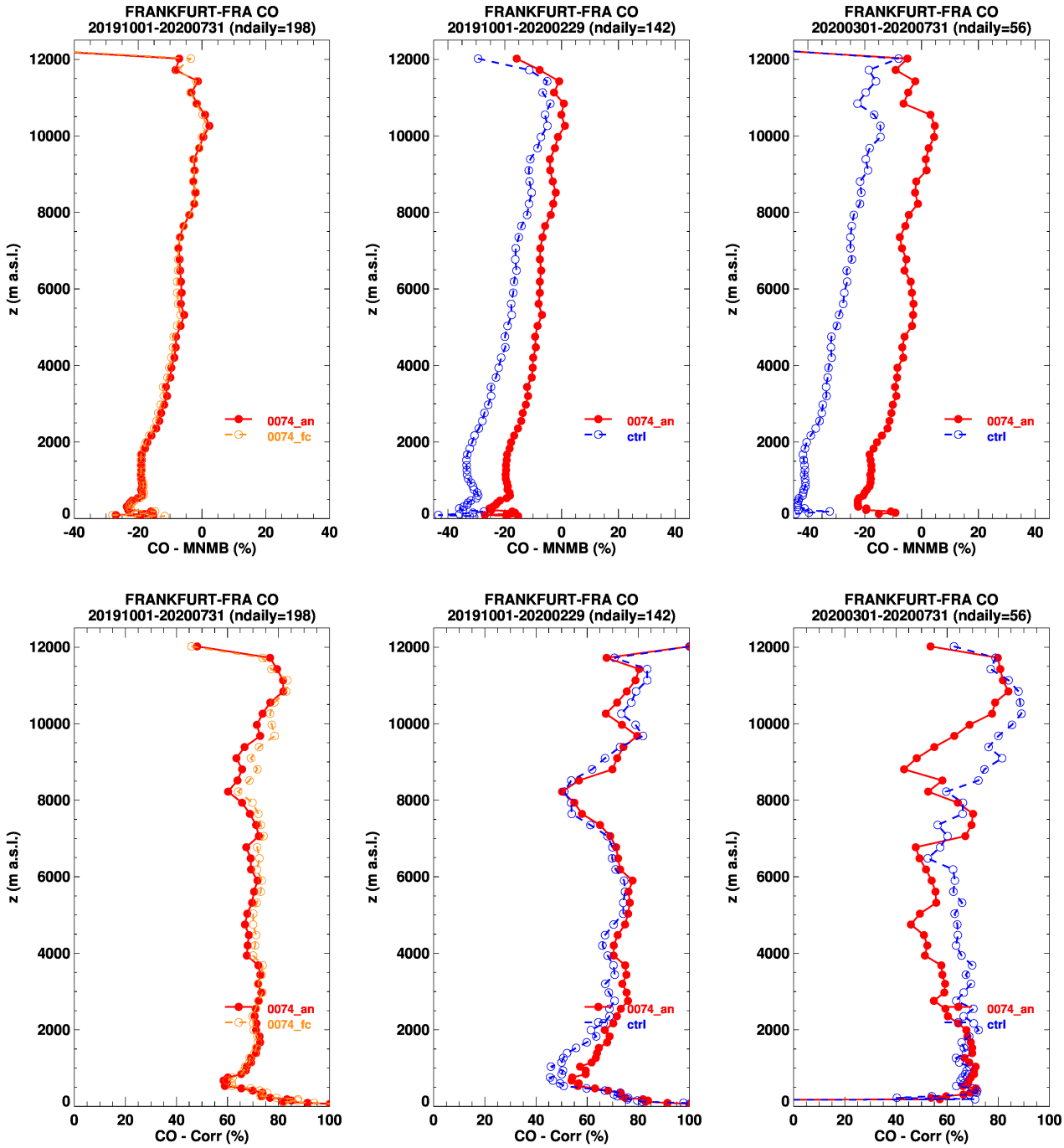

Fig. 2.10.5: Profile of MNMB and Correlation coefficient for CO at Frankfurt. Results are presented for three periods, the full evaluation period October 2019 - July 2020 (left) and two sub-periods: October 2019 - February 2020 (middle) and March 2019 - July 2020 (right). Left panels show the e-suite analysis and forecast, the middle and right panels show the e-suite and associated control run. The e-suite analysis and forecast present a very similar bias and correlation as shown in the left panels. The middle and right panels show that both bias and correlation show differences between the sub-periods before and after March 2020. On average the bias at all levels increases significantly for the control run in the second period. For the correlation coefficient, it is slightly higher in the mid to upper troposphere for control run than for the e-suite analysis in the second period, while the results are rather similar for both runs in the first period.

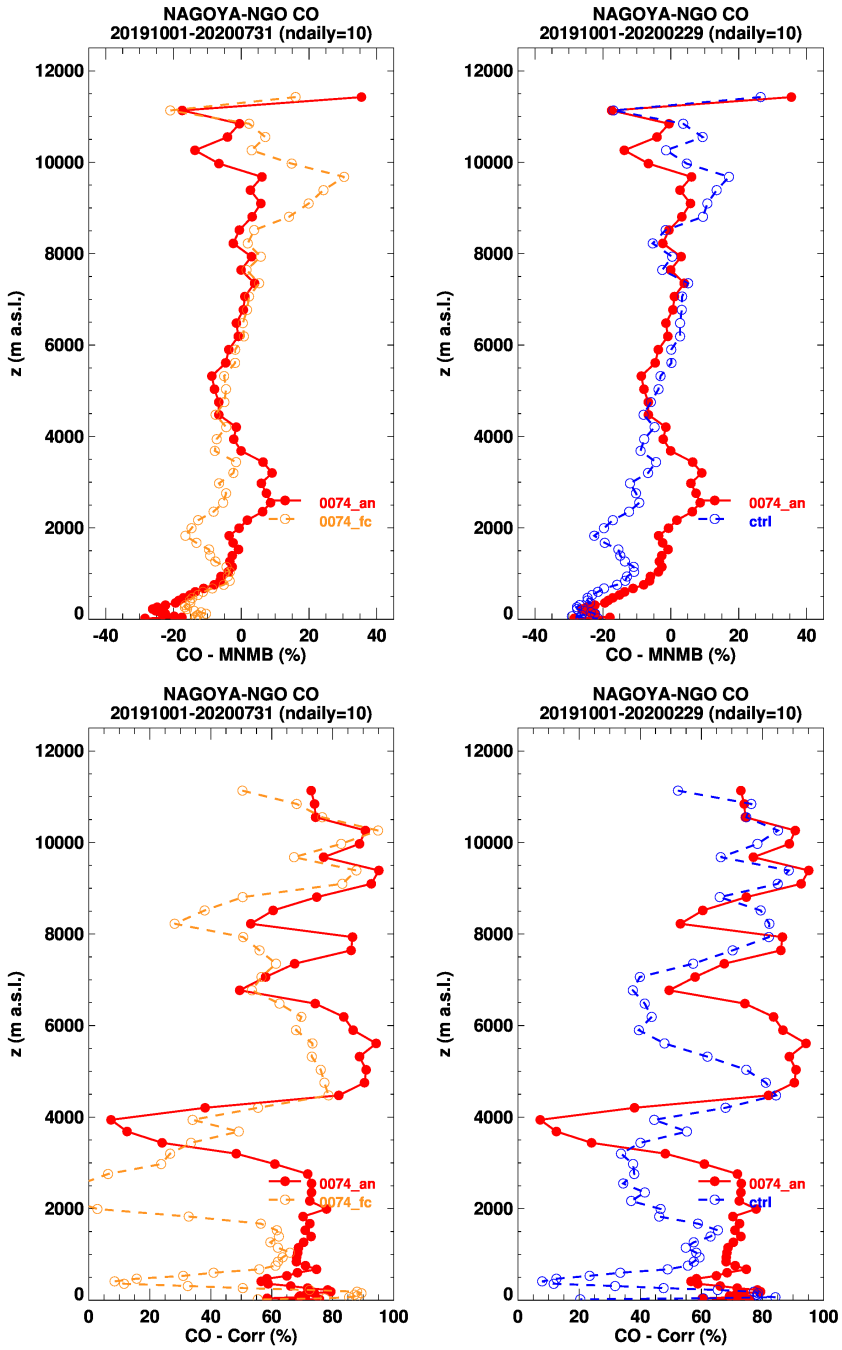

Fig. 2.10.6: Profile of MNMB and Correlation coefficient for CO at Nagoya where observations are available only until February 2020. Left panels show the e-suite analysis and forecast, the middle and right panels show the e-suite and associated control run. Unlike for Europe, some differences are found in MNMB and correlation coefficient between analysis and forecast from the e-suite at Shanghai, with better performances from the analysis.

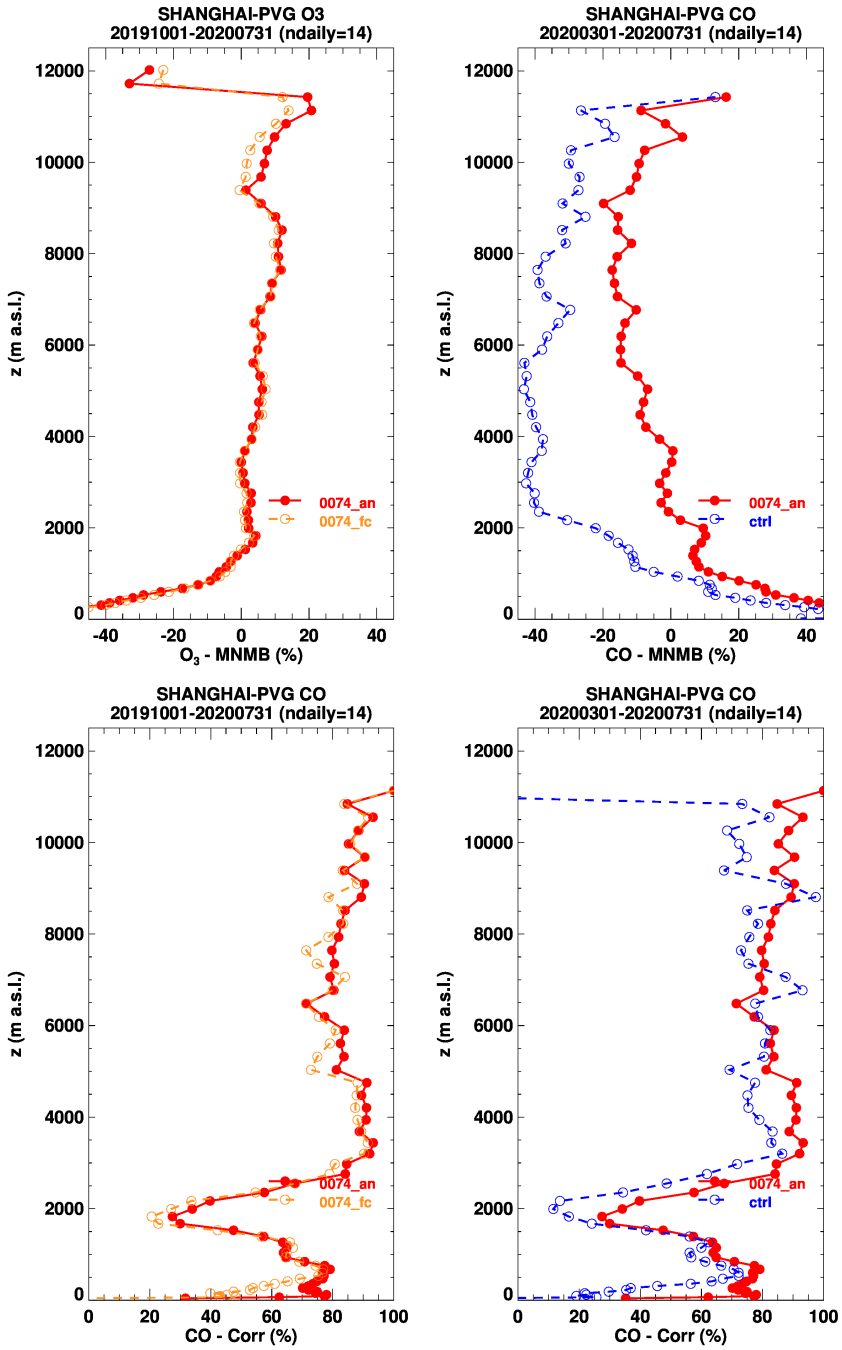

Fig. 2.10.7: Profile of MNMB and Correlation coefficient for CO at Shanghai where CO observations are available only starting from April 2020. Left panels show the e-suite analysis and forecast, the middle and right panels show the e-suite and associated control run. Unlike in Shanghai and similarly to Europe, the results from the e-suite analysis and forecast are very similar. The bias at Shanghai is much larger than at Nagoya (see Fig. 2.10.6), however this might not be related to the airport location but to the aforementioned increase of the bias from control run in the second half of the evaluation period, as this effect is also noted at other location over East Asia (Shanghai and Nagoya being the East Asia airports with the highest number of observations during the entire period) as well as over Europe (Fig. 2.10.5).

2.11 Comparisons with MOPITTv8 CO data

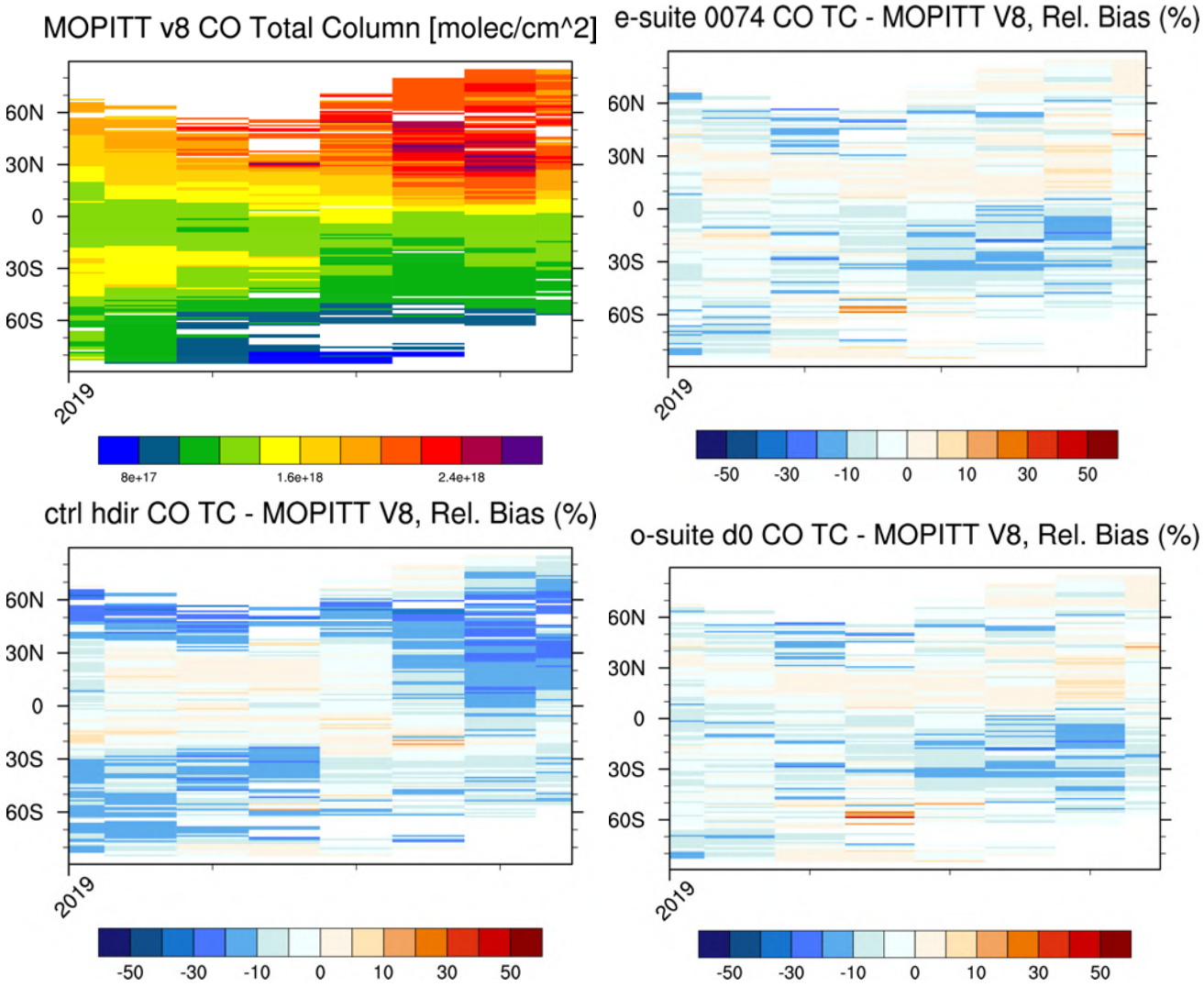

Fig. 2.11.1: MOPITT V8 CO total column as a function of latitude and time (top-left), from October 2019 till May 2020. Relative difference (in %) with CAMS e-suite 0074 d0 (top-right), CAMS o-suite 0001 d0 (bottom-right) and control hdir (bottom-left). In general, the o-suite and e-suite are very similar and agree very well with MOPITT. The control run shows higher negative bias, especially over the SH during autumn/winter (up to 30%) and over the NH during spring (up to 40%).

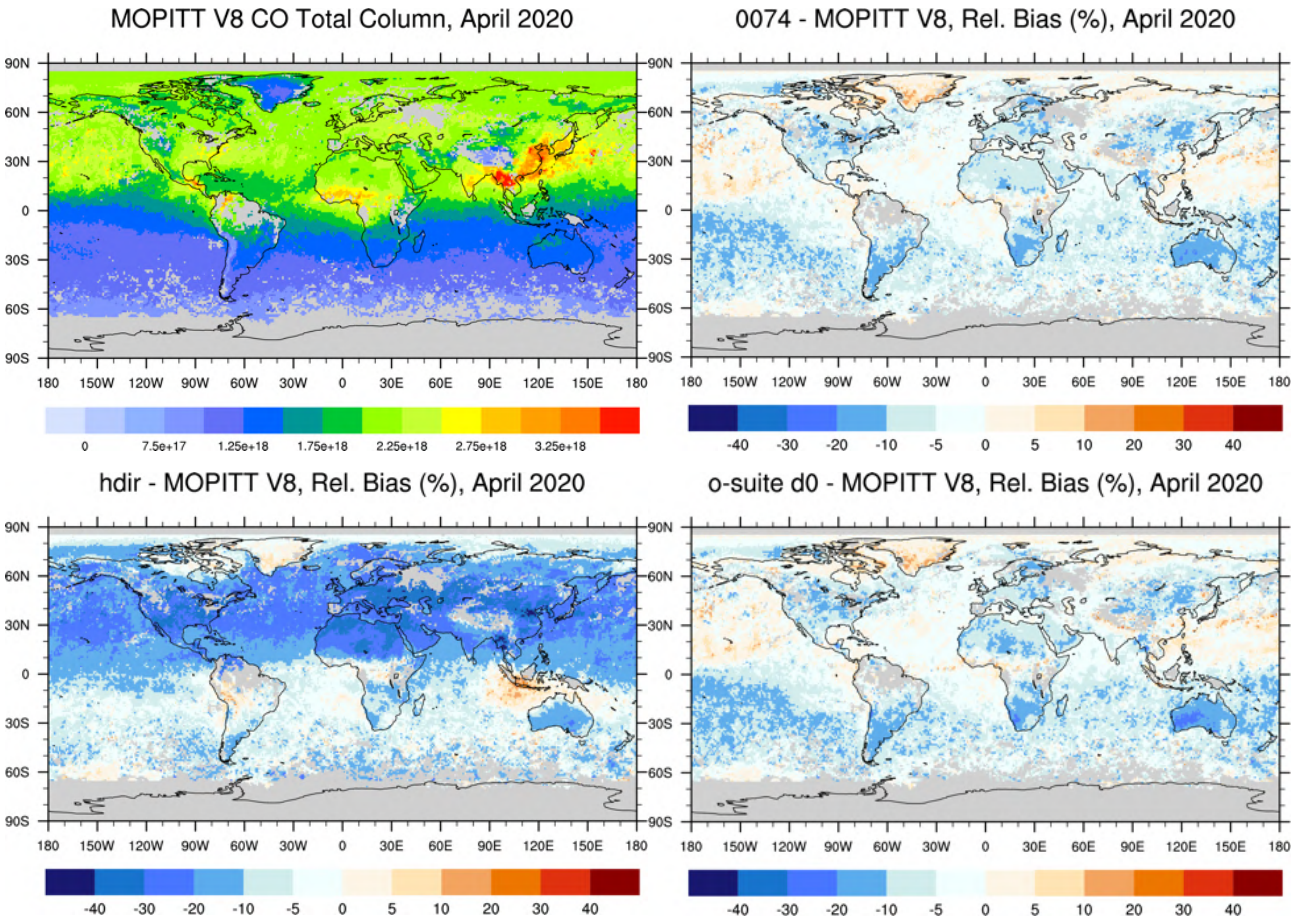

Fig. 2.11.2: Map of MOPITT CO total column (top-left) and relative difference (in %) with CAMS e-suite d0 (top-right), control run (bottom-left) and o-suite (bottom-right) for April 2020. In general, the o-suite and e-suite are very similar and agree very well with MOPITT. The control run shows higher negative bias, especially over the NH during spring (up to 40%).

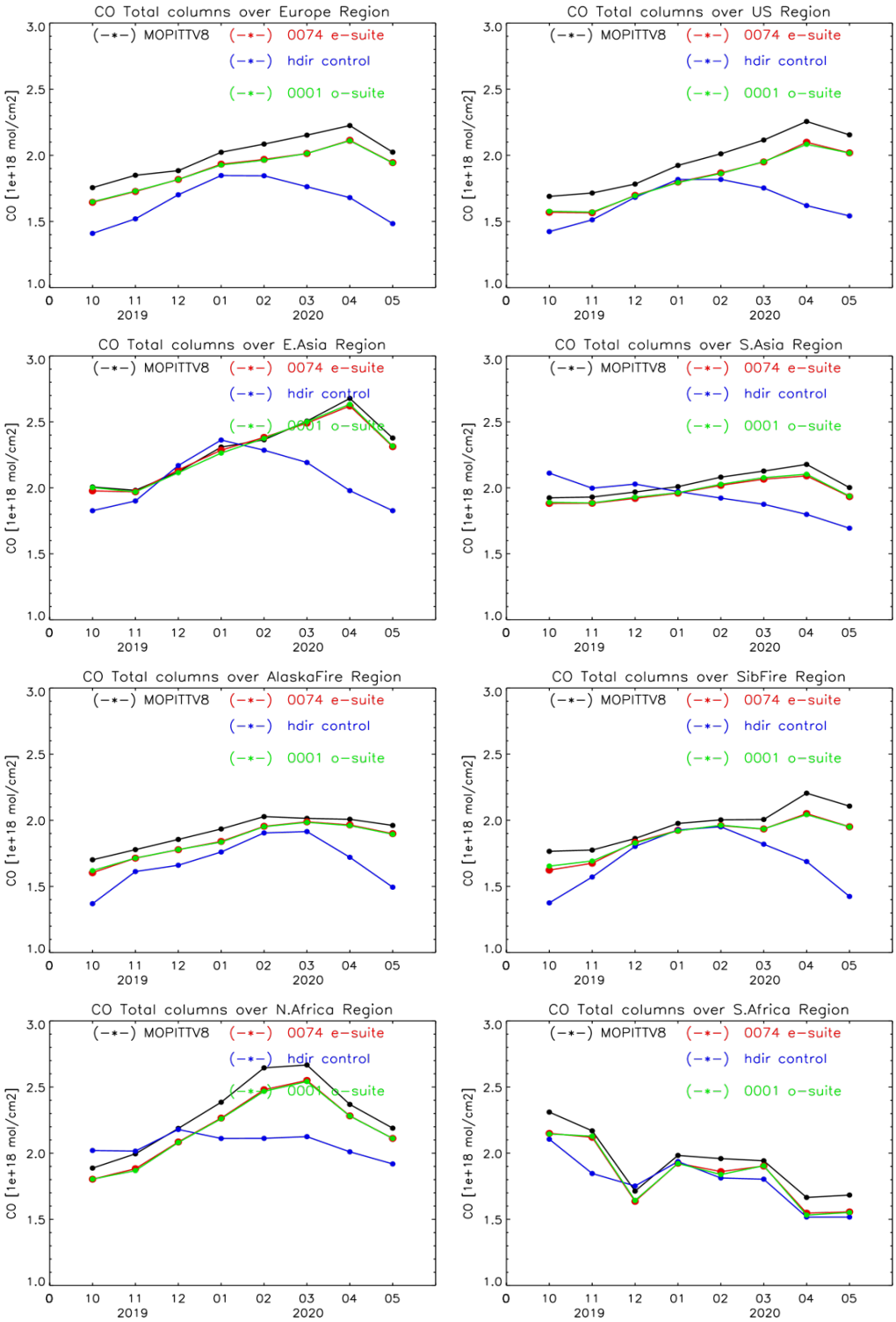

Fig. 2.11.3: Time series of CO total columns for MOPITT V8 and the model runs over the selected regions: e-suite 0074 (red, solid), control hdir (blue, solid), o-suite (green, solid). Period: October 2019 – May 2020. The e-suite is in very good agreement with the observations with a bias less than 10% and very similar to o-suite. The control run shows bigger negative bias especially during the spring season over most of the regions (except south African region).

2.12 CO validation with NDACC and TCCON surface remote-sensing observations

In order to understand the NDACC and TCCON results, it is important to mention that there is an overall bias between NDACC and TCCON of approximately 6%, where TCCON is biased low compared to NDACC .

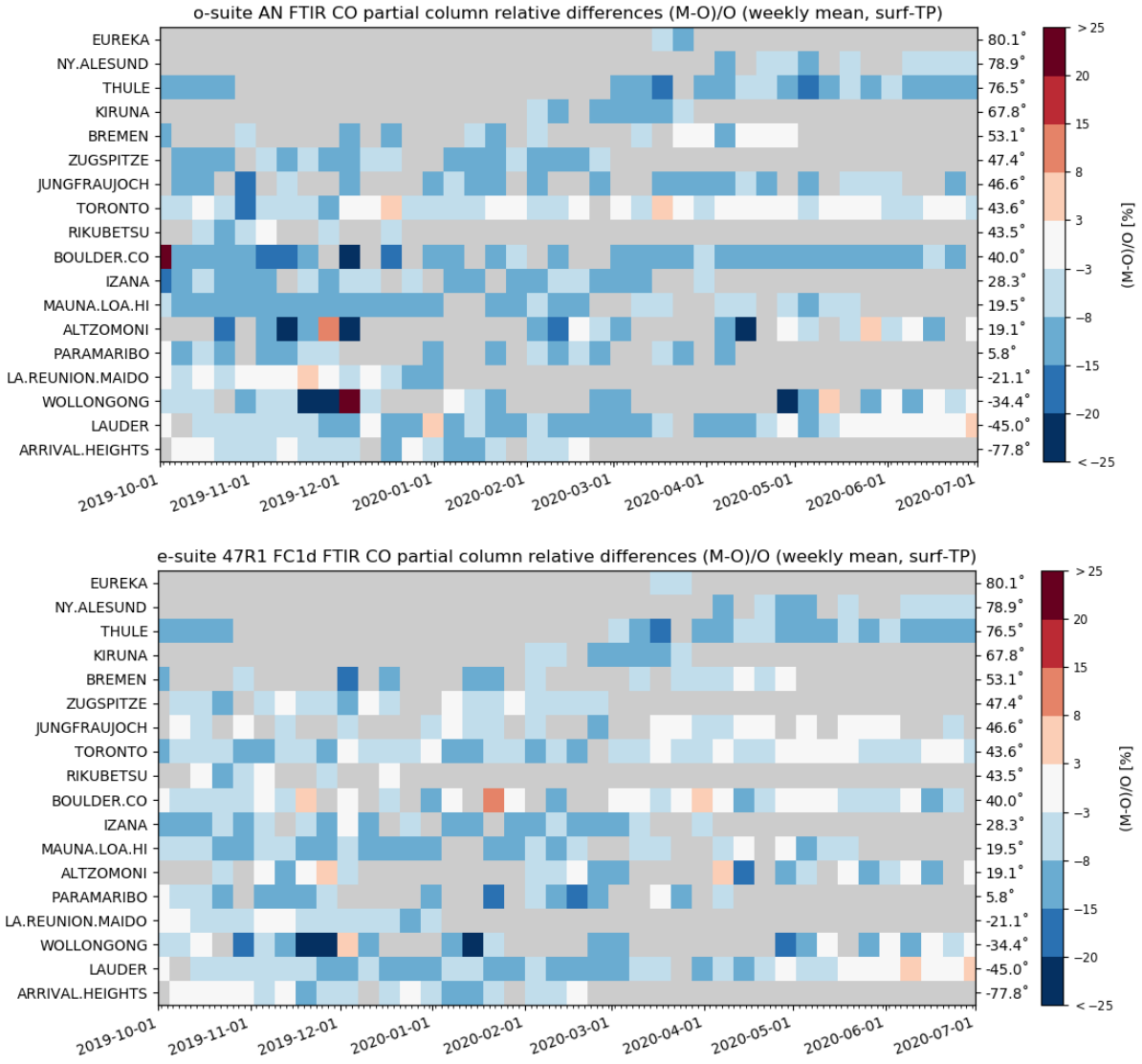

Fig. 2.12.1.: Relative weekly mean bias for tropospheric NDACC CO columns (MB, %) for the period October 2019-June 2020 for the 1d FC o-suite (top) and e-suite (bottom). The overall uncertainty for the CO measurements is approximately 3%. Stations are sorted with decreasing latitude (northern to southern hemisphere). The overall bias has slightly decreased in the e-suite.

	o-suite analysis					e-suite analysis					
NDACC troposphere	#	rel. std	Correlation	rel diff bias(%)	rel diff std(%)	#	rel. std	Correlation	rel diff bias(%)	rel diff std(%)	lat
EUREKA	6	0.7	0.93	-7.61	4.25	6	0.7	0.93	-6.88	4.07	80.1
NY.ALESUND	12	1.2	0.99	-6.78	3.09	12	1.2	0.99	-6.47	3.04	78.9
THULE	71	1.1	0.97	-9.93	3.46	71	1.1	0.98	-9.6	3.37	76.5
KIRUNA	17	1	0.92	-9.9	3.35	17	1	0.93	-9.44	3.23	67.8
BREMEN	22	0.8	0.93	-4.72	5.23	22	0.8	0.93	-4.51	4.96	53.1
ZUGSPITZE	49	0.9	0.91	-10.04	4.33	49	0.9	0.91	-10.27	4.24	47.4
JUNGFRAUJOCH	54	0.9	0.91	-10.44	4.73	54	0.9	0.92	-9.51	4.83	46.6
TORONTO	105	0.8	0.88	-2.99	5.32	105	0.9	0.88	-3.31	5.3	43.6
RIKUBETSU	8	0.9	0.89	-5.49	4.17	8	1	0.9	-5.86	3.86	43.5
BOULDER.CO	89	0.9	0.86	-11.78	7.22	89	1	0.94	-12.34	4.61	40
IZANA	39	1	0.88	-9.68	3.82	39	1.1	0.9	-9.46	3.59	28.3
MAUNA.LOA.HI	86	1	0.98	-9.15	3.56	86	1	0.98	-8.28	3.41	19.5
ALTZOMONI	49	0.9	0.83	-7.63	10.04	49	0.9	0.82	-6	10.91	19.1
PARAMARIBO	18	0.9	0.91	-8	3.55	18	0.9	0.91	-8.14	3.64	5.8
LA.REUNION.MAIDO	69	1	0.98	-2.74	4.02	69	0.9	0.98	-2.43	4.67	-21.1
WOLLONGONG	77	1.1	0.88	-6.25	14.77	77	1.4	0.91	-8.75	12.81	-34.4
LAUDER	121	1	0.93	-5.27	5.43	121	1.1	0.95	-5.69	5.04	-45
ARRIVAL.HEIGHTS	44	0.9	0.97	-4.71	2.99	44	0.9	0.96	-4.58	3.29	-77.8
		0.9	0.92	-7.4	5.19	--	1	0.93	-7.31	4.94	

Table 2.12.1 Overview of o-suite/e-suite analysis performance against the NDACC FTIR tropospheric CO column. The e-suite has a slightly improved overall bias and averaged correlation.

	o-suite analysis					e-suite analysis					
TCCON xCO	#	rel. std	Correlation	diff bias(ppb)	diff std(ppb)	#	rel. std	Correlation	diff bias(ppb)	diff std(ppb)	lat
EASTTROUTLAKE	78	1.1	0.88	-8.47	4.07	78	1.1	0.9	-8.1	3.68	54.3
KARLSRUHE	45	0.8	0.96	-1.3	3.65	45	0.8	0.95	-1.19	3.82	49.1
ORLEANS	71	0.9	0.91	1.49	3.9	71	0.9	0.91	1.85	3.9	48
GARMISCH	4	0.9	0.97	-3.22	0.97	4	0.9	0.97	-2.84	0.91	47.5
ZUGSPITZE	6	0.5	0.89	-7.72	2.62	6	0.6	0.95	-7.48	2.15	47.4
PARKFALLS	67	0.9	0.87	-4.1	4.65	67	0.9	0.89	-3.85	4.43	45.9
LAMONT	90	0.8	0.93	-6.17	3.88	90	0.8	0.94	-5.92	3.71	36.6
NICOSIA	196	0.8	0.92	-1.83	4.1	196	0.8	0.92	-1.54	3.81	35.1
EDWARDS	158	0.7	0.95	-4.01	4.79	158	0.7	0.95	-3.5	4.39	35
PASADENA	135	0.7	0.85	-3.83	7.18	135	0.8	0.89	-5.63	6.07	34.1
SAGA	19	0.8	0.95	-1.31	5.2	19	0.8	0.97	-0.97	4.44	33.2
IZANA	46	0.8	0.93	-4.35	4.22	46	0.8	0.93	-3.48	4.16	28.3
REUNION	107	0.8	0.98	-2.78	3.85	107	0.8	0.98	-2.14	4.28	-20.9
LAUDER	61	1.1	0.97	-2.46	2.73	61	1.1	0.98	-2.78	2.55	-45
		0.8	0.92	-3.57	3.99		0.8	0.94	-3.4	3.74	

Table 2.12.2. Overview of o-suite/pre e-suite analysis performance against the TCCON FTIR dry air averaged CO column. Similar to the NDACC results, the averaged bias of the e-suite has decreased. Correlations and the standard deviation on the relative difference behave similar: slight improvement in the e-suite.

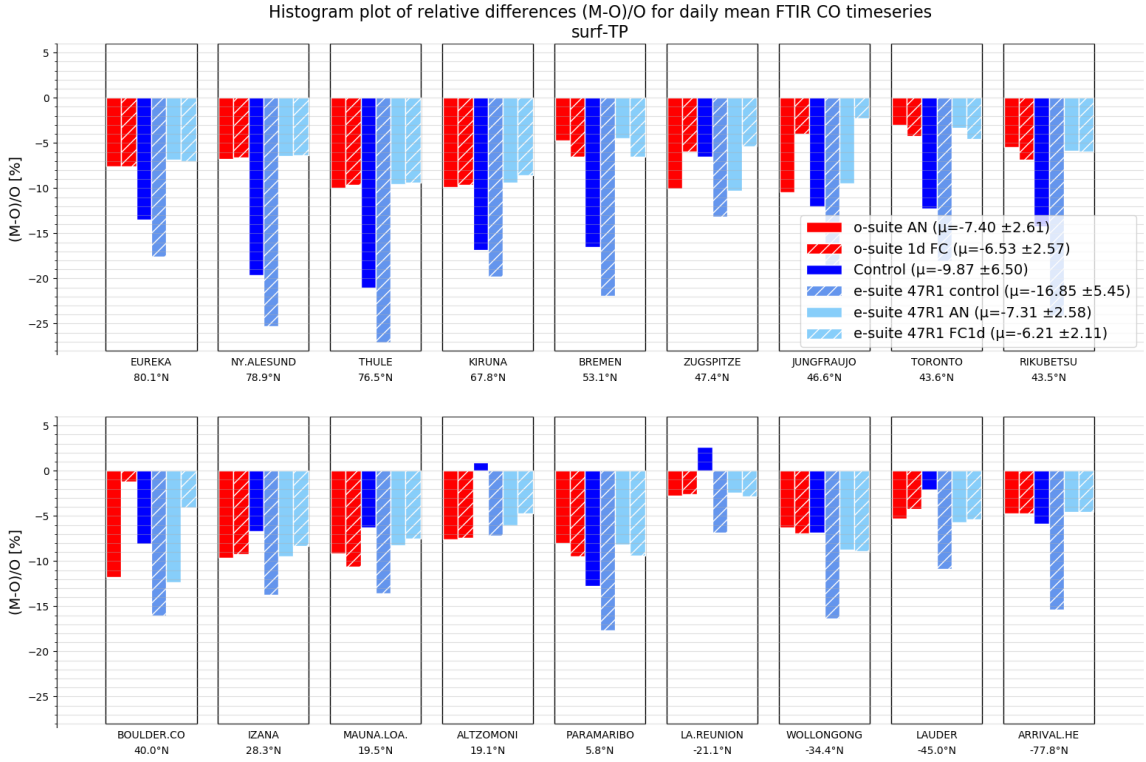

Fig. 2.12.2.: Averaged relative bias for tropospheric CO columns compared to NDACC FTIR. The e-suite control (hdir) has a significantly increased low bias.

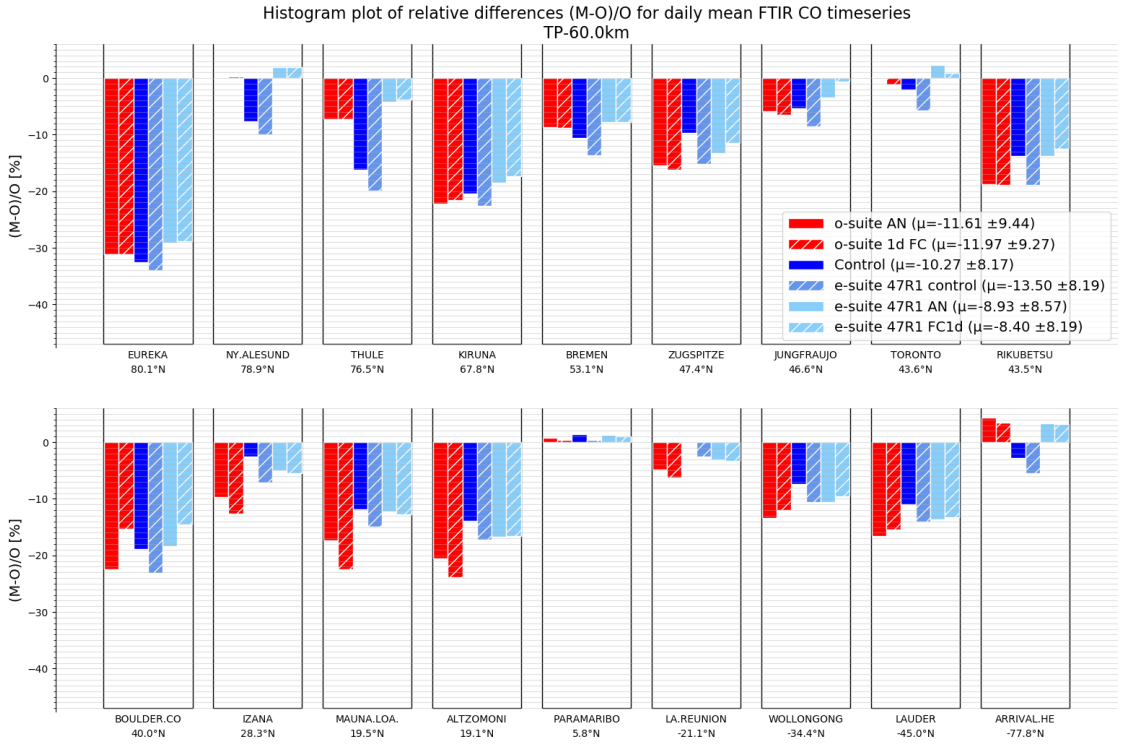

Fig. 2.12.3.: Averaged relative bias for stratospheric CO columns compared to NDACC FTIR. Both the e-suite analysis and day 1 forecast have a reduced bias compared to the o-suite analysis and day 1 forecast respectively at almost all sites (Ny Alesund and Toronto are exceptions).

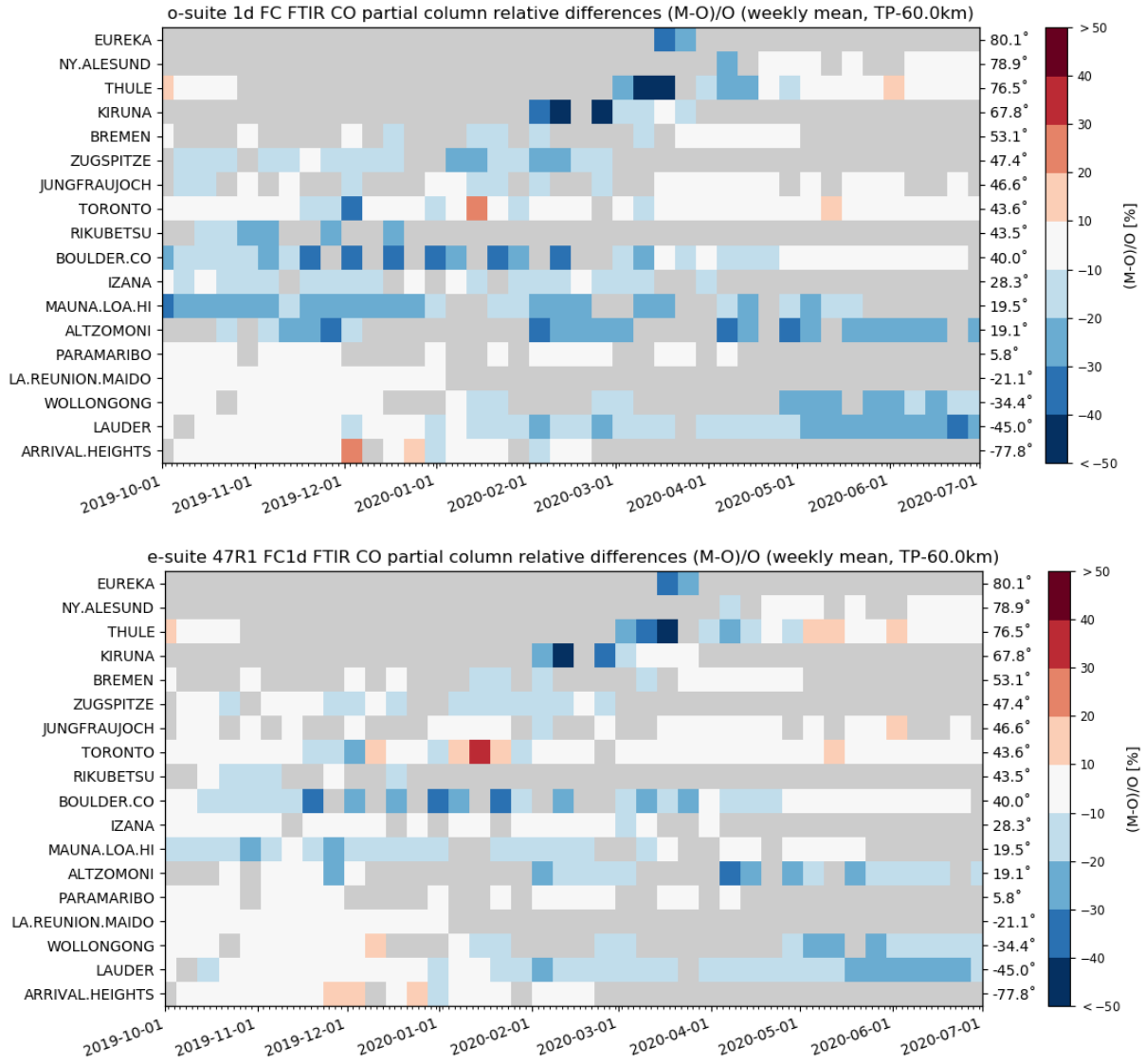

Fig. 2.12.4.: Relative mean bias for stratospheric NDACC FTIR CO columns (MB, %) for the considered period October 2019 – June 2020 (top, o-suite day 1 forecast and bottom pre-e-suite day 1 forecast). The overall uncertainty for the CO measurements is approximately 10%. Stations are sorted with decreasing latitude (northern to southern hemisphere). A clear improvement is seen at the mountain sites of Izana, Mauna Loa and Altzomoni.

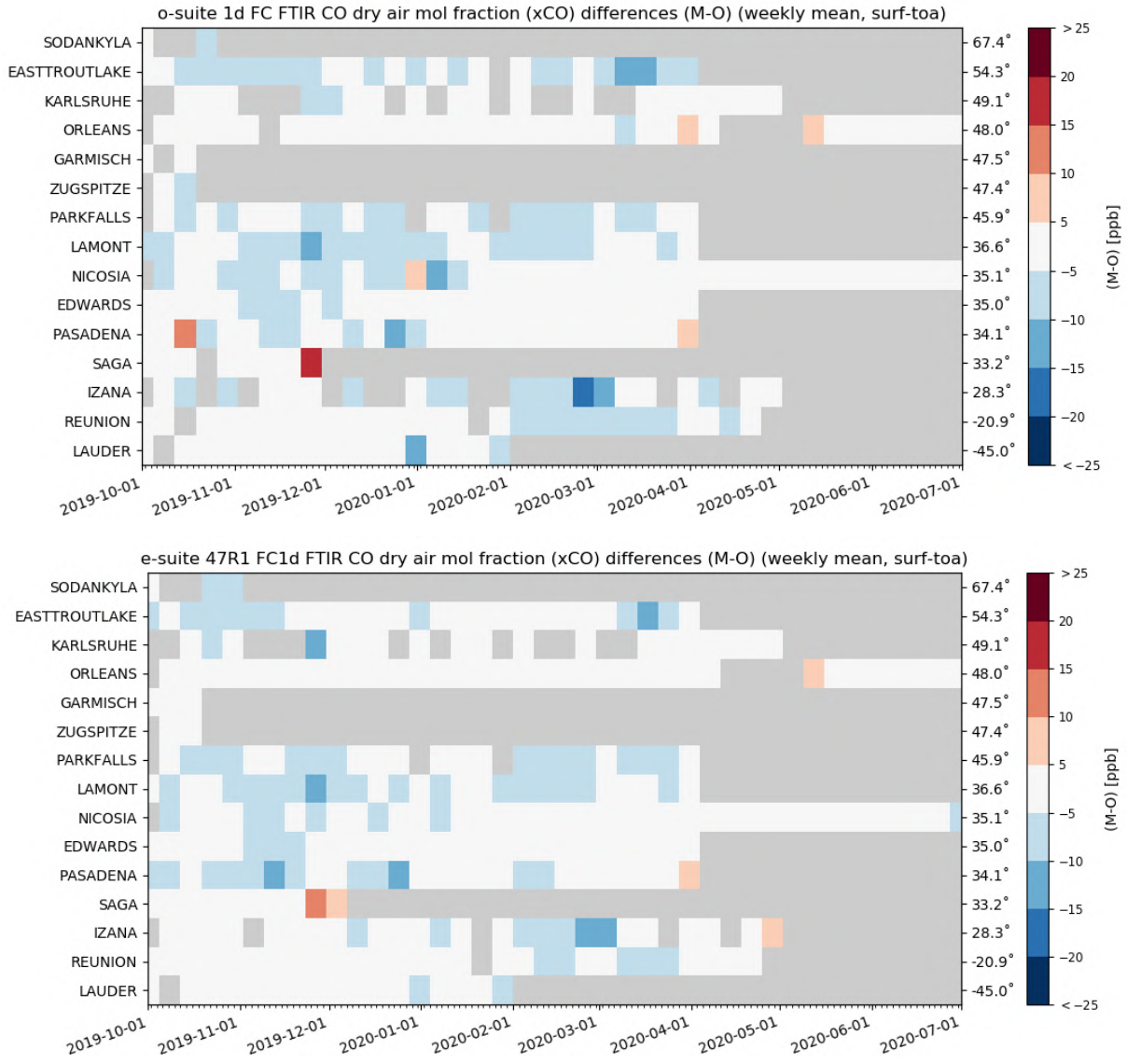

Fig. 2.12.5.: Relative mean bias for stratospheric TCCON FTIR CO columns (MB, %) for the period October 2019-June 2020 (top: o-suite day 1 forecast; bottom: e-suite day 1 forecast). The overall uncertainty for the CO measurements is approximately 5ppb. Stations are sorted with decreasing latitude (northern to southern hemisphere). A slight improved bias is observed in the e-suite. This is in agreement with the NDACC comparison.

2.13 Tropospheric nitrogen dioxide comparisons with GOME-2

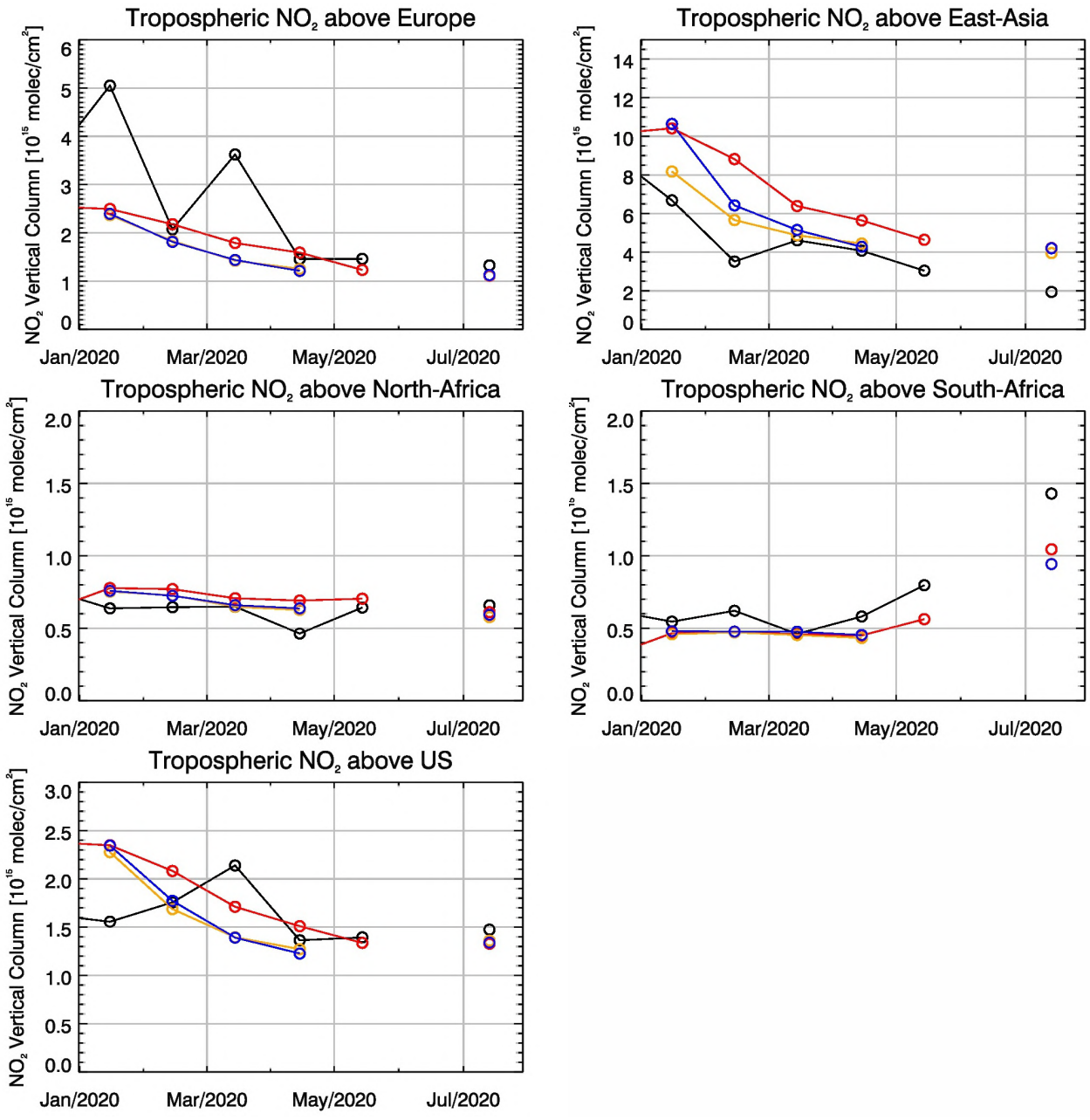

Figure 2.13.1: Time series of average tropospheric NO_2 columns [10^{15} molec. cm-2] from (black) GOME-2 compared to (red) o-suite, (orange) e-suite, (blue) e-suite control for different regions. Upper panels represent regions dominated by anthropogenic emissions, lower panels represent those dominated by biomass burning. The e-suite compares better than the o-suite to GOME-2 retrievals over East-Asia and North-Africa, but slightly worse for Europe.

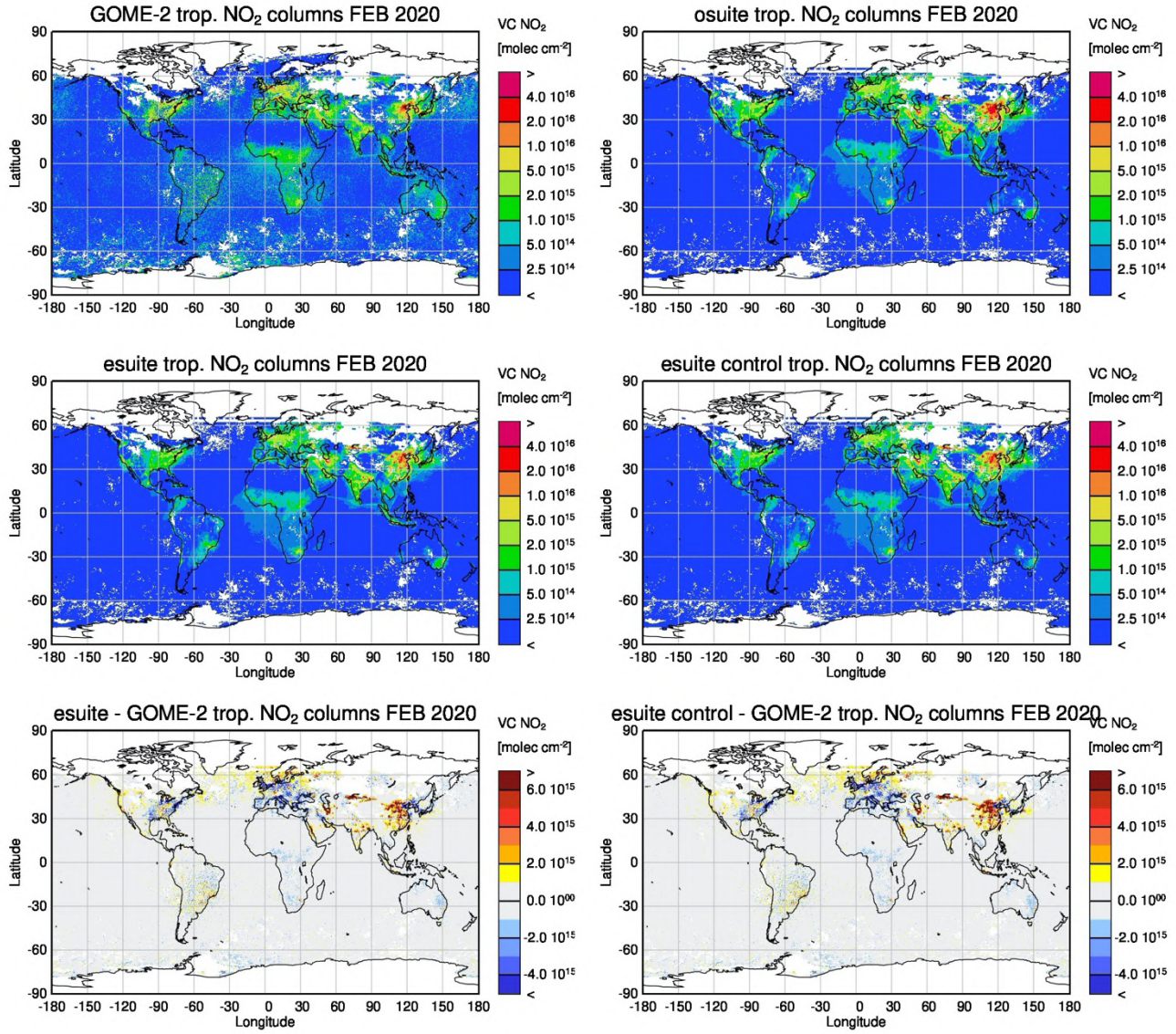

Figure 2.13.2: Monthly mean tropospheric NO_2 columns [molec. cm^{-2}] from GOME-2 compared to model runs for February 2020. GOME-2 is shown at the top left and the o-suite at top right. The middle row shows e-suite results on the left and e-suite control on the right. The lower row shows the difference between e-suite and GOME-2 on the left and the same for e-suite control on the right. GOME-2 and model data were gridded to 0.4 degree resolution. Model data were treated with the same reference sector subtraction approach as the satellite data. The e-suite shows an improved performance compared to the o-suite over emission hotspots in East-Asia. There are only very small differences between e-suite and e-suite control.

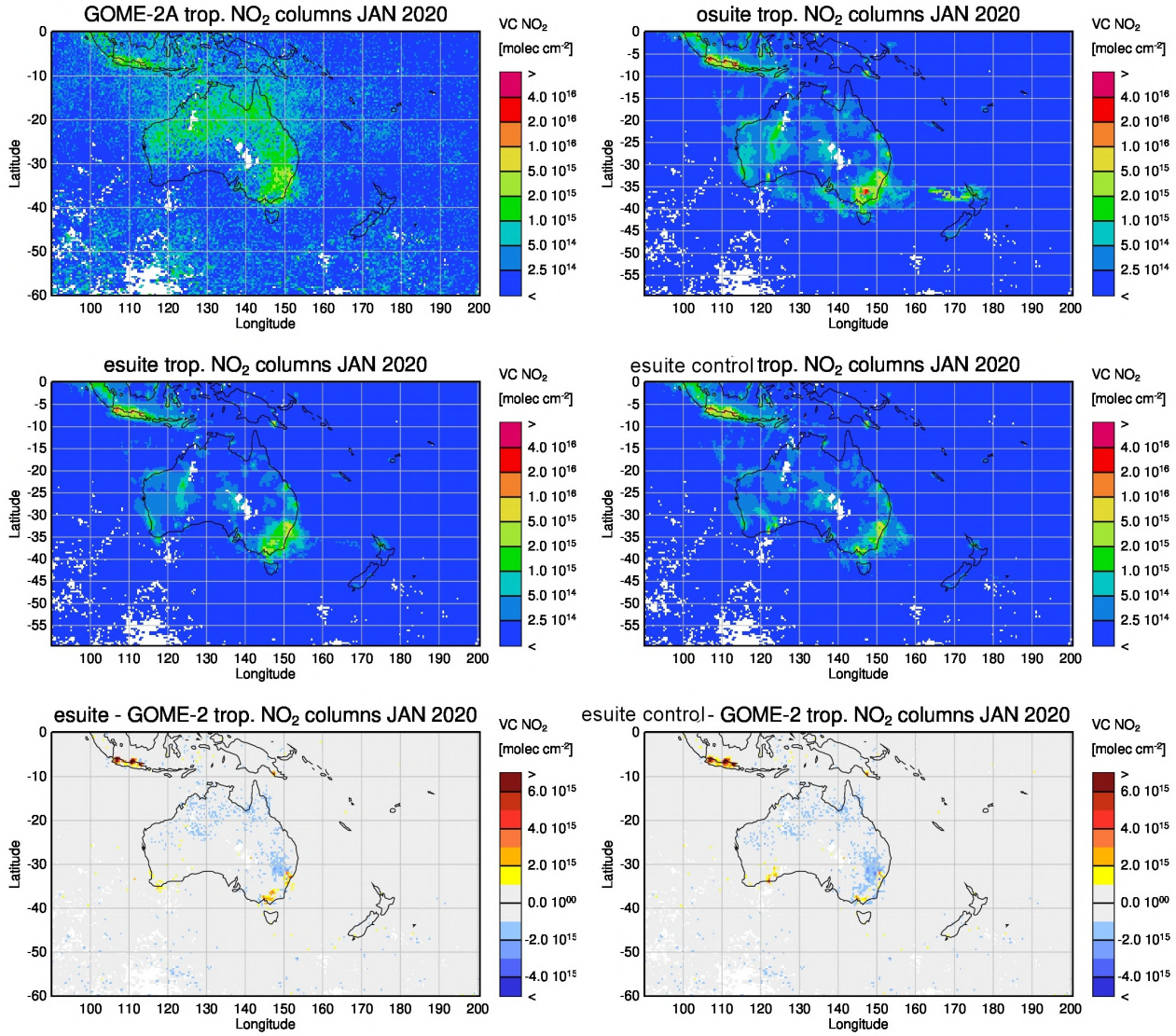

Figure 2.13.3: Same as in Figure 2.13.2 but for January 2020 over Australia. The e-suite and e-suite control compare better to GOME-2 than the o-suite over regions associated with the fire plume from South-Eastern Australia.

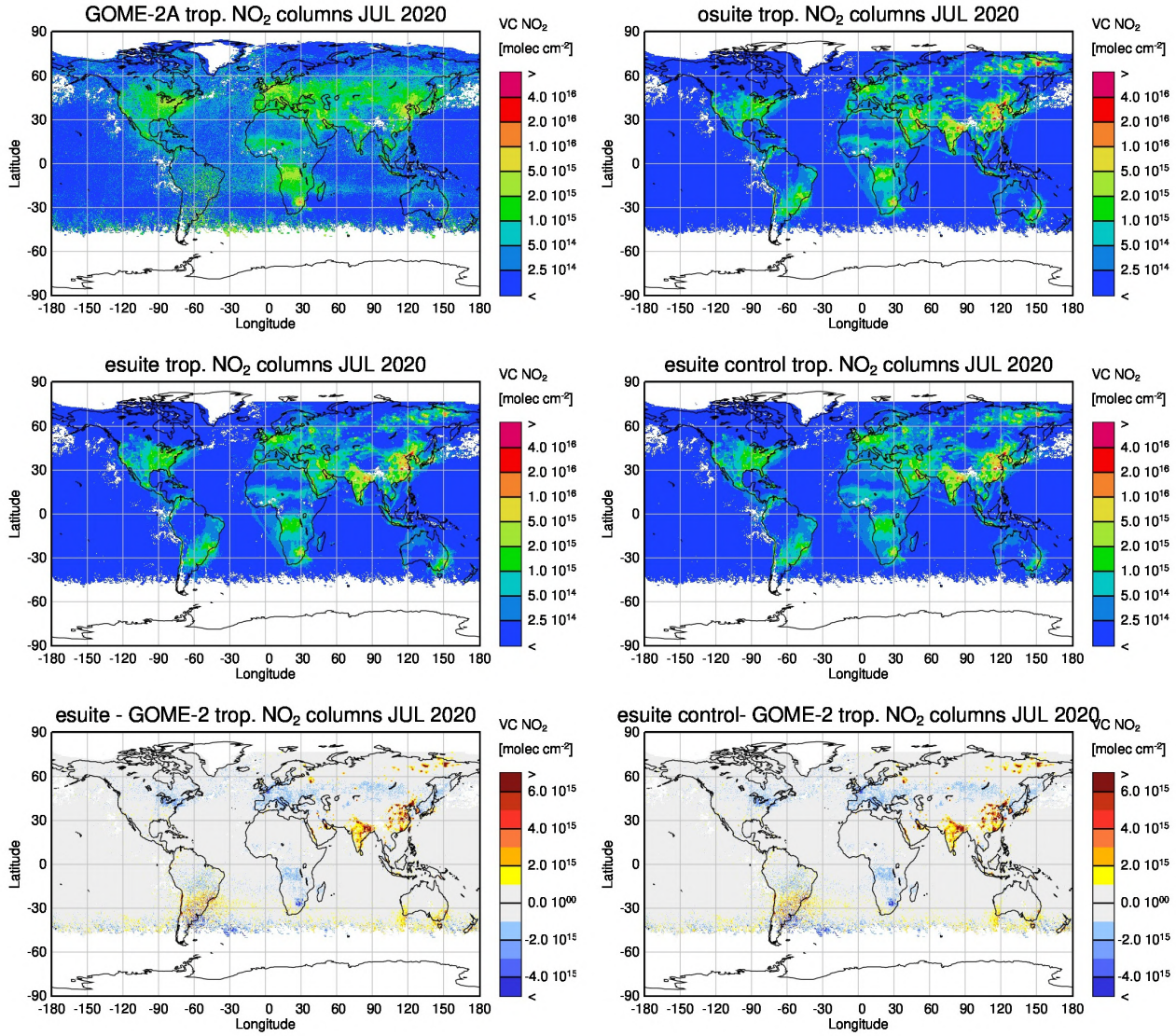

Figure 2.13.4: Same as in Figure 2.13.2 but for July 2020. The e-suite and e-suite control compare better to GOME-2 over regions associated with boreal forest fires in Siberia.

2.14 Tropospheric nitrogen dioxide comparisons with MAXDOAS

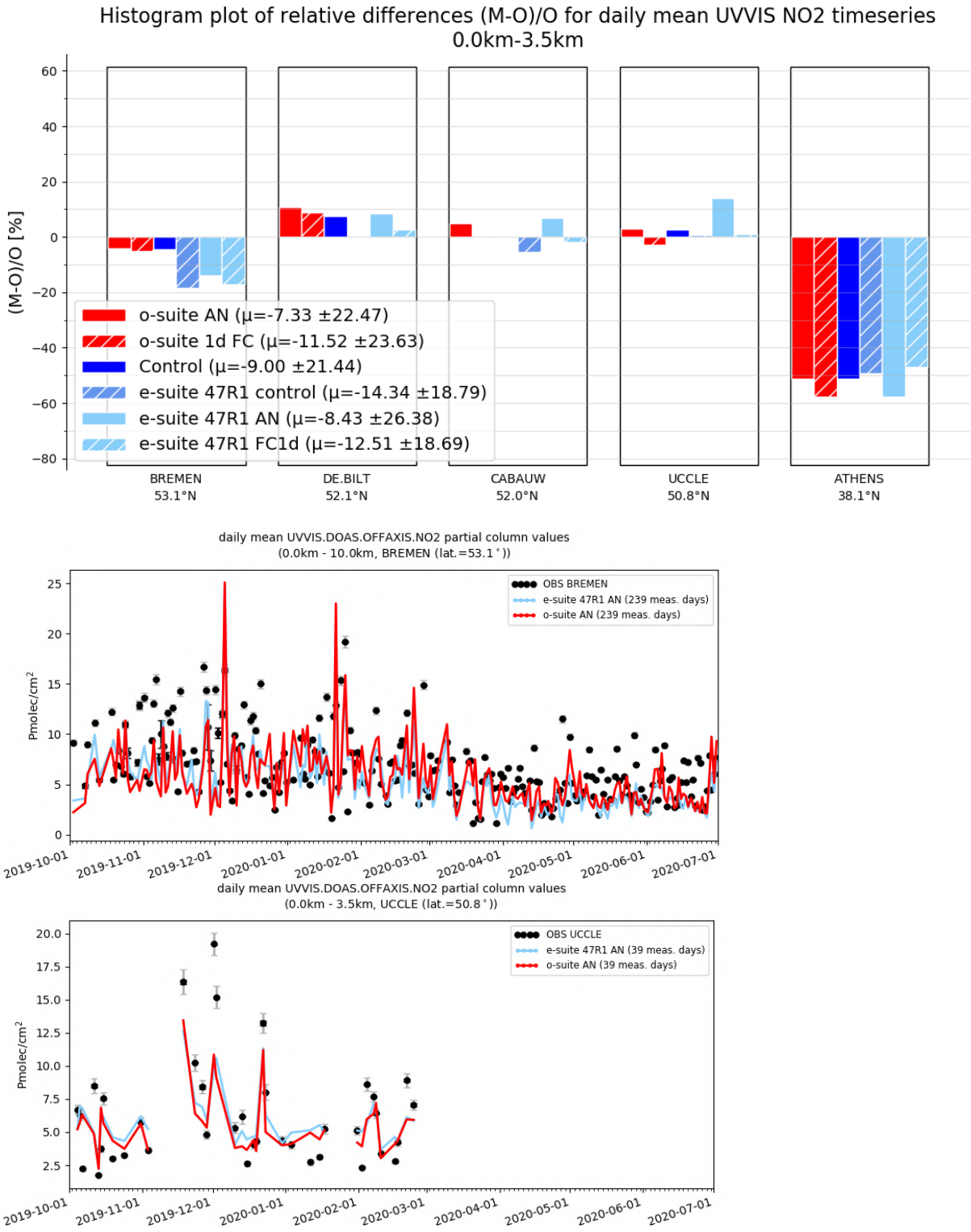

Fig. 2.14.1.: Top: Overview of the relative bias against MAXDOAS tropospheric columns for the entire time period Oct 2019 – June 2020 for the o-suite and e-suite. Bottom: at Bremen the e-suite shows a slightly increased bias due to a shift in the baseline concentrations.

2.15 Formaldehyde (HCHO)

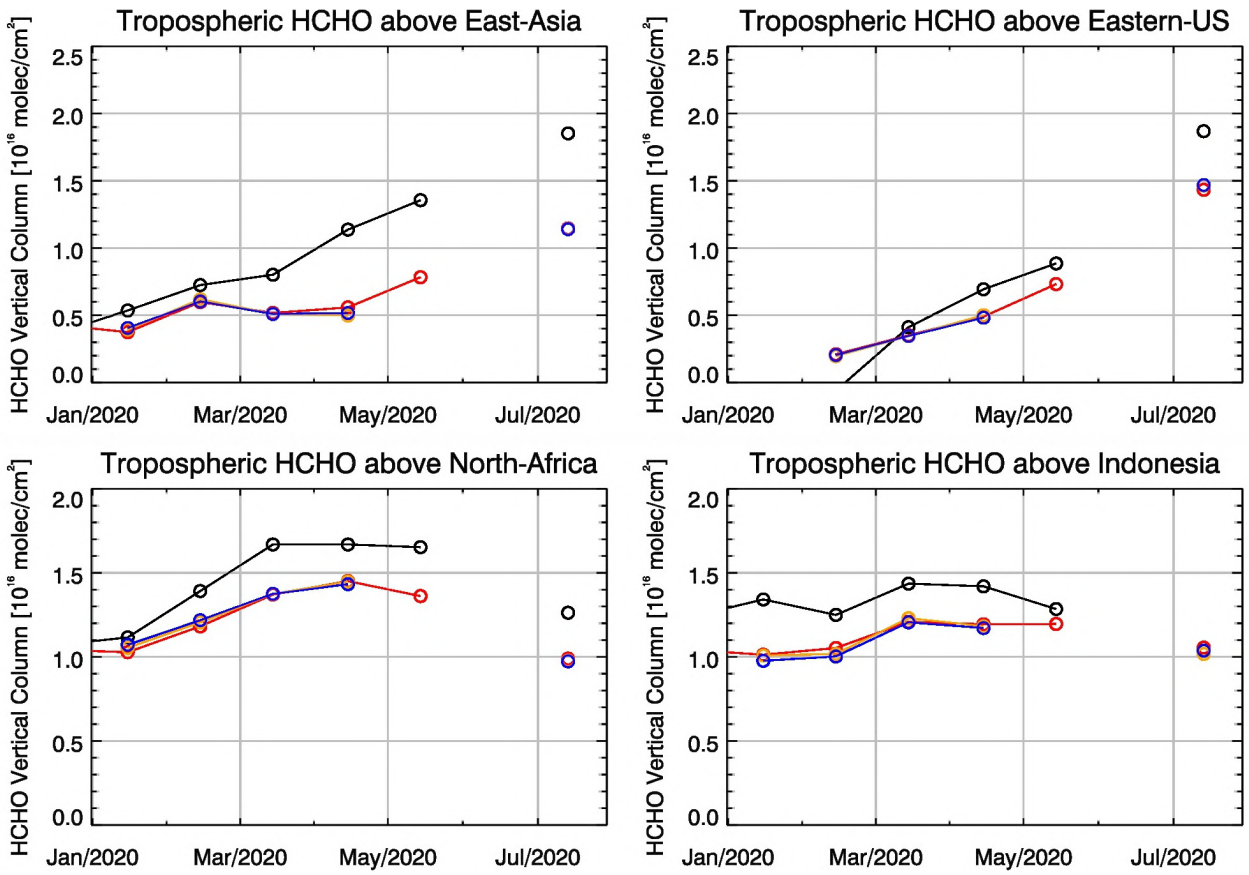

Figure 2.15.1. Time series of average tropospheric HCHO columns [10^{16} molec cm-2] from (black) GOME-2 compared to (red) o-suite, (orange) e-suite, (blue) e-suite control for different regions. The regions differ from those used for NO2 to better focus on HCHO hotspots: East-Asia (25-40°N, 110-125°E), Eastern US (30-40°N, 75-90°W), Northern Africa (0-15°N, 15°W-25°E) and Indonesia (5°S-5°N, 100-120°E). Negative satellite retrieved values and large variability over Eastern US during Northern Hemisphere winter months are due to a lack of data (caused by instrument degradation) for this region. Results are very similar for all model runs.

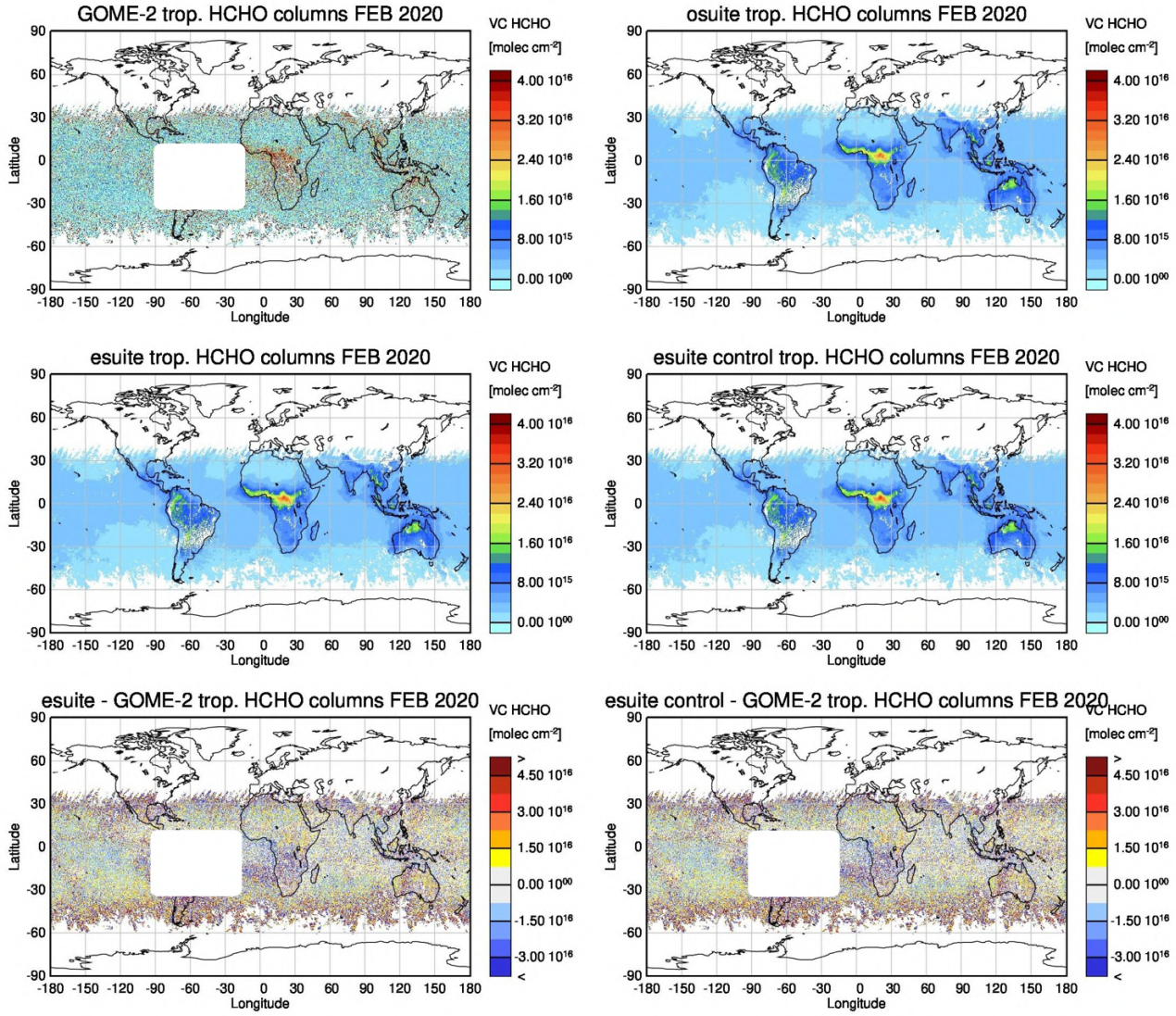

Figure 2.15.2: Monthly mean tropospheric HCHO columns [molec cm-2] from GOME-2 compared to model runs for February 2020. GOME-2 is shown at the top left and the o-suite at top right. The middle row shows e-suite results on the left and e-suite control on the right. The lower row shows the difference between e-suite and GOME-2 on the left and the same for e-suite control on the right. GOME-2 and model data were gridded to 0.4 degree resolution. Satellite retrieved values in the region of the South Atlantic Anomaly are not valid and therefore masked out (white boxes). All model runs show a very similar spatial distributions and therefore basically no differences in the performance compared to GOME-2. There are mismatches over Central Africa, possibly related to fire emissions incorporated the model runs.

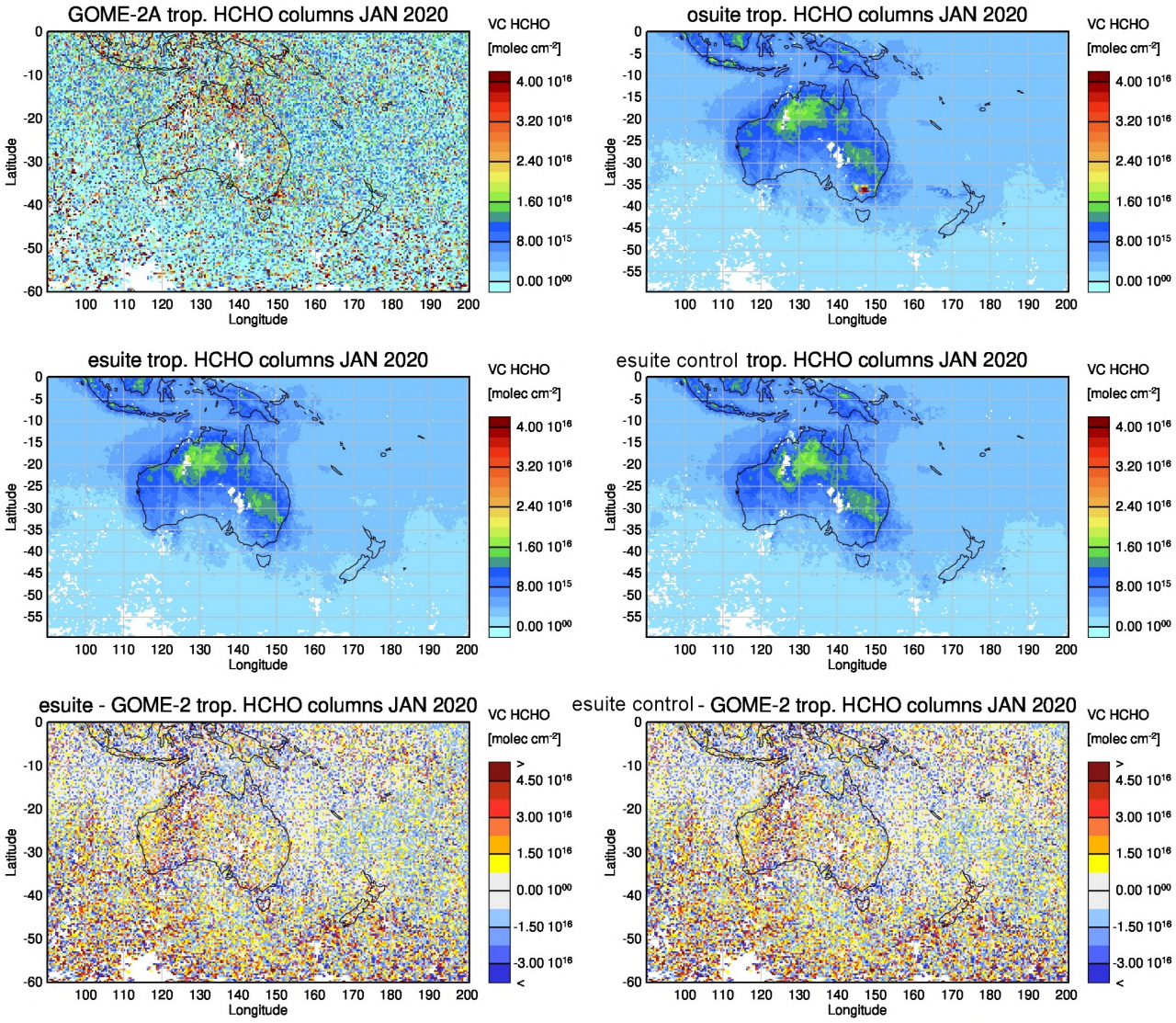

Figure 2.15.3: Same as in Figure 2.15.2 but for January 2020 over Australia. The e-suite and e-suite control compare better to GOME-2 than the o-suite over regions associated with the fire plume from South-Eastern Australia.

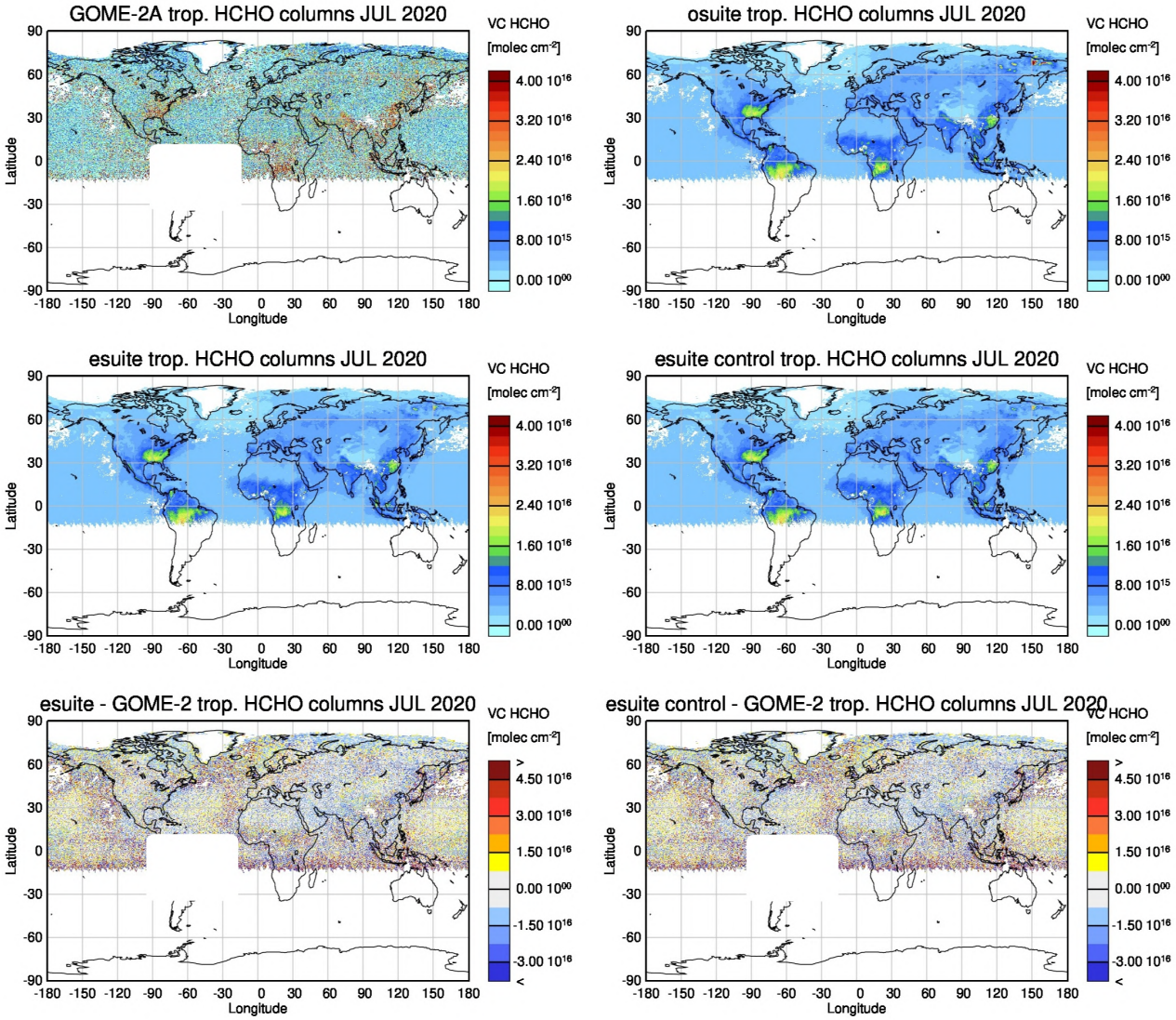

Figure 2.15.4: Same as in Figure 2.15.2 but for July 2020. The e-suite and e-suite control compare better to GOME-2 over regions associated with boreal forest fires in Siberia.

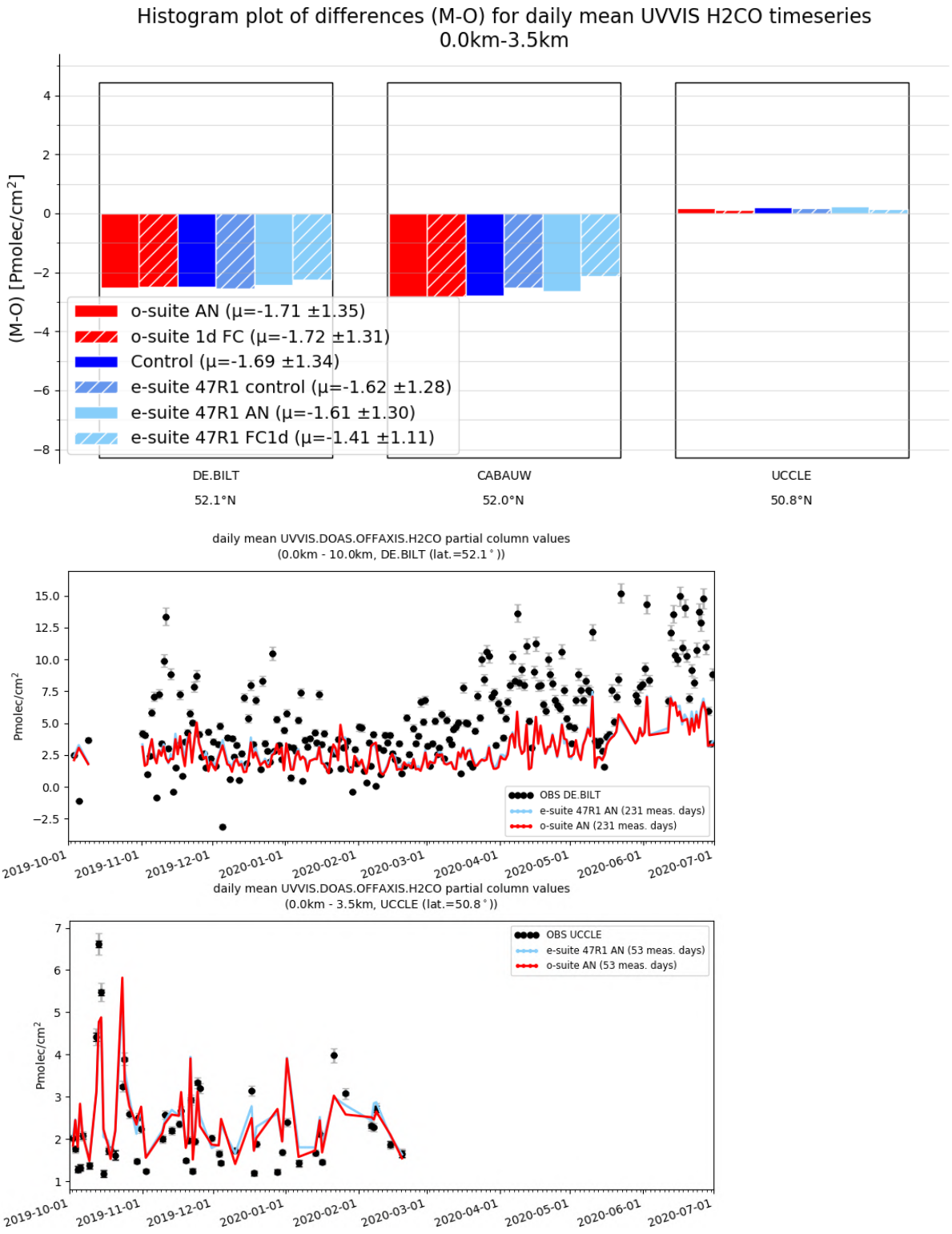

Figure 2.15.5. Top: Overview of the relative bias against UV-Vis MAXDOAS measurements for the entire time period Oct 2019 – June 2020 for the o-suite and e-suite. Little difference is observed in the performance of both runs. This is confirmed when looking at the timelines for De Bilt and Uccle in the bottom plots.

2.16 Stratosphere: comparisons with ozone sondes

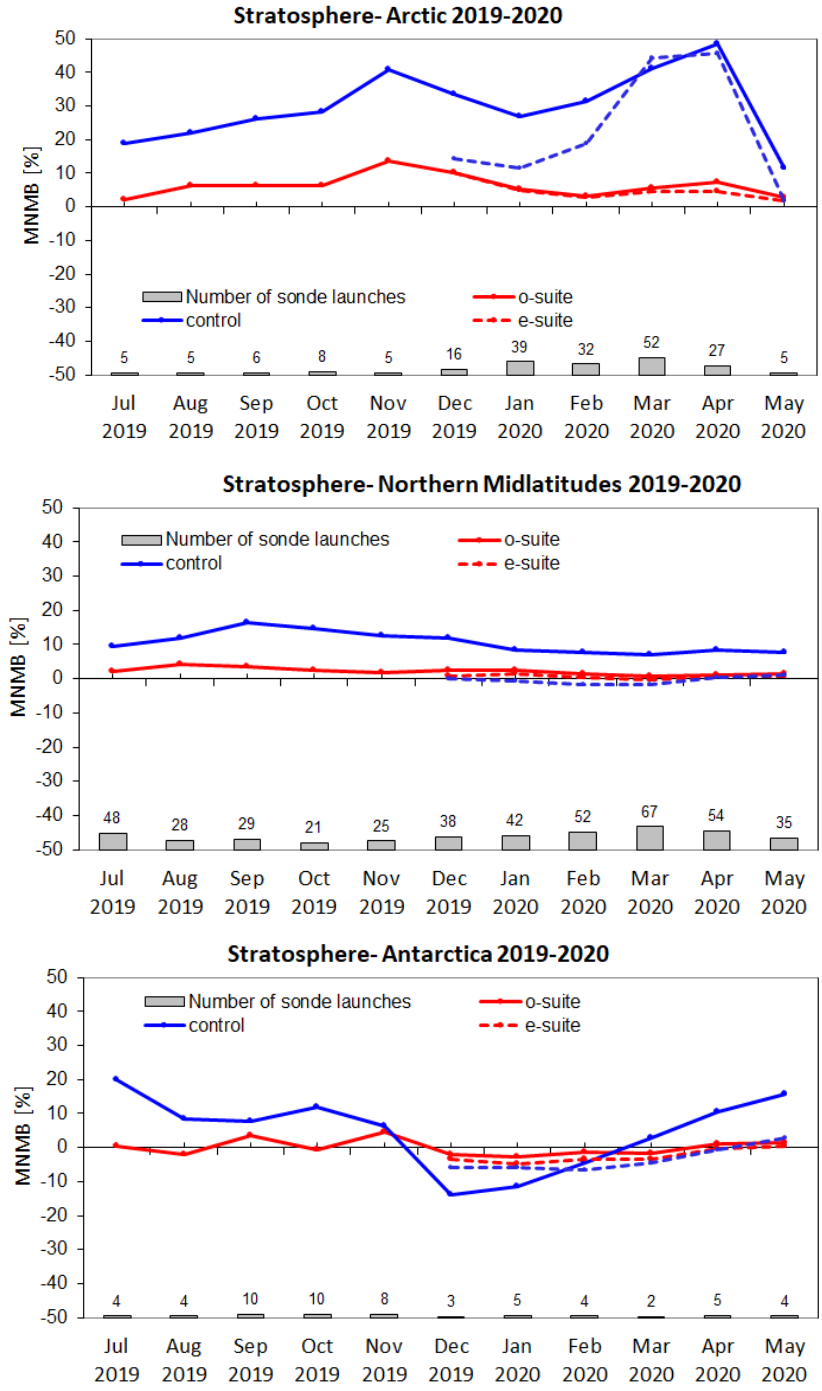

Fig. 2.16.1: Bias (MNMB) from the comparison of o-suite, e-suite and control runs with ozonesonde measurements in the stratosphere. The profiles are averaged over the range 10-90 hPa. Differences between e-suite and o-suite are small. The e-suite control has improved considerably compared to the o-suite control run.

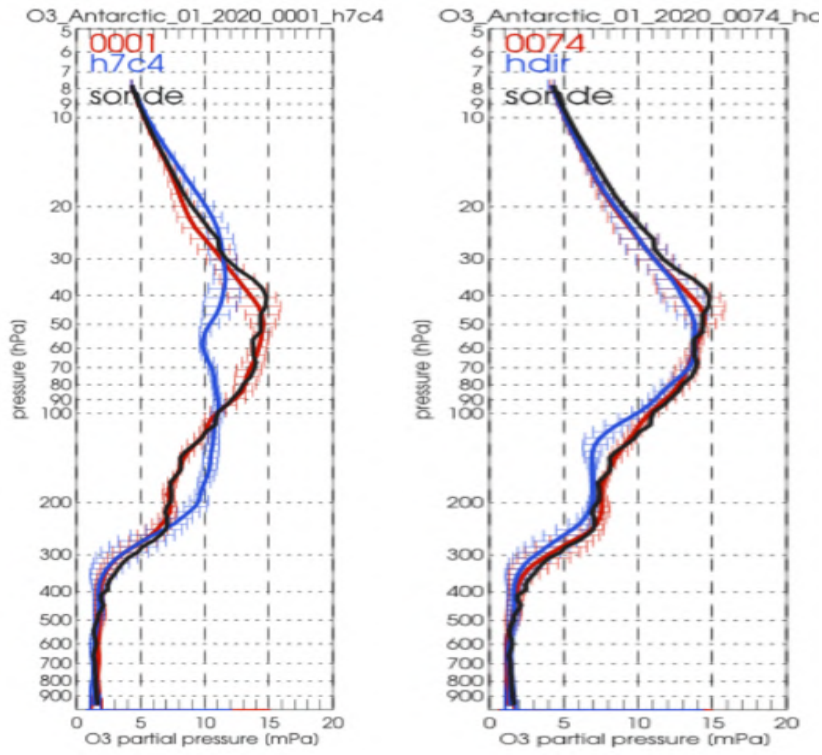

Fig.2.16.2: Mean O3 profiles for the o-suite and control (left) and e-suite and control (right) for the month of January 2020 for Antarctica. The e-suite shows improvements around 20 hPa.

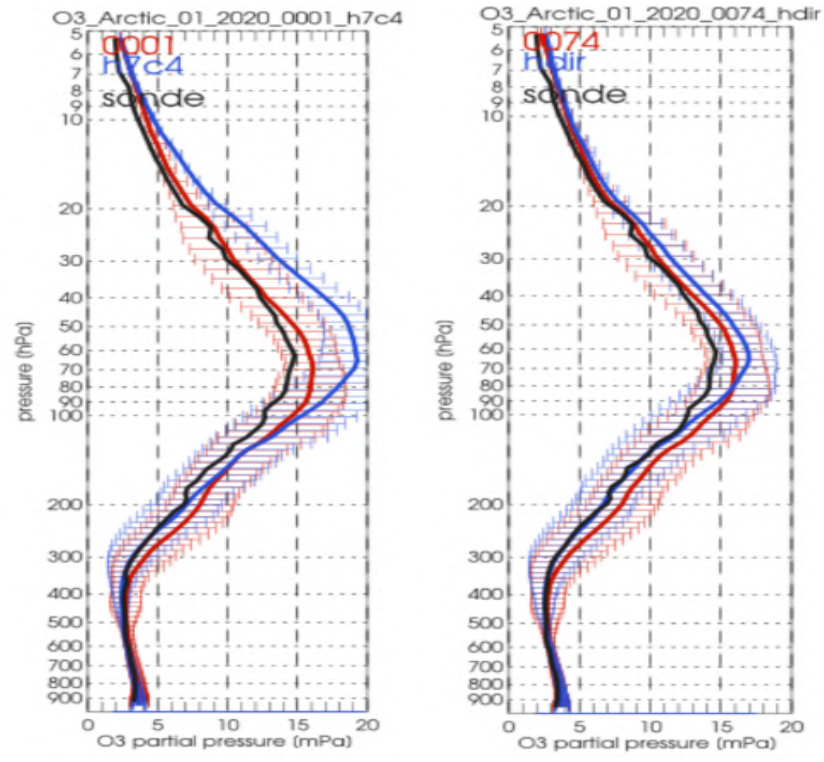

Fig. 2.16.3: Mean O_3 profiles for the o-suite and control (left) and e-suite and control (right) for the month of January 2020 for the Arctic. The e-suite control run is much improved compared to the o-suite control, both in the Arctic and Antarctic.

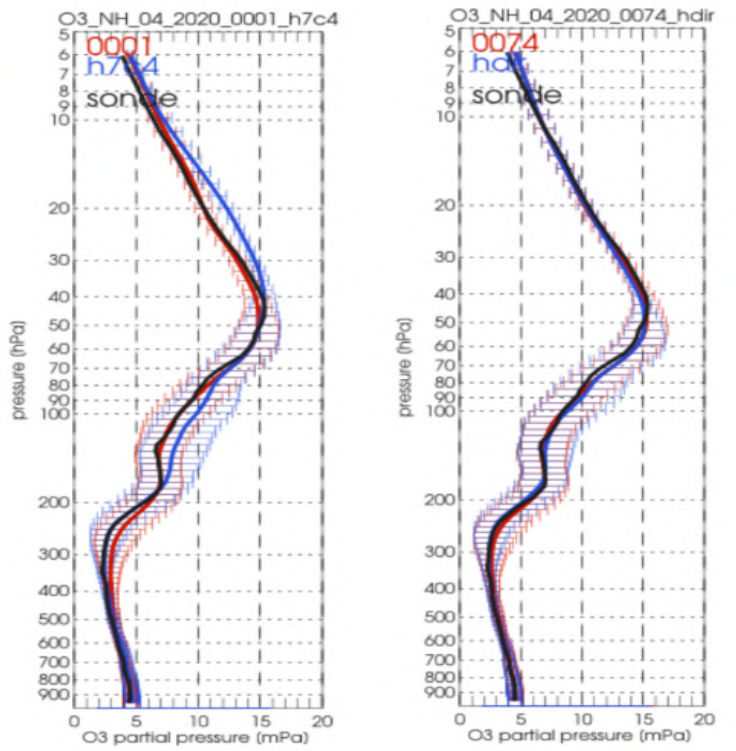

Fig.2.16.4: Mean O_3 profiles for the o-suite and control (left) and e-suite and control (right) for the month of April 2020 for the Northern Hemisphere. Improvements of the o-suite compared to the e-suite are observed in the range 10-40 hPa and around 250 hPa.

2.17 Stratospheric ozone: Comparison with satellite observations

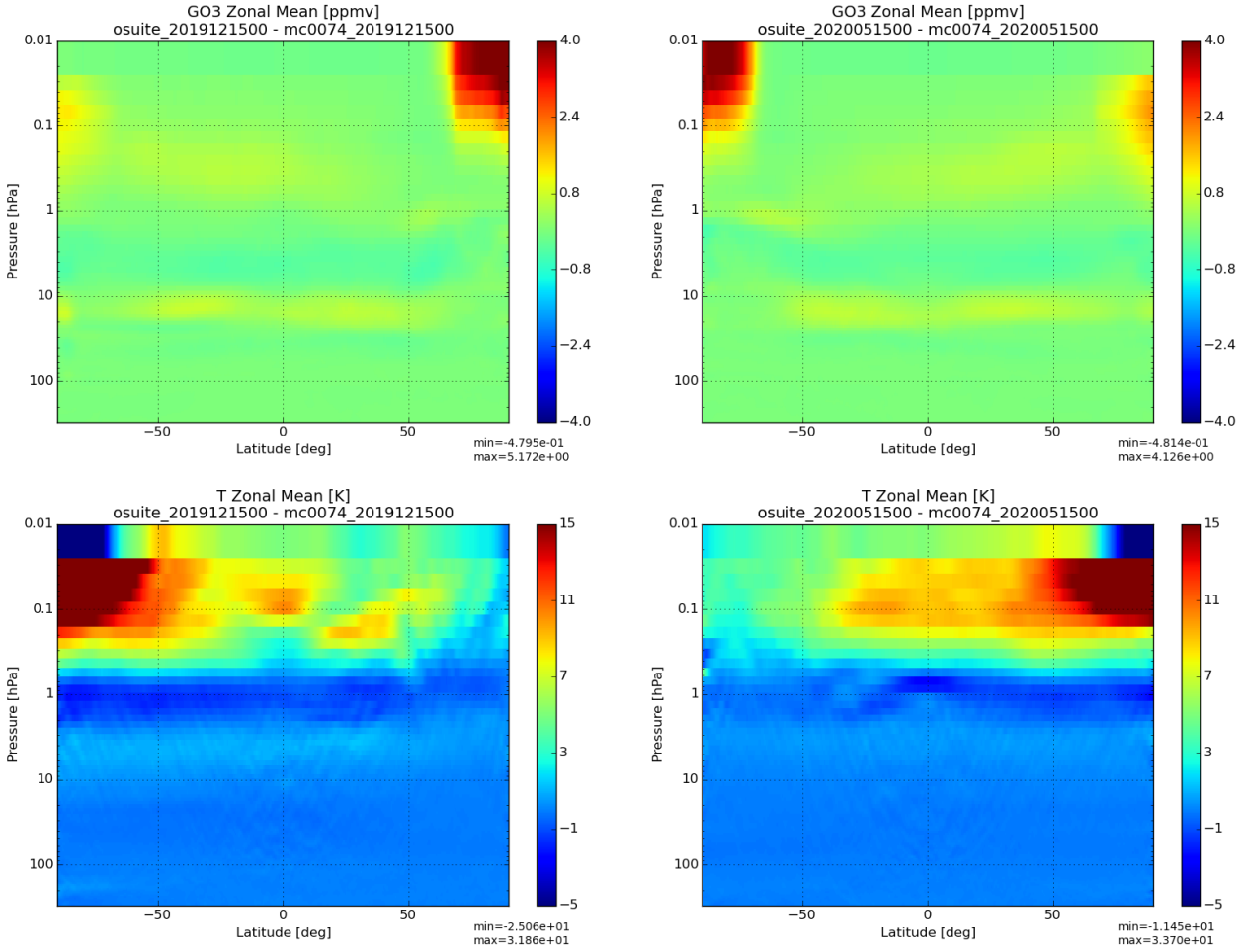

Figure 2.17.1: Zonal means of the difference between the o-suite and the e-suite mc.0074 at 2019-12-15 (left) and 2020-05-15 (right). For the ozone volume mixing ratio (ppmv, top row), up to ~20hPa, the differences are within ±0.7 ppmv; in the upper stratosphere above 20hPa, the differences are alternating from positive (~1ppmv, up to ~10hPa), then slightly negative (up to ~1hPa), then again slightly positive; at the polar regions in fall and winter, a strong difference of up to +5ppmv is observed. The temperature biases (K, bottom row) are within ±1K up to ~7hPa; above, a latitude-dependent positive difference of up to more than 15K is present (the topmost level is inconsistent with the levels below).

Figure 2.17.2 (next 3 pages): Comparison with satellite observations: monthly mean profiles (top panels) and mean biases (bottom panels) in January 2020 (a,b,c) and March 2020 (d,e,f): against ACE-FTS (a,d), SAGE3 ISS (b,e) and MLS (c,f); for the o-suite (red) and the e-suite (blue), analysis (solid) and 4th day forecast (96-120h) (dotted). The shaded area represents the standard deviations of the bias of the o-suite analysis. The profiles from the e-suite are generally closer to the observations in the 25-45km / 30 to 3 hPa altitude range; above ~45km / 3hPa, the results are less conclusive: biases wrt observation profiles are more distributed between the e-suite and the o-suite, depending on the altitude and the latitude band.

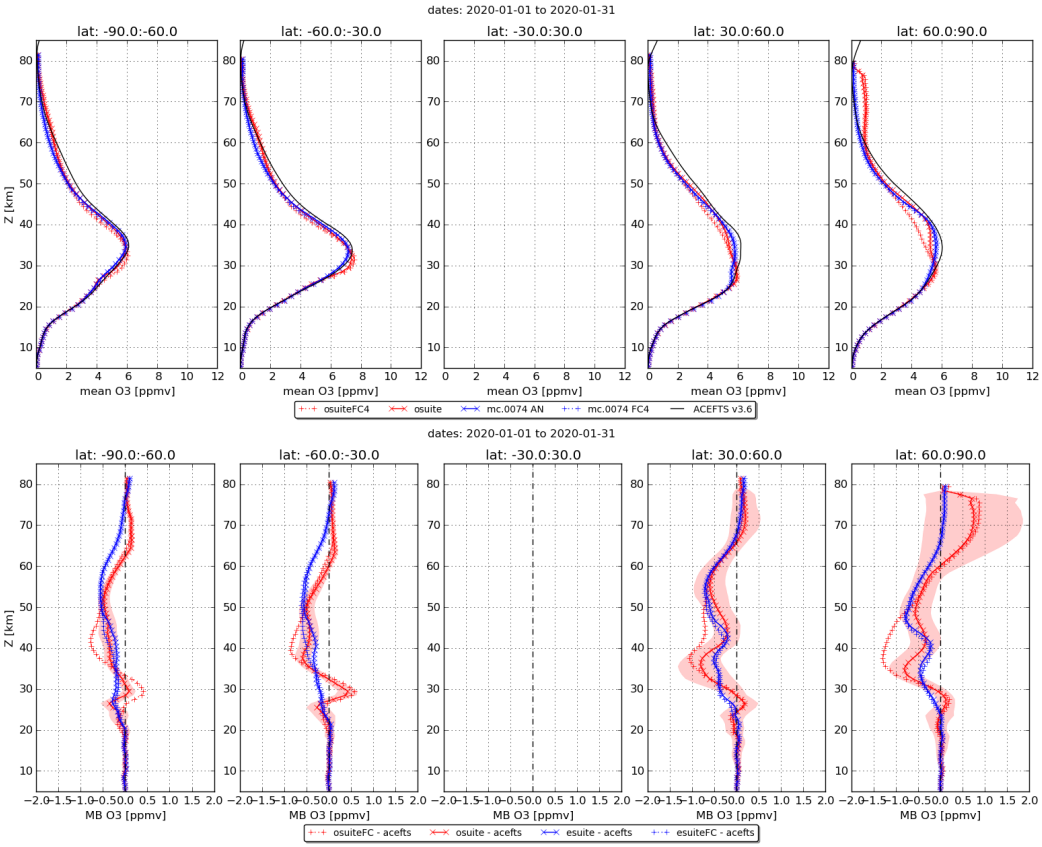
dates: 2020-01-01 to 2020-01-31
lat: -90.0:-60.0
lat: -60.0:-30.0
lat: -30.0:30.0
lat: 30.0:60.0
lat: 60.0:90.0
Z [km]
mean O3 [ppmv]
osuiteFC4
osuite
mc.0074 AN
mc.0074 FC4
ACEFTS v3.6
dates: 2020-01-01 to 2020-01-31
MB O3 [ppmv]
osuiteFC - acefts
osuite - acefts
esuite - acefts
esuiteFC - acefts

(a)

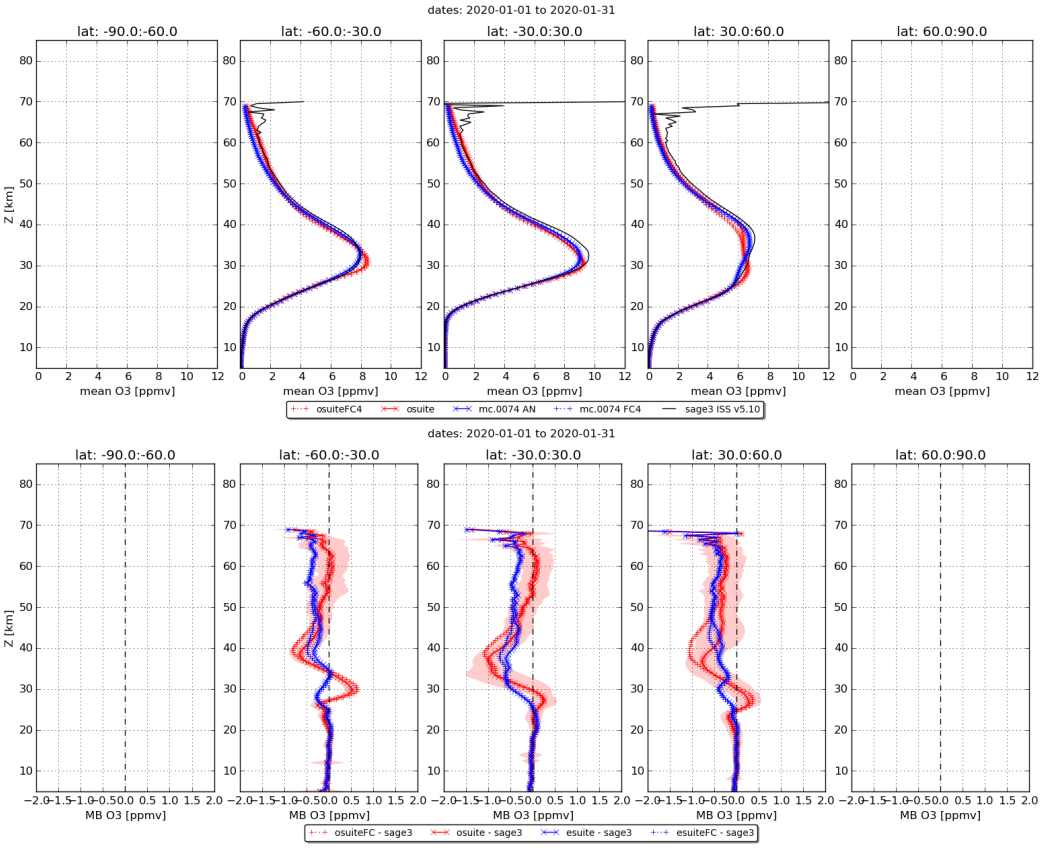
dates: 2020-01-01 to 2020-01-31
lat: -90.0:-60.0
lat: -60.0:-30.0
lat: -30.0:30.0
lat: 30.0:60.0
lat: 60.0:90.0
Z [km]
mean O3 [ppmv]
osuiteFC4
osuite
mc.0074 AN
mc.0074 FC4
sage3 ISS v5.10
dates: 2020-01-01 to 2020-01-31
MB O3 [ppmv]
osuiteFC - sage3
osuite - sage3
esuite - sage3
esuiteFC - sage3

(b)

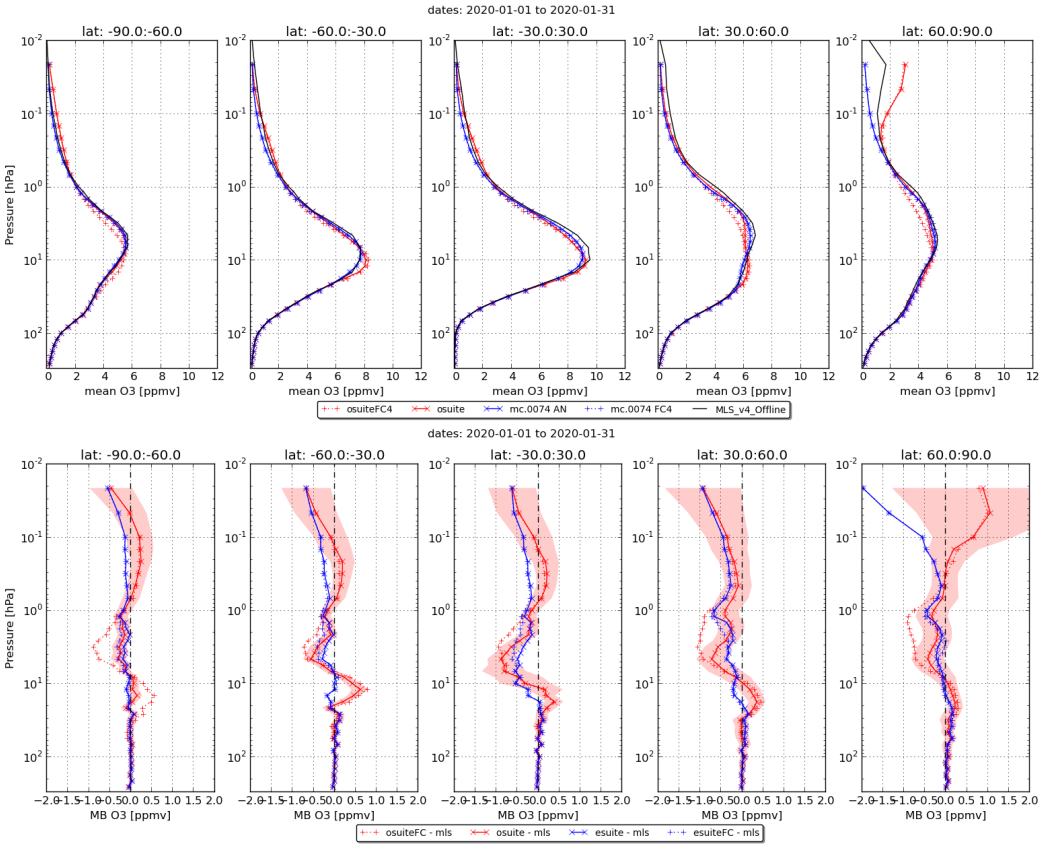
dates: 2020-01-01 to 2020-01-31
lat: -90.0:-60.0
lat: -60.0:-30.0
lat: -30.0:30.0
lat: 30.0:60.0
lat: 60.0:90.0
Pressure [hPa]
mean O3 [ppmv]
osuiteFC4
osuite
mc.0074 AN
mc.0074 FC4
MLS_v4_Offline
dates: 2020-01-01 to 2020-01-31
MB O3 [ppmv]
osuiteFC - mls
osuite - mls
esuite - mls
esuiteFC - mls

(c)

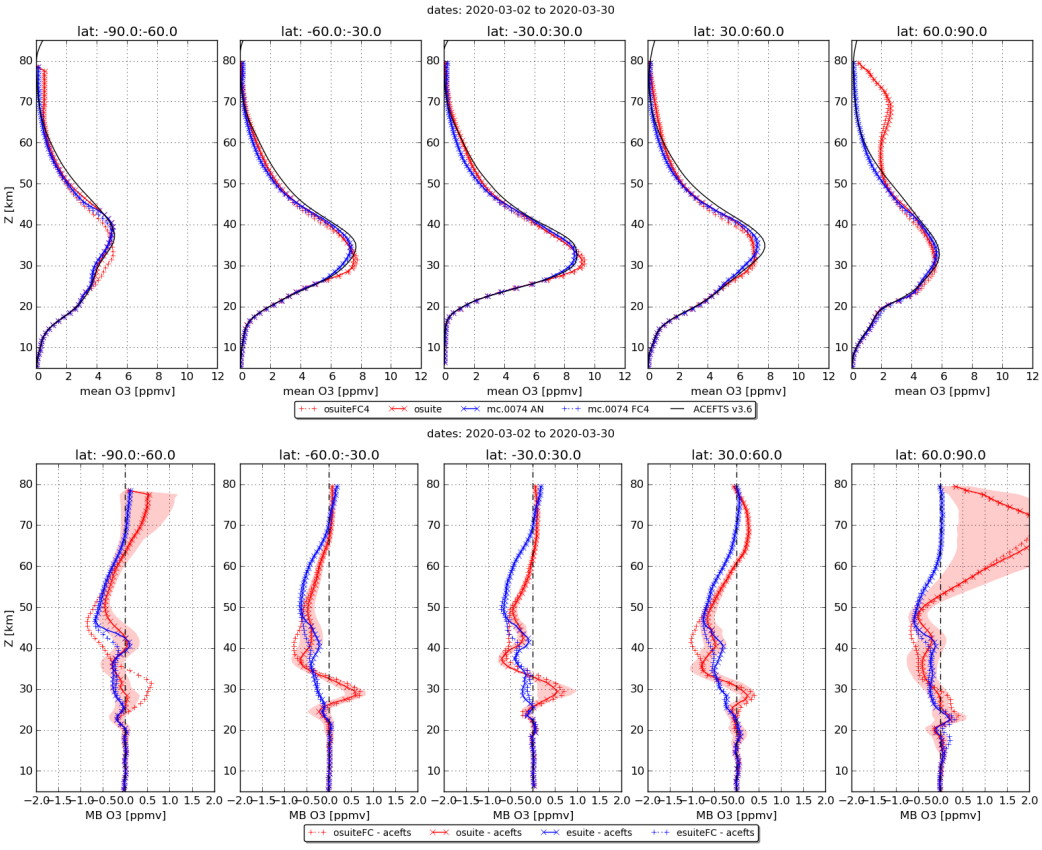
dates: 2020-03-02 to 2020-03-30
lat: -90.0:-60.0
lat: -60.0:-30.0
lat: -30.0:30.0
lat: 30.0:60.0
lat: 60.0:90.0
Z [km]
mean O3 [ppmv]
osuiteFC4
osuite
mc.0074 AN
mc.0074 FC4
ACEFTS v3.6
dates: 2020-03-02 to 2020-03-30
MB O3 [ppmv]
osuiteFC - acefts
osuite - acefts
esuite - acefts
esuiteFC - acefts

(d)

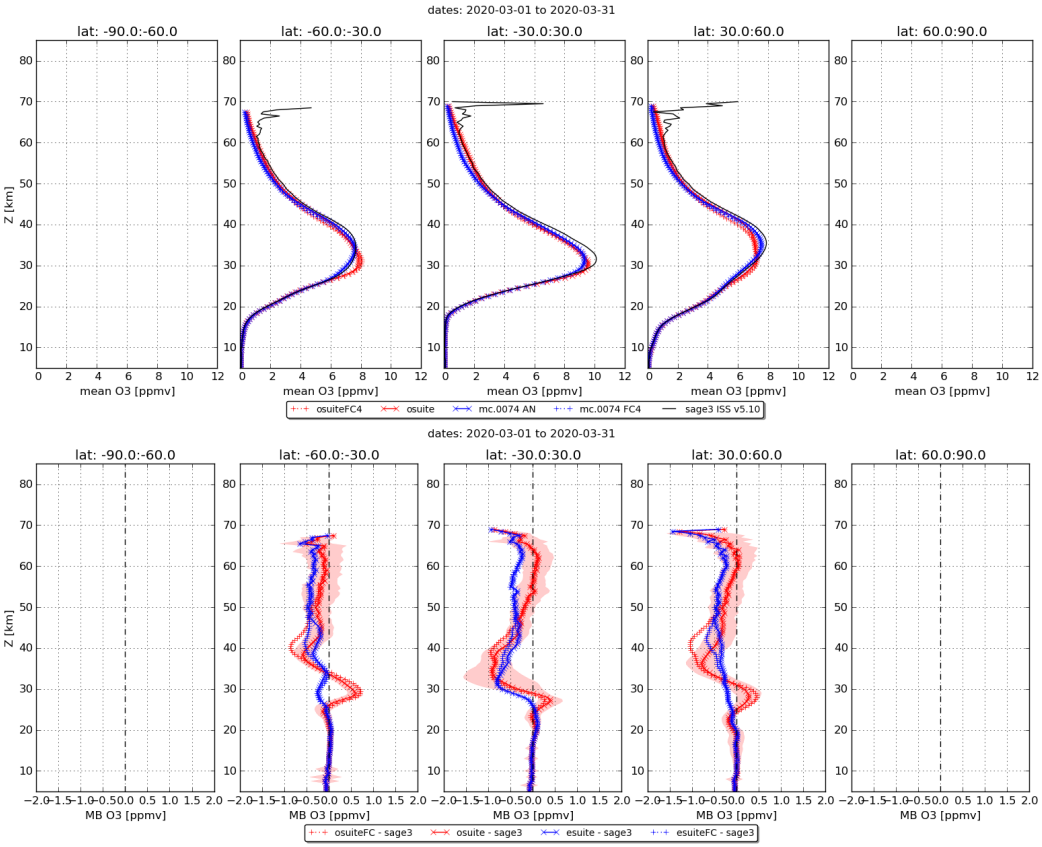
dates: 2020-03-01 to 2020-03-31
lat: -90.0:-60.0
lat: -60.0:-30.0
lat: -30.0:30.0
lat: 30.0:60.0
lat: 60.0:90.0
Z [km]
mean O3 [ppmv]
osuiteFC4
osuite
mc.0074 AN
mc.0074 FC4
sage3 ISS v5.10
dates: 2020-03-01 to 2020-03-31
MB O3 [ppmv]
osuiteFC - sage3
osuite - sage3
esuite - sage3
esuiteFC - sage3

(e)

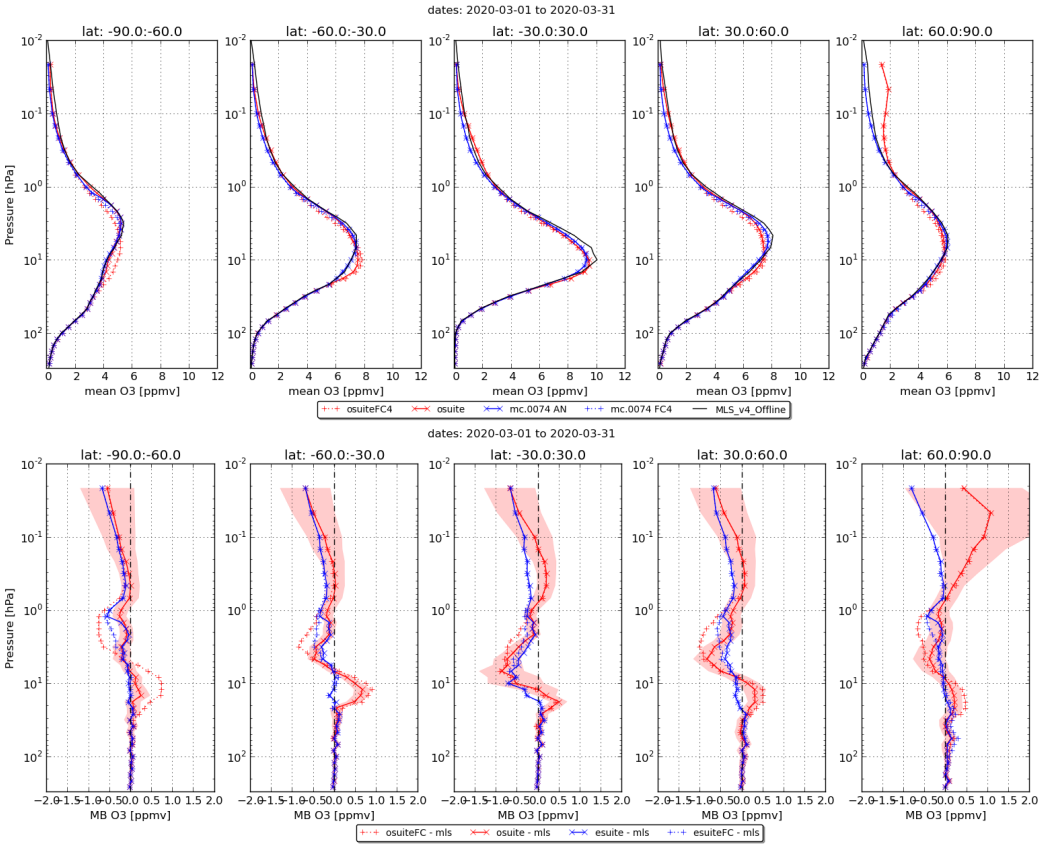
dates: 2020-03-01 to 2020-03-31
lat: -90.0:-60.0
lat: -60.0:-30.0
lat: -30.0:30.0
lat: 30.0:60.0
lat: 60.0:90.0
Pressure [hPa]
mean O3 [ppmv]
osuiteFC4
osuite
mc.0074 AN
mc.0074 FC4
MLS_v4_Offline
dates: 2020-03-01 to 2020-03-31
MB O3 [ppmv]
osuiteFC - mls
osuite - mls
esuite - mls
esuiteFC - mls

(f)

2.18 Stratospheric ozone: Comparison with NDACC observations

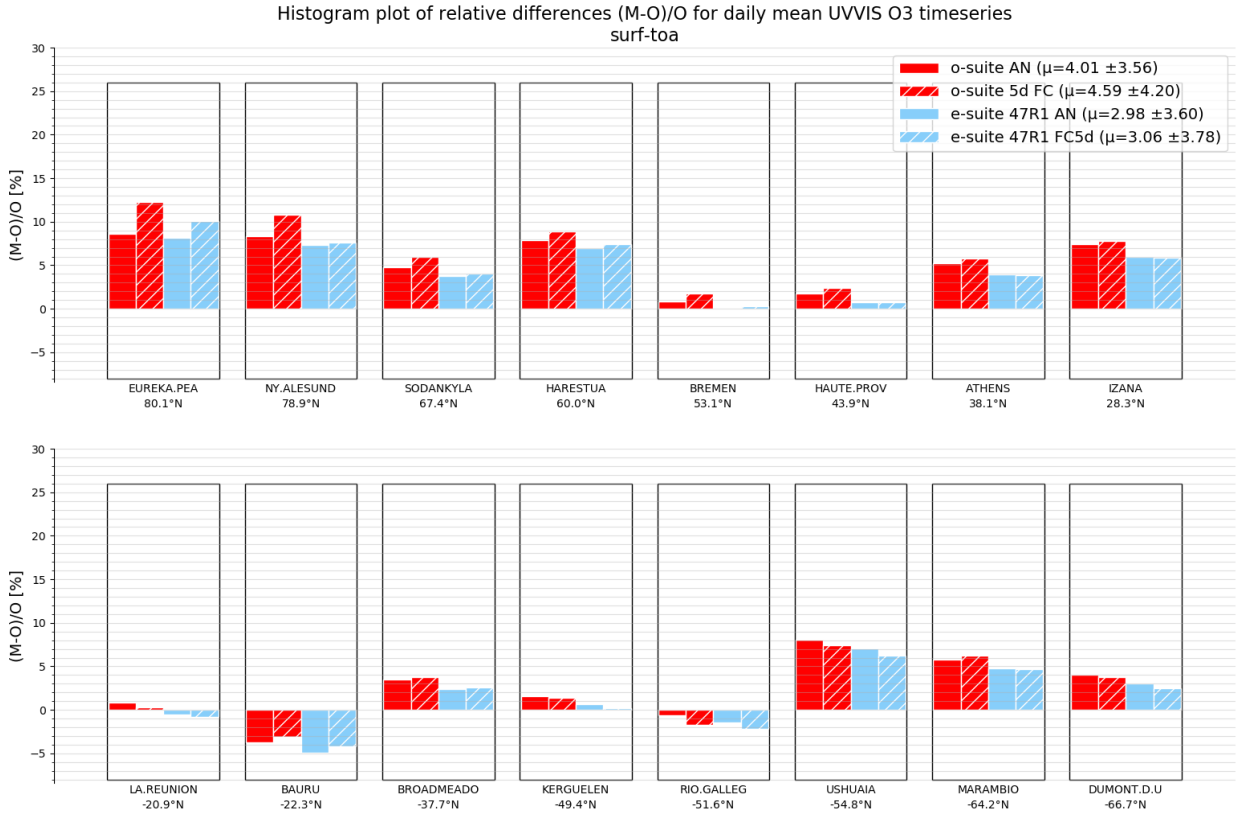

Fig. 2.18.1.: Comparison of averaged relative differences for stratospheric ozone columns between the o-suite and e-suite analysis and 5-day forecast. Stratospheric column bias in the e-suite decreased and falls within the measurement uncertainty of 5% at most sites.

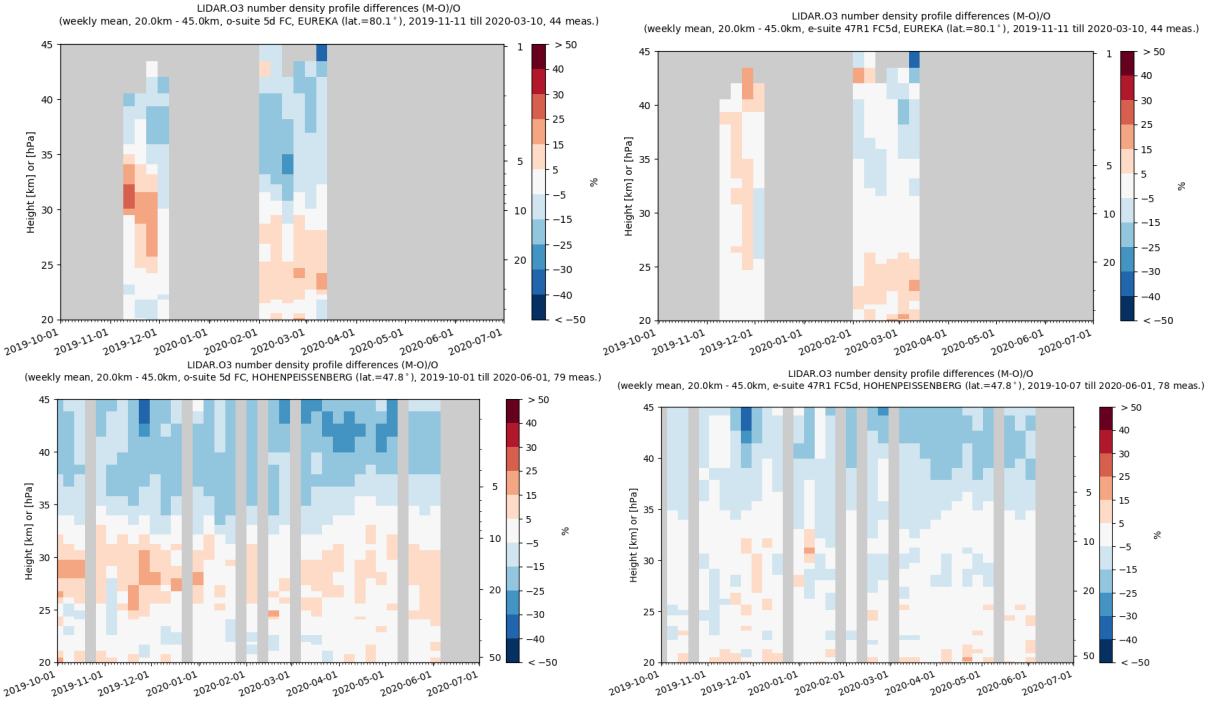

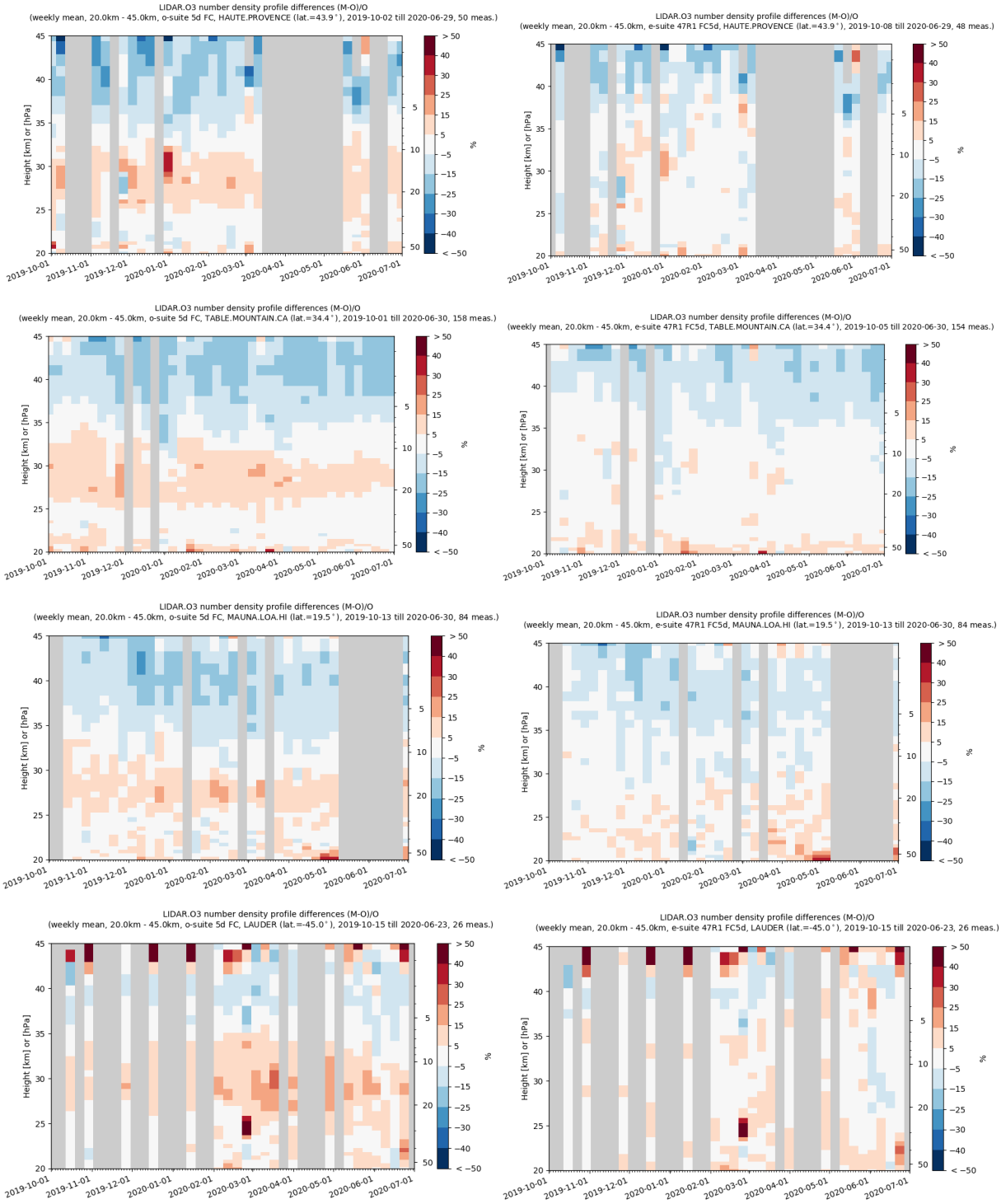

Fig. 2.18.2.: Comparison of weekly mean relative difference of the 5-day FC ozone profiles against LIDAR between the o-suite (left column) and e-suite (right column). All LIDAR stations see an improved profile shape performance of the e-suite. LIDAR measurements have increased uncertainty at higher altitudes and above 35km the biases are comparable to the measurement's uncertainty.

2.19 Stratospheric NO2

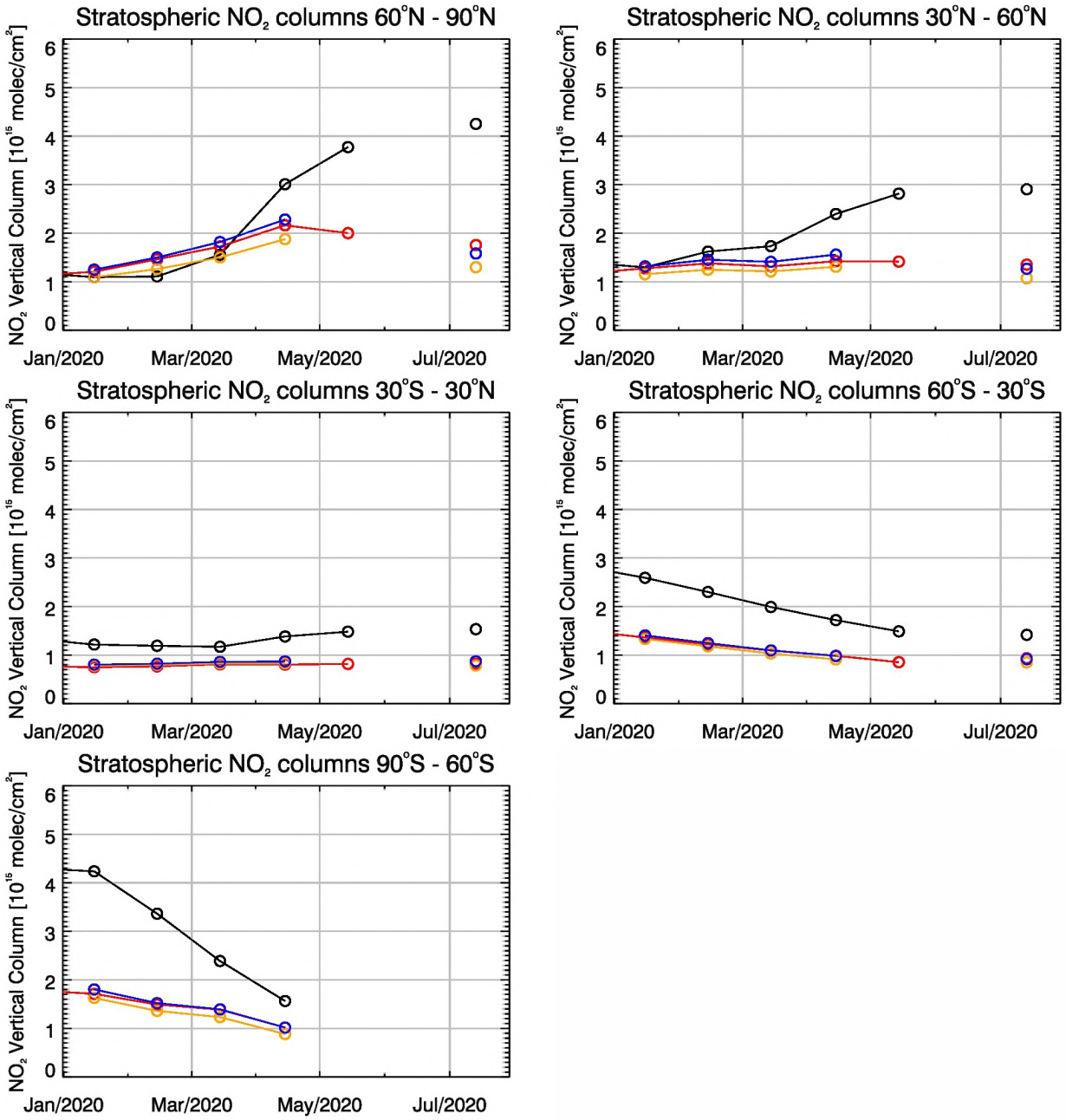

Figure 2.19.1: Time series of average stratospheric NO_2 columns [10^{15} molec cm-2] from (black) GOME-2 compared to the (red) o-suite and (orange) e-suite and (blue) e-suite control for different latitude bands. All model runs show similar values, a good agreement of model results and GOME-2 is not expected as stratospheric chemistry is not implemented in the runs.

2.20 UV radiation

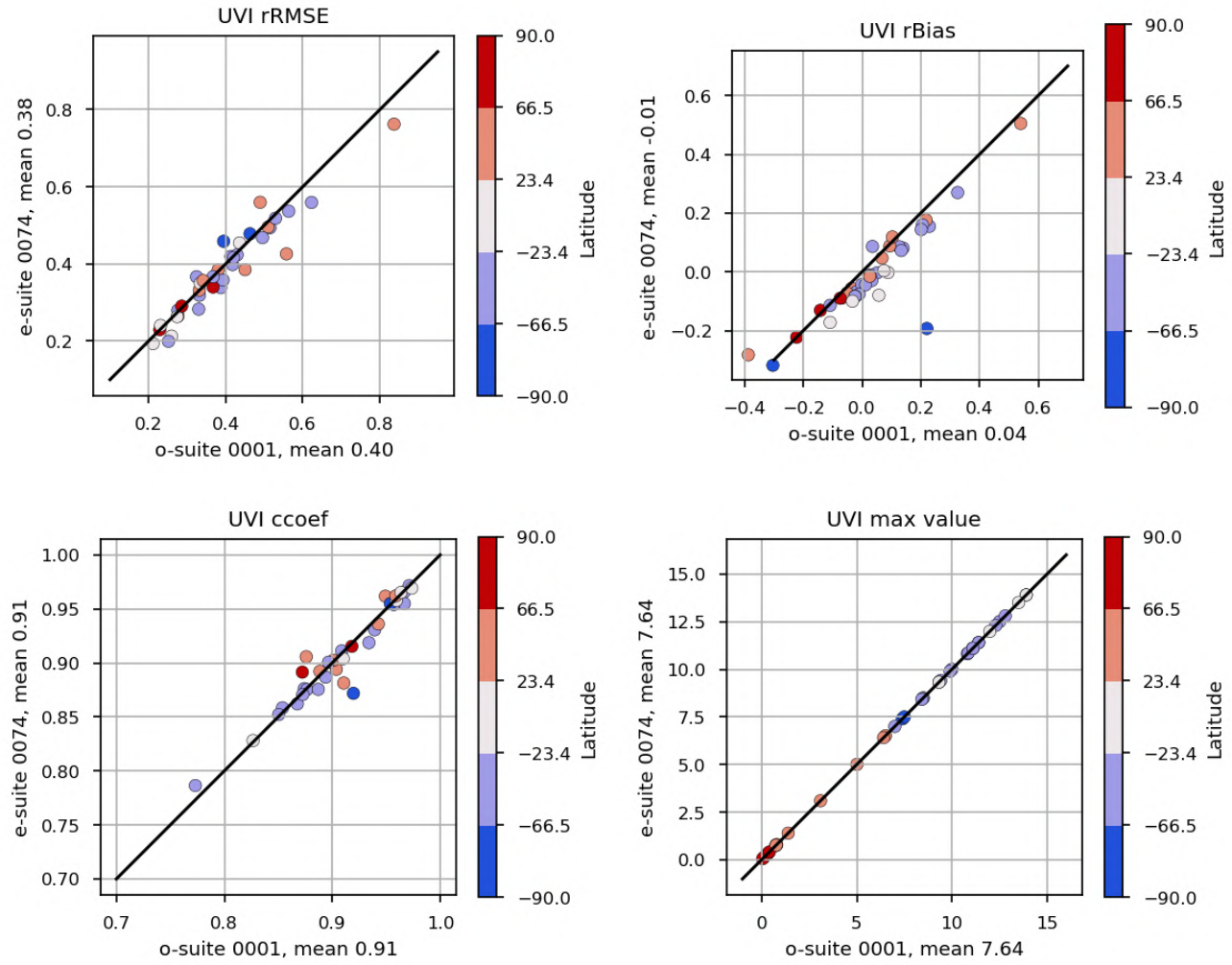

Fig. 2.20.1. Relative RMSE (rRMSE, top left), relative bias (rBias, top right), correlation coefficient (ccoef, bottom left), and maximum UV-Index value (bottom right) between 1 hourly CAMS UV index (1h to 24h forecast) and ground based reference measurements from 2019-12-01 to 2020-02-29. The x-axes show the statistics for the baseline model 46R1 (0001 o-suite) and y-axes show the same statistics for 47R1 (0074, e-suite). Each dot corresponds to one ground-based measurement site (presented in CAMS deliverable D72.2.2.1-2019) at a latitude given in colour bar. The outlier (e.g. rBias) is the Davis station, see Fig. 2.20.2.

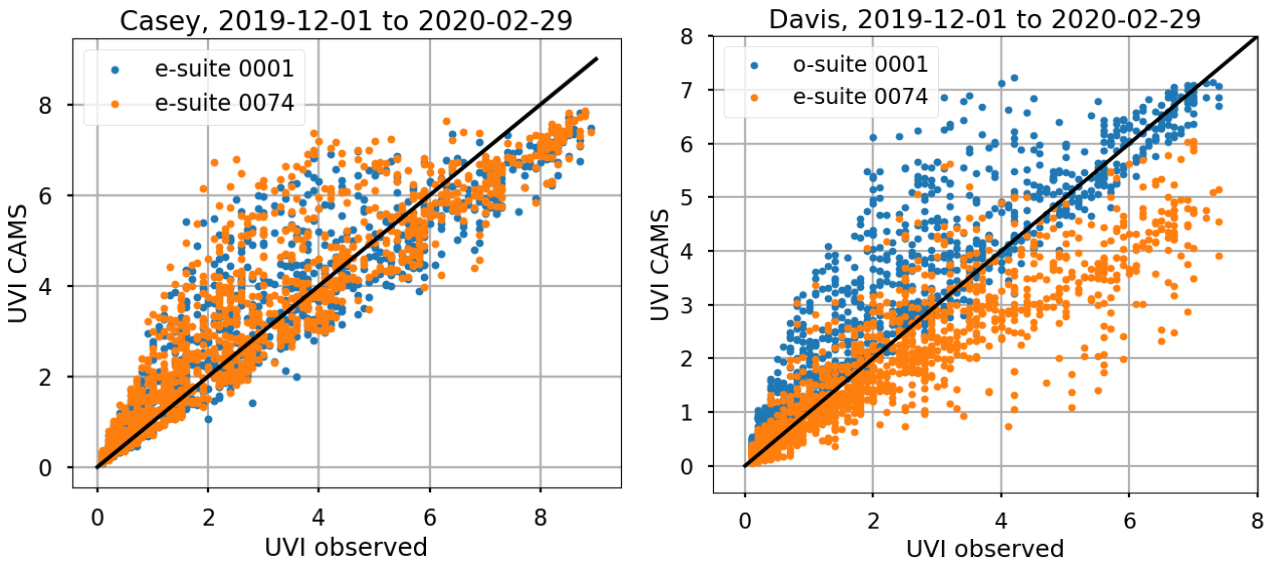

Fig. 2.20.2. UV-Index (UVI) scatter plot: observations against e-suite (orange) and o-suite (blue). In Casey (Antarctica) there is a good match, but Davis (Antarctica) shows a major reduction in the UVI. This difference between the stations indicates that some local and noticeable features degrades the CAMS UVI performance in the Antarctic summer in the e-suite.

3. Greenhouse gases CO2 and CH4

3.1 Comparison against NDACC methane

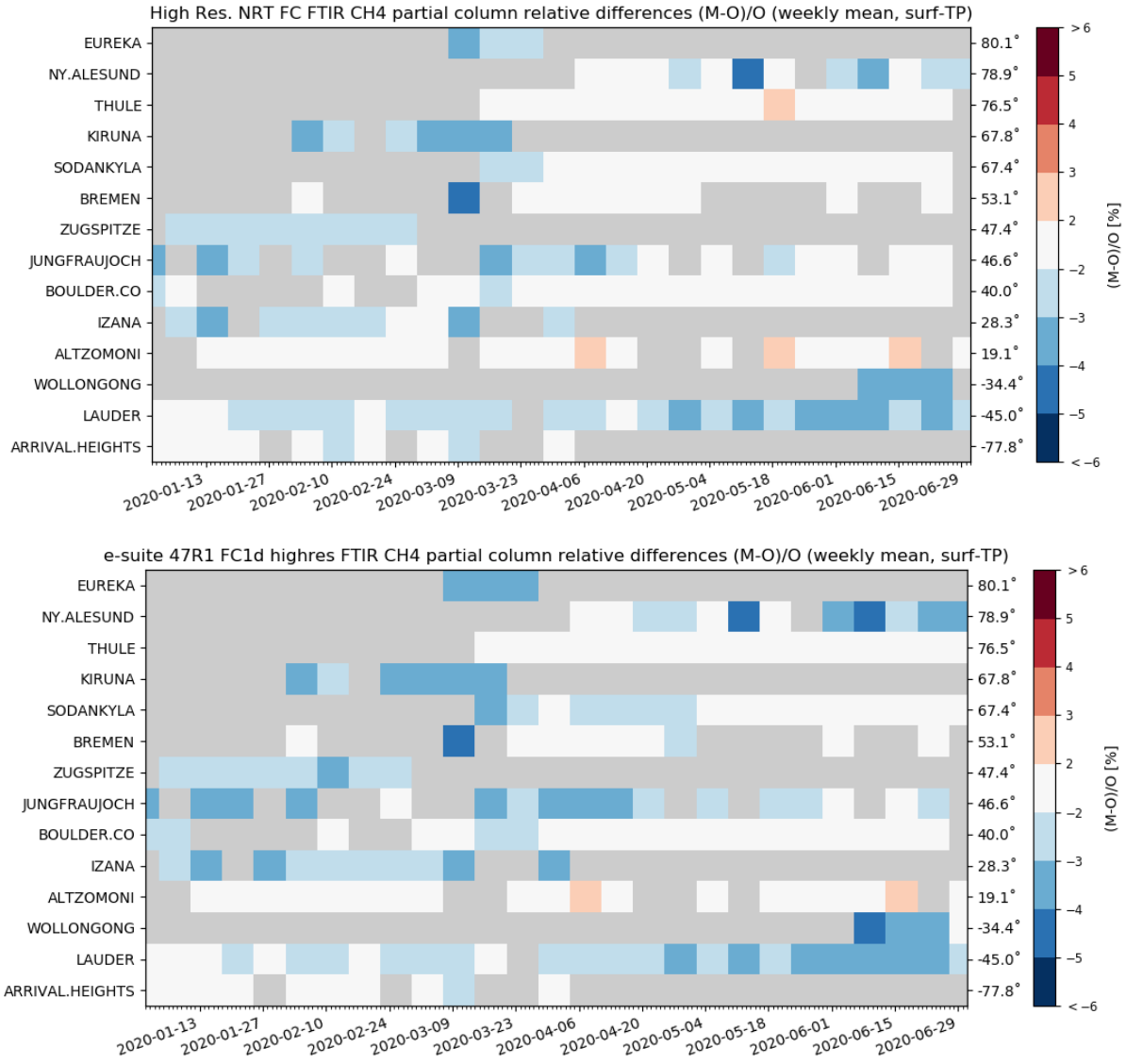

Fig. 3.1.1.: Relative weekly mean bias for tropospheric NDACC CH_4 tropospheric columns (MB, %) for the period Jan 2020-June 2020 for the 1d FC o-suite high resolution (top) and e-suite high-resolution (bottom). The overall uncertainty for the tropospheric CH_4 measurements is approximately 3%. Stations are sorted with decreasing latitude (northern to southern hemisphere). The overall bias has slightly increased (underestimation) in the e-suite.

	o-suite highres					e-suite highres					
NDACC troposphere	#	rel. std	correlation	rel diff bias(%)	rel diff std(%)	#	rel. std	correlation	rel diff bias(%)	rel diff std(%)	lat
EUREKA	11	1	0.99	-2.69	0.61	11	1	0.99	-3.14	0.53	80.1
NY.ALESUND	24	0.9	0.97	-1.94	1.29	23	1	0.97	-2.62	1.24	78.9
THULE	58	1	0.99	0.73	0.97	63	1	0.99	-0.1	0.83	76.5
KIRUNA	17	1	1	-3.31	0.41	16	1	1	-3.53	0.44	67.8
SODANKYLA	55	1	1	-1.22	0.67	55	1	1	-1.96	0.57	67.4
BREMEN	19	1.1	0.87	-0.86	1.6	19	1	0.88	-1.46	1.55	53.1
ZUGSPITZE	22	1	1	-2.53	0.34	20	1	1	-2.71	0.3	47.4
JUNGFRAUJOCH	45	1	0.99	-2.42	0.92	43	1	0.99	-2.97	0.79	46.6
BOULDER.CO	61	0.9	1	-0.54	0.79	60	0.9	1	-1	0.77	40
IZANA	21	1	1	-2.53	0.66	21	1	1	-2.71	0.62	28.3
ALTZOMONI	49	1.1	0.92	1.01	0.7	47	1	0.87	1.01	0.89	19.1
WOLLONGONG	7	1	1	-3.3	0.39	8	1	0.98	-3.17	0.96	-34.4
LAUDER	92	1	0.99	-2.54	0.89	92	1	0.98	-2.57	0.95	-45
ARRIVAL.HEIGHTS	21	1	0.99	-1.74	0.7	19	1	0.99	-1.76	0.74	-77.8
		1	0.98	-1.71	0.78		1	0.97	-2.05	0.8	

Table 3.1.1 Overview of o-suite/e-suite high resolution 1d FC performance against the NDACC FTIR tropospheric CH_4 column. While the correlations are similar, the e-suite high resolution 1d FC has a slightly higher negative bias for all stations in the northern hemisphere. In the southern hemisphere the biases are very similar. Similar conclusions are found for the analysis.

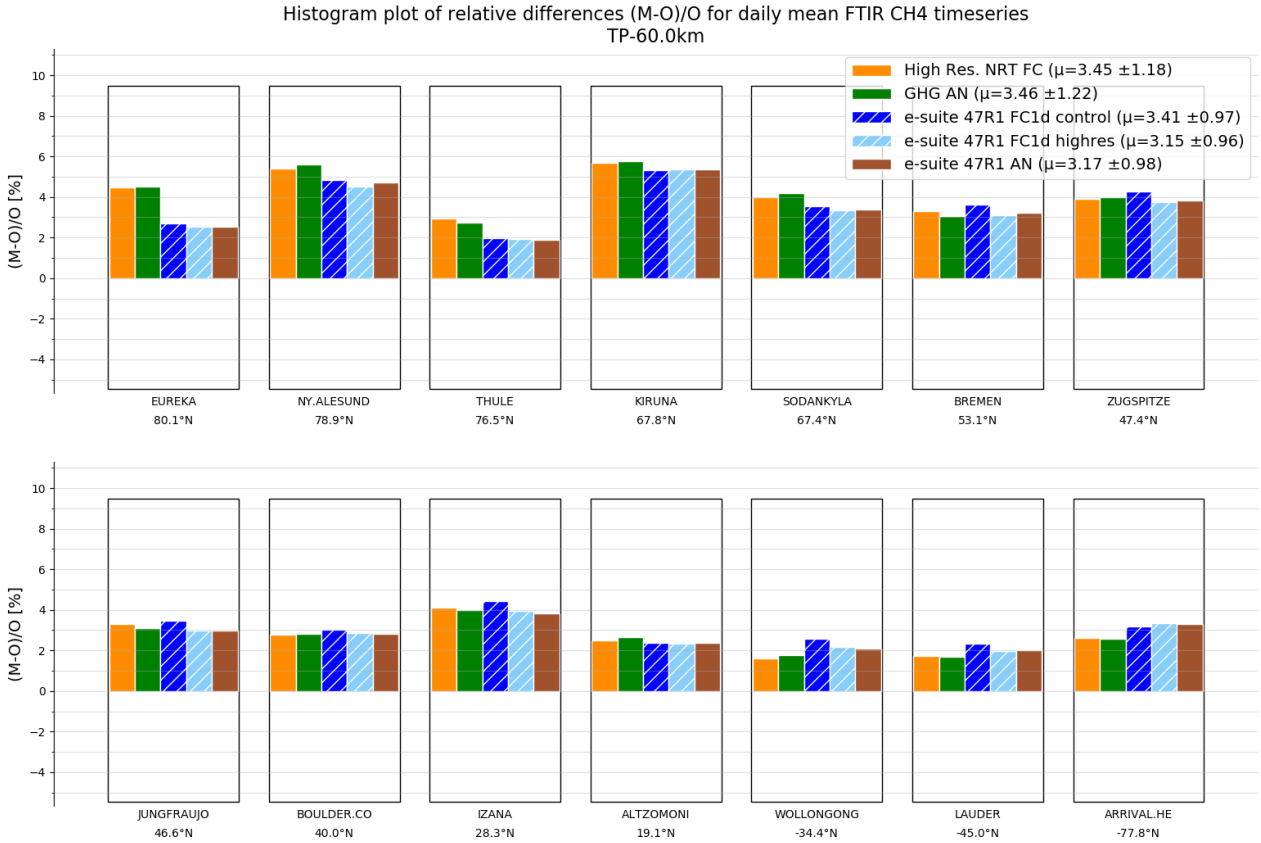

Fig. 3.1.2.: Averaged relative bias for stratospheric CH_4 columns compared against FTIR observations. The o-suite analysis and high-resolution simulation, and e-suite analysis and high-resolution simulation behave similar in the stratosphere

3.2 Comparison against TCCON methane

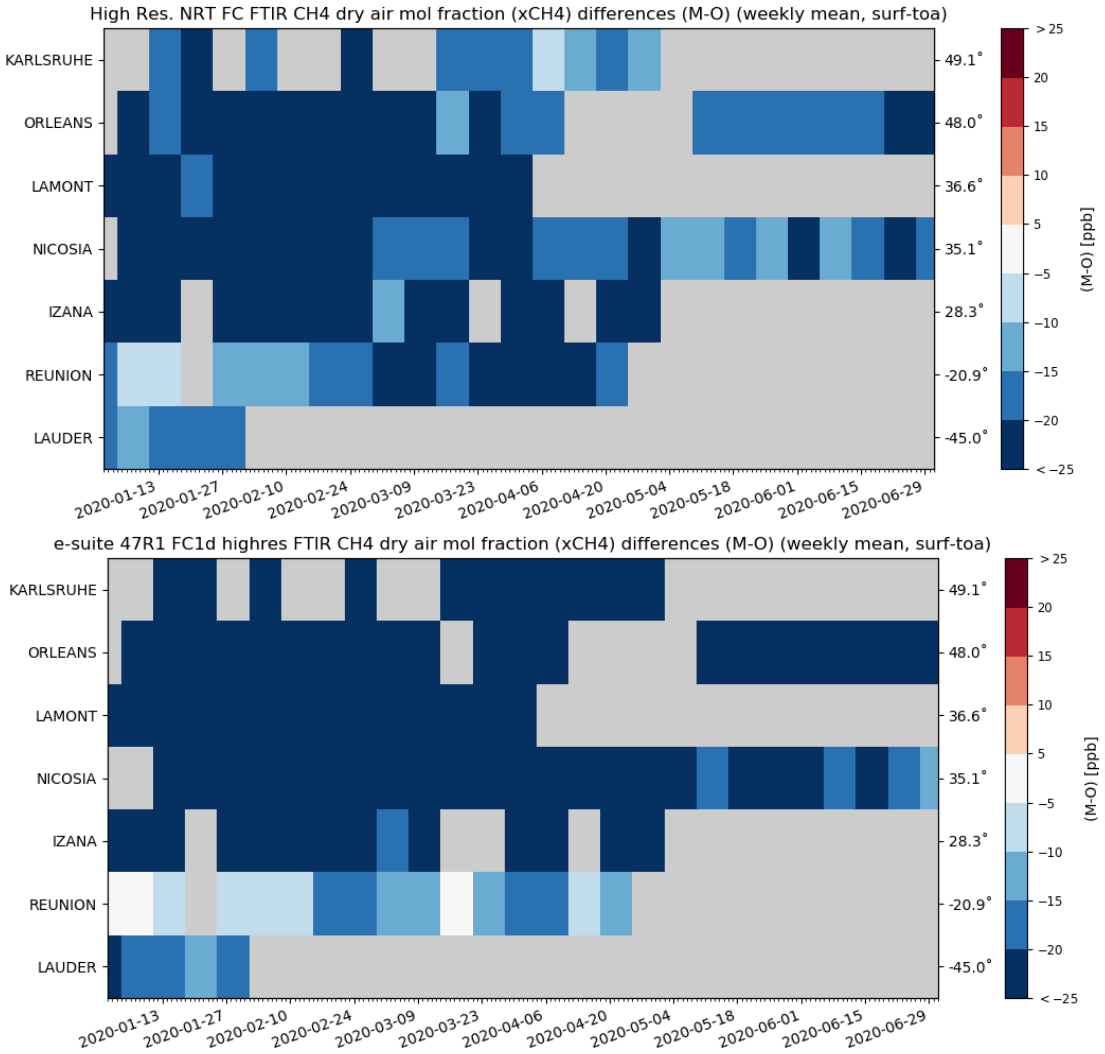

Fig. 3.2.1. Comparison against TCCON methane. Weekly mean differences for the period Jan 2020-June 2020 for the 1d FC o-suite high resolution (top) and e-suite high resolution (bottom). Stations are sorted with decreasing latitude (northern to southern hemisphere). The overall bias (negative, underestimation) has slightly increased in the e-suite.

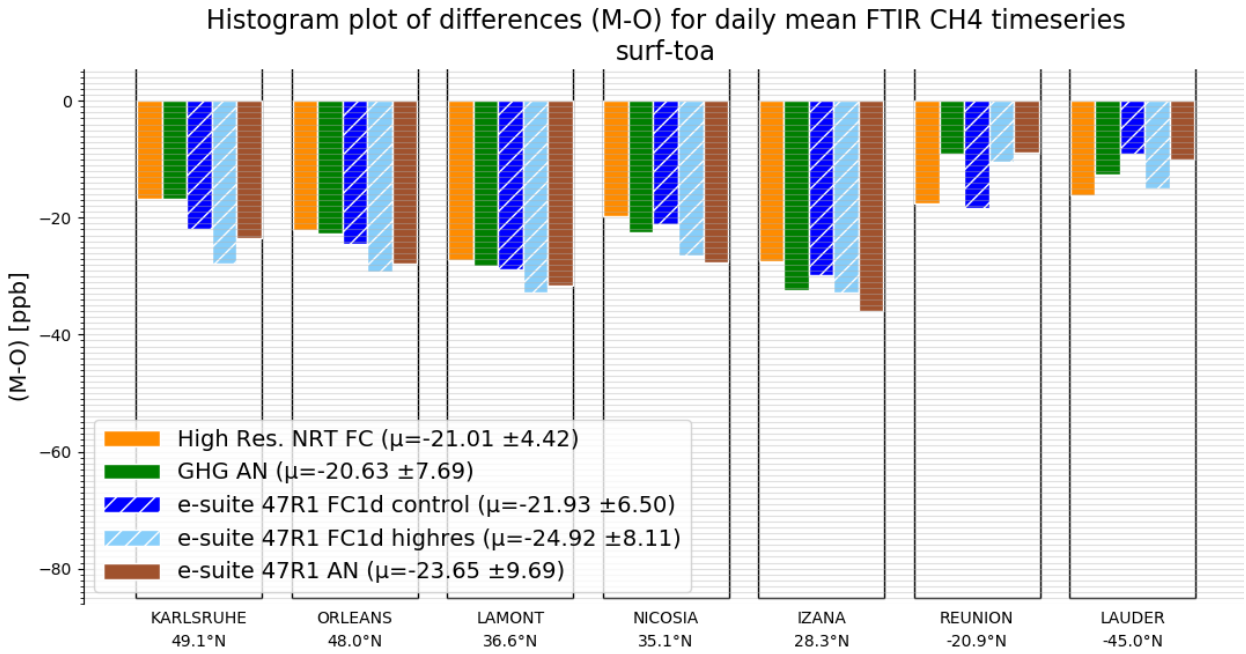

Fig. 3.2.2. Comparison against TCCON methane. Averaged differences for the column averaged mole fractions.

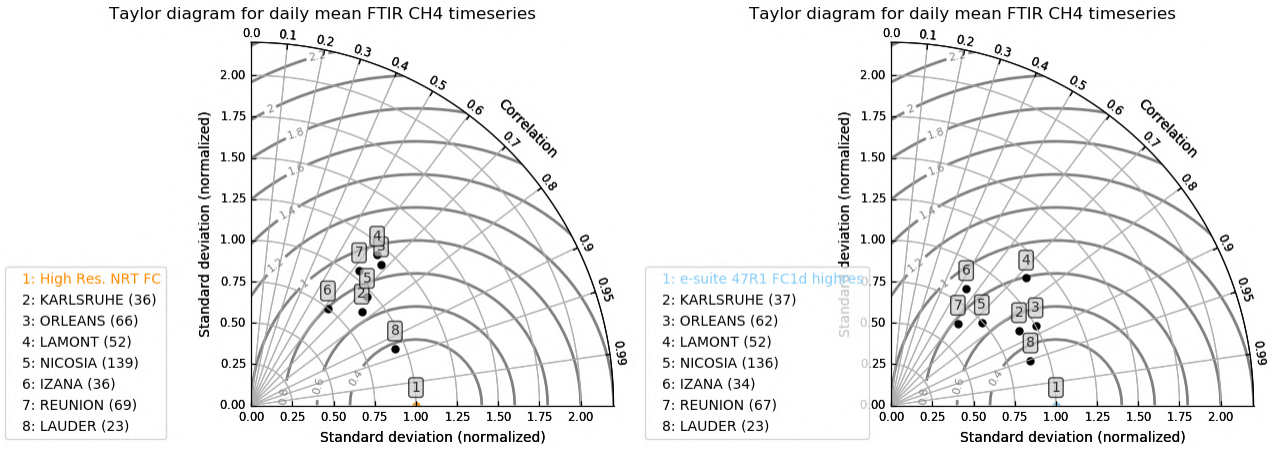

Fig. 3.2.3. Comparison against TCCON methane. Taylor diagrams for the 1d forecast o-suite high-resolution (left) and e-suite high-resolution (right).

3.3 Comparison against TCCON carbon dioxide

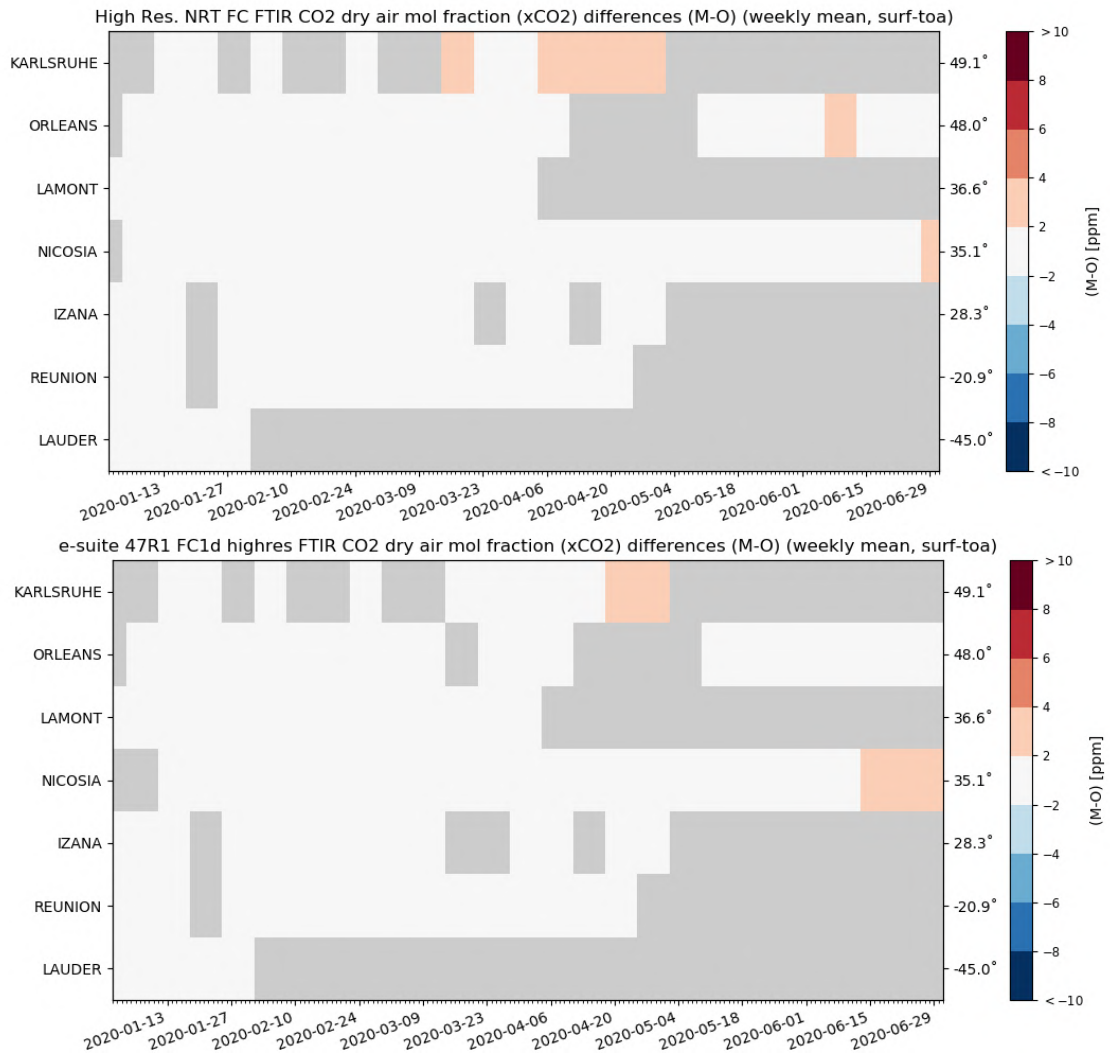

Fig. 3.3.1. Comparison with TCCON CO_2. Weekly mean differences for the period Jan 2020-June 2020 for the 1d FC o-suite high-resolution (top) and e-suite high-resolution (bottom). Stations are sorted with decreasing latitude (northern to southern hemisphere). The overall bias has slightly increased (underestimation) in the e-suite.

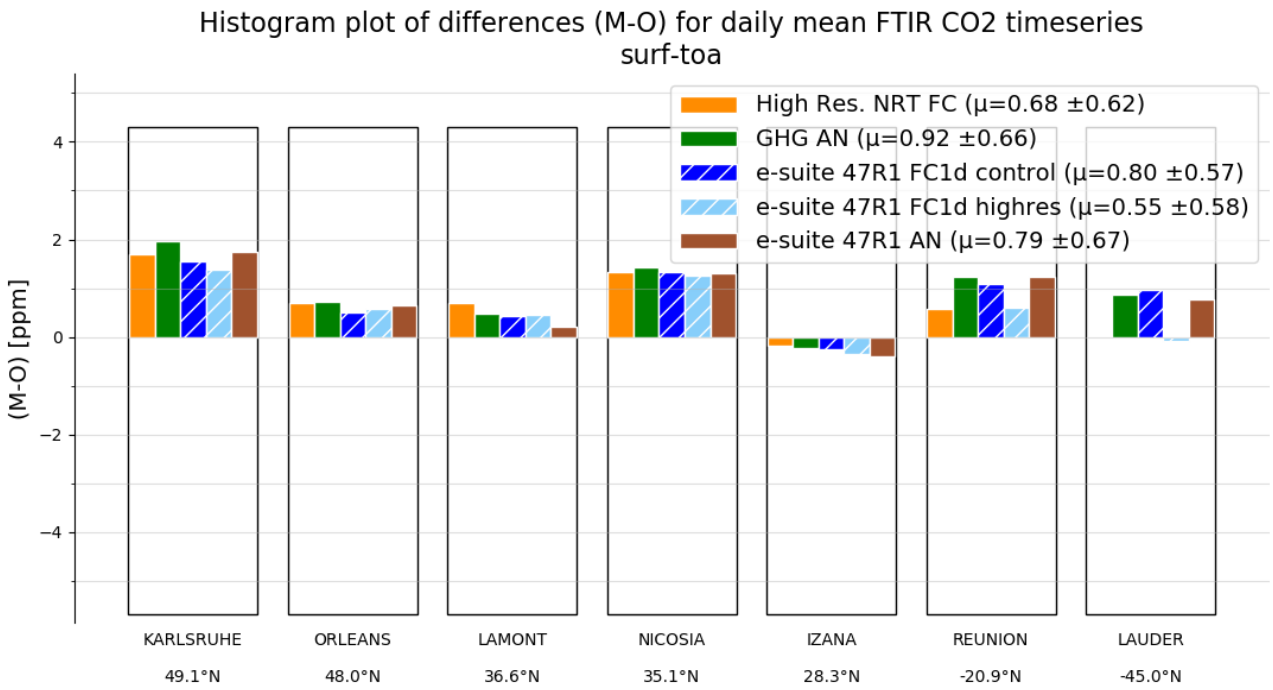

Fig. 3.3.2. Comparison with TCCON CO_2. Averaged differences for the column averaged mole fractions. The new 47R1 configurations perform comparably to the 46R1 (o-suite) runs.

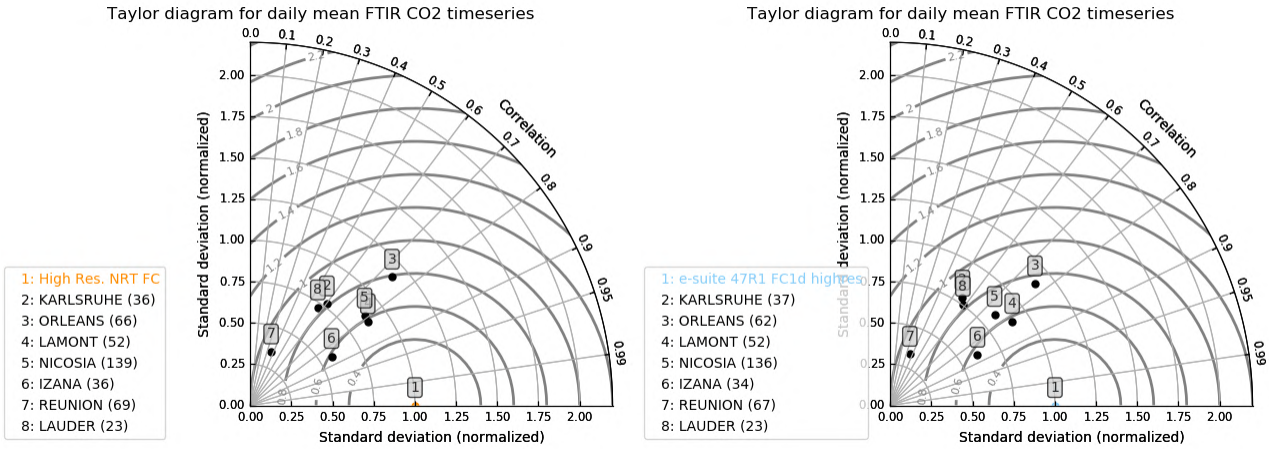

Fig. 3.3.3.: Comparison with TCCON CO_2. Taylor diagrams for the 1d FC o-suite high-resolution (left) and e-suite high-resolution (right). The performance is comparable.

3.4 Comparison against ICOS methane surface data

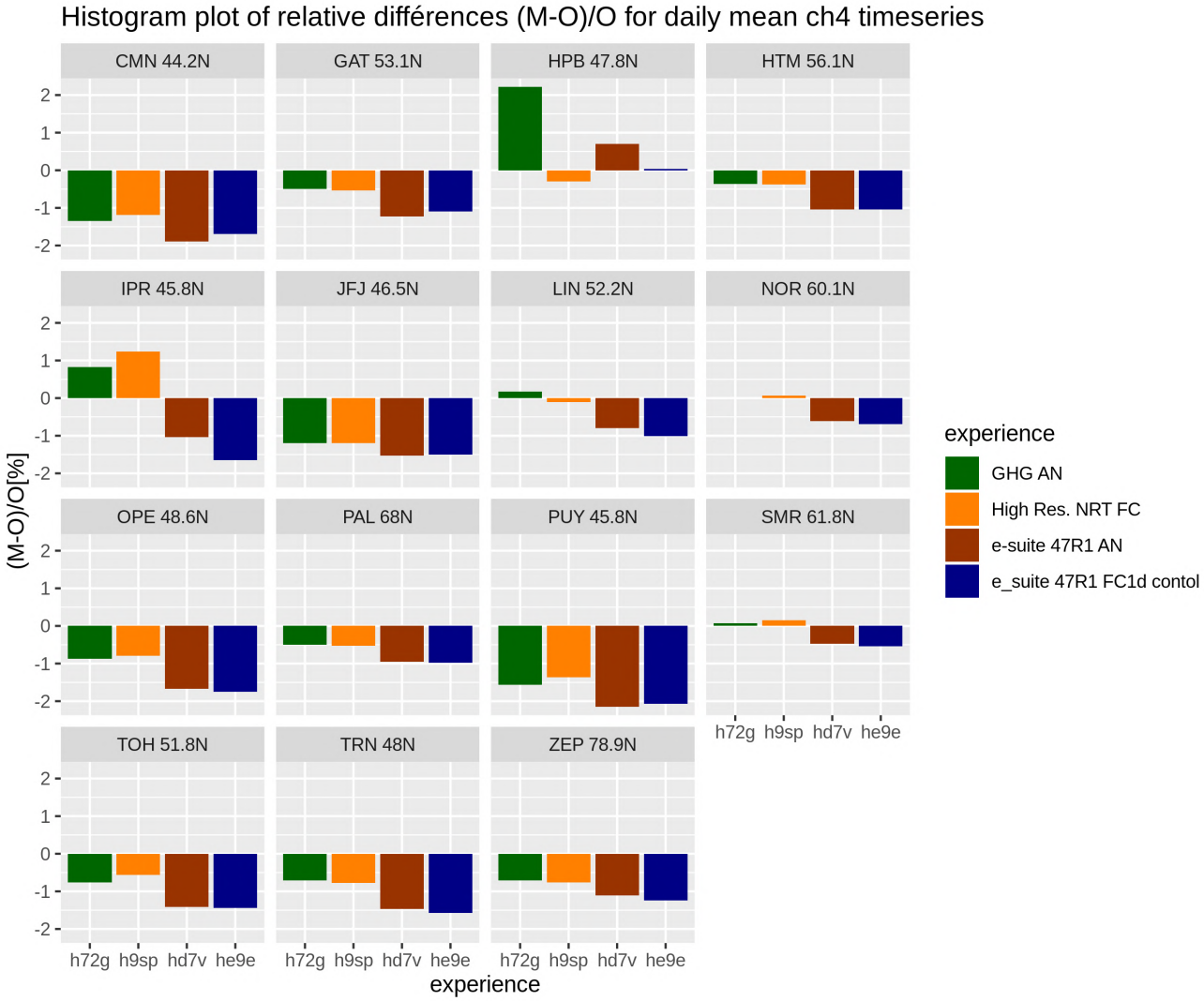

Figure 3.4.1: Comparison against ICOS methane data. Averaged relative bias for surface CH_4 measurements (1st Jan to 1st June 2020). The o-suite analysis and high-resolution forecasts are shown in green and orange respectively. The e-suite analysis and control run are shown in brick and blue colors. All sites, except HPB, show higher negative biases for e-suites runs compared to o-suite. The differences are on the order of 1%.

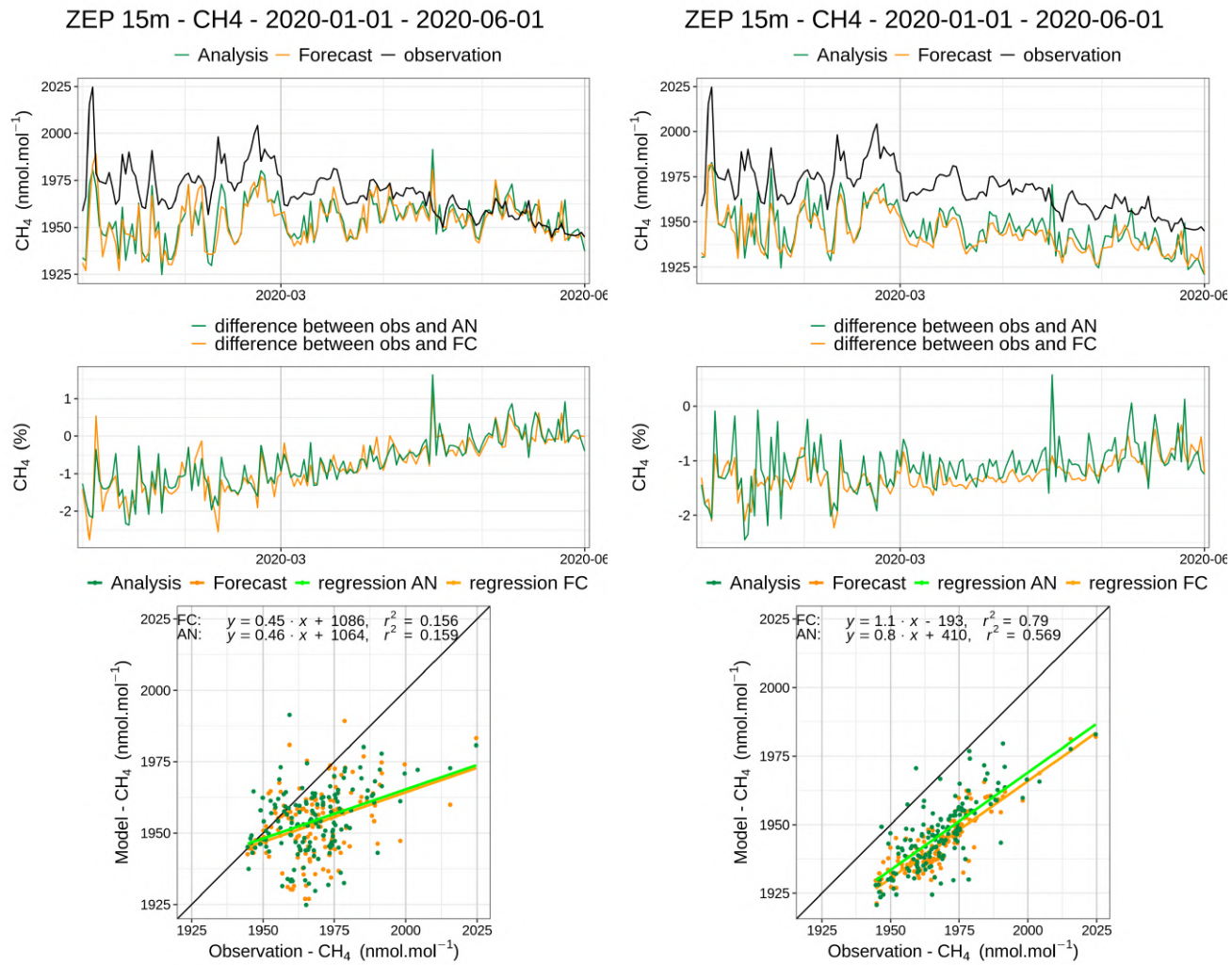

Figure 3.4.2: Comparison of the o-suite (left) and e-suite (right) runs for CH_4 at Zeppelin. This comparison shows a seasonal effect. Both o-suite and e-suite runs perform similarly in early 2020, but from March on the o-suite runs get closer from observations. Similar behaviour is observed at most sites.

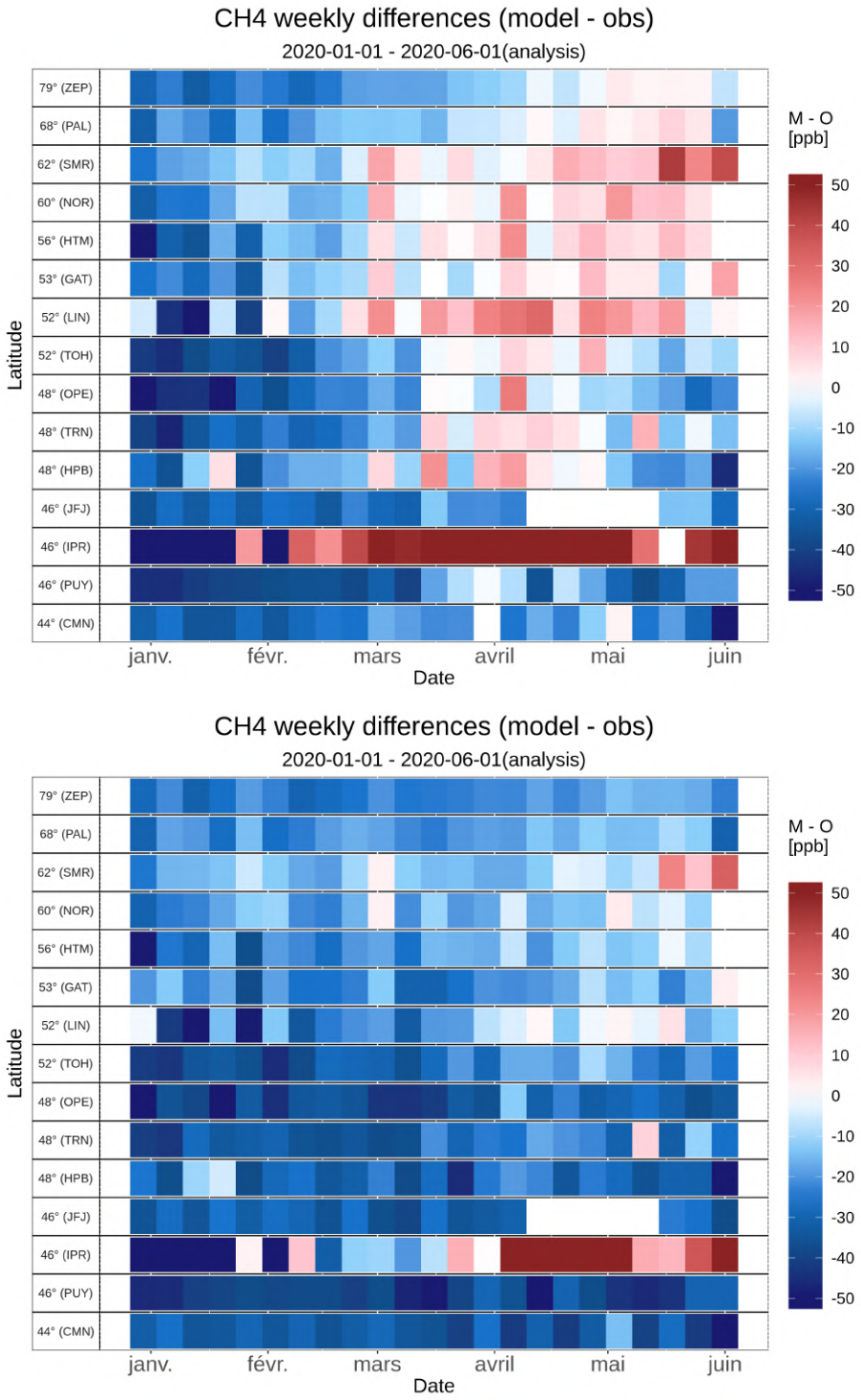

Figure 3.4.3. Comparison against ICOS methane data. Weekly mean differences for the period Jan 2020-June 2020 for the o-suite analysis (top) and e-suite analysis (bottom). Stations are sorted with decreasing latitude (northern to southern hemisphere). Similar negative biases are observed in early 2020, but the e-suite biases are not decreasing in spring, contrary to the o-suite.

3.5 Comparison against ICOS carbon dioxide surface data

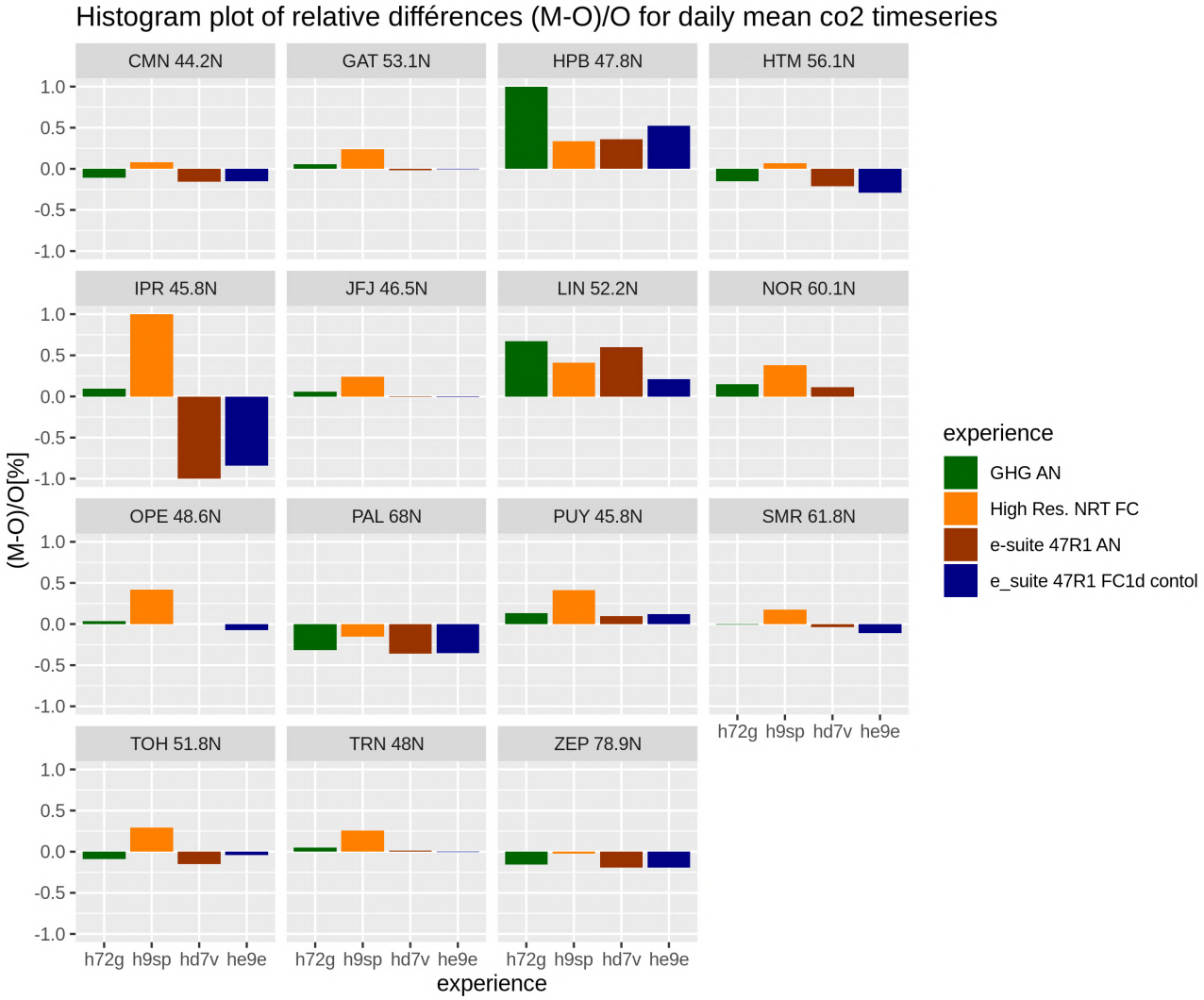

Figure 3.5.1: Same as Figure 3.4.1, but for CO_2. There is no significant difference emerging between o-suite and e-suite experiments.

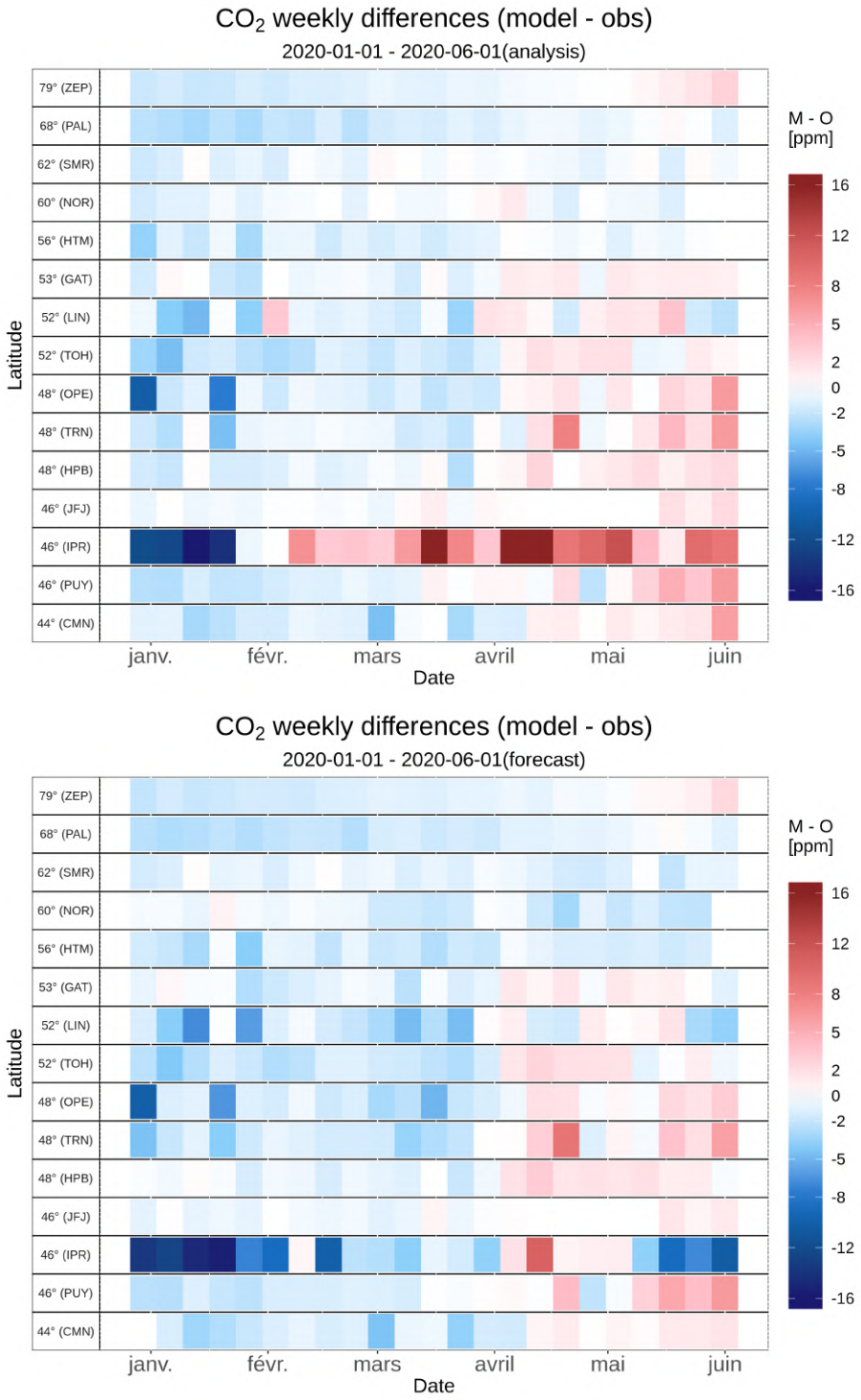

Figure 3.5.2: Same as Figure 3.4.3, but for CO_2. There are no significant differences emerging between o-suite and e-suite experiments.

4. References

Albert, M. F. M. A., Anguelova, M. D., Manders, A. M. M., Schaap, M., and de Leeuw, G.: Parameterization of oceanic whitecap fraction based on satellite observations, Atmos. Chem. Phys., 16, 13725–13751, https://doi.org/10.5194/acp-16-13725-2016, 2016.

Agusti-Panareda, A., Monitoring upgrades of analysis/forecast system, MACC-III Deliverable D44.04, June 2015.

Basart, S, A. Benedictow, Y. Bennouna, A.-M. Blechschmidt, S. Chabrillat, Y. Christophe, E. Cuevas, H. J. Eskes, K. M. Hansen, O. Jorba, J. Kapsomenakis, B. Langerock, T. Pay, A. Richter, N. Sudarchikova, M. Schulz, A. Wagner, C. Zerefos, Upgrade verification note for the CAMS real-time global atmospheric composition service: Evaluation of the e- suite for the CAMS upgrade of July 2019, Copernicus Atmosphere Monitoring Service (CAMS) report, CAMS84_2018SC1_D3.2.1-201907_esuite_v1.pdf, July 2019, doi:10.24380/fcwq-yp50.

Benedetti, A., J.-J. Morcrette, O. Boucher, A. Dethof, R. J. Engelen, M. Fisher, H. Flentjes, N. Huneeus, L. Jones, J. W. Kaiser, S. Kinne, A. Mangold, M. Razinger, A. J. Simmons, M. Suttie, and the GEMS-AER team: Aerosol analysis and forecast in the ECMWF Integrated Forecast System. Part II : Data assimilation, J. Geophys. Res., 114, D13205, doi:10.1029/2008JD011115, 2009.

Bergamaschi, P., Frankenberg, C., Meirink, J. F., Krol, M., Villani, M. G., Houweling, S., Dentener, F., Dlugokencky, E. J., Miller, J. B., Gatti, L. V., Engel, A., and Levin, I.: Inverse modeling of global and regional CH4 emissions using SCIAMACHY satellite retrievals, J. Geophys. Res., 114, D22301, doi:10.1029/2009JD012287, 2009.

Boussetta, S., Balsamo, G., Beljaars, A., Agusti-Panareda, A., Calvet, J.-C., Jacobs, C., van den Hurk, B., Viterbo, P., Lafont, S., Dutra, E., Jarlan, L., Balzarolo, M., Papale, D., and van der Werf, G.: Natural carbon dioxide exchanges in the ECMWF Integrated Forecasting System: implementation and offline validation, J. Geophys. Res.-Atmos., 118, 1–24, doi: 10.1002/jgrd.50488, 2013.

Cariolle, D. and Teyssèdre, H.: A revised linear ozone photochemistry parameterization for use in transport and general circulation models: multi-annual simulations, Atmos. Chem. Phys., 7, 2183-2196, doi:10.5194/acp-7-2183-2007, 2007.

Carn, S. A., V. E. Fioletov, C. A. McLinden, C. Li & N. A. Krotkov, A decade of global volcanic SO2 emissions measured from space, Scientific Reports volume 7, Article number: 44095 (2017).

Dee, D. P. and S. Uppala, Variational bias correction of satellite radiance data in the ERA-Interim reanalysis. Quart. J. Roy. Meteor. Soc.,135, 1830-1841, 2009.

Eskes, H., Huijnen, V., Arola, A., Benedictow, A., Blechschmidt, A.-M., Botek, E., Boucher, O., Bouarar, I., Chabrillat, S., Cuevas, E., Engelen, R., Flentje, H., Gaudel, A., Griesfeller, J., Jones, L., Kapsomenakis, J., Katragkou, E., Kinne, S., Langerock, B., Razinger, M., Richter, A., Schultz, M., Schulz, M., Sudarchikova, N., Thouret, V., Vrekoussis, M., Wagner, A., and Zerefos, C.: Validation of reactive gases and aerosols in the MACC global analysis and forecast system, Geosci. Model Dev., 8, 3523-3543, doi:10.5194/gmd-8-3523-2015, 2015.

Eskes, H.J., S. Basart, A. Benedictow, Y. Bennouna, A.-M. Blechschmidt, S. Chabrillat, Y. Christophe, E. Cuevas, H. Flentje, K. M. Hansen, J. Kapsomenakis, B. Langerock, M. Ramonet, A. Richter, M. Schulz, N. Sudarchikova, A. Wagner, T. Warneke, C. Zerefos, Observation characterisation and validation methods document, Copernicus Atmosphere Monitoring Service (CAMS) report, December 2019, doi: 10.24380/0nsd- wb26, December 2019.

Eskes, H. J., S. Basart, A. Benedictow, Y. Bennouna, A.-M. Blechschmidt, S. Chabrillat, Y. Christophe, H. Clark, E. Cuevas, K. M. Hansen, U. Im, J. Kapsomenakis, B. Langerock, K. Petersen, M. Schulz, A. Wagner, C. Zerefos, Upgrade verification note for the CAMS near-real time global atmospheric composition service, Copernicus Atmosphere Monitoring Service (CAMS) report, CAMS84_2015SC3_D84.3.1.5_201802_esuite_v1.pdf, February 2018 (2018)

Eskes et al., Upgrade verification note for the CAMS near-real time global atmospheric composition service, Addendum July 2018, CAMS84_2015SC3_D84.3.1.5_201802_esuite_v1.pdf (2018c).

Flemming, J., Huijnen, V., Arteta, J., Bechtold, P., Beljaars, A., Blechschmidt, A.-M., Diamantakis, M., Engelen, R. J., Gaudel, A., Inness, A., Jones, L., Josse, B., Katragkou, E., Marecal, V., Peuch, V.-H., Richter, A., Schultz, M. G., Stein, O., and Tsikerdekis, A.: Tropospheric chemistry in the Integrated Forecasting System of ECMWF, Geosci. Model Dev., 8, 975-1003, doi:10.5194/gmd-8-975-2015, 2015.

Flemming, J., Benedetti, A., Inness, A., Engelen, R. J., Jones, L., Huijnen, V., Remy, S., Parrington, M., Suttie, M., Bozzo, A., Peuch, V.-H., Akritidis, D., and Katragkou, E.: The CAMS interim Reanalysis of Carbon Monoxide, Ozone and Aerosol for 2003–2015, Atmos. Chem. Phys., 17, 1945-1983, doi:10.5194/acp-17-1945-2017, 2017.

Granier, C. et al.: Evolution of anthropogenic and biomass burning emissions of air pollutants at global and regional scales during the 1980–2010 period. Climatic Change (109), 2011

Huijnen, V., et al.: The global chemistry transport model TM5: description and evaluation of the tropospheric chemistry version 3.0, Geosci. Model Dev., 3, 445-473, doi:10.5194/gmd-3-445-2010, 2010.

Inness, A., Blechschmidt, A.-M., Bouarar, I., Chabrillat, S., Crepulja, M., Engelen, R. J., Eskes, H., Flemming, J., Gaudel, A., Hendrick, F., Huijnen, V., Jones, L., Kapsomenakis, J., Katragkou, E., Keppens, A., Langerock, B., de Mazière, M., Melas, D., Parrington, M., Peuch, V. H., Razinger, M., Richter, A., Schultz, M. G., Suttie, M., Thouret, V., Vrekoussis, M., Wagner, A., and Zerefos, C.: Data assimilation of satellite-retrieved ozone, carbon monoxide and nitrogen dioxide with ECMWF's Composition-IFS, Atmos. Chem. Phys., 15, 5275-5303, doi:10.5194/acp-15-5275-2015, 2015.

Janssens-Maenhout, G., Dentener, F., Aardenne, J. V., Monni, S., Pagliari, V., Orlandini, L., Klimont, Z., Kurokawa, J., Akimoto, H., Ohara, T., Wankmueller, R., Battye, B., Grano, D., Zuber, A., and Keating, T.: EDGAR-HTAP: a Harmonized Gridded Air Pollution Emission Dataset Based on National Inventories, JRC68434, EUR report No EUR 25 299–2012, ISBN 978-92-79- 23122-0, ISSN 1831-9424, European Commission Publications Office, Ispra (Italy), 2012.

Kaiser, J. W., Heil, A., Andreae, M. O., Benedetti, A., Chubarova, N., Jones, L., Morcrette, J.-J., Razinger, M., Schultz, M. G., Suttie, M., and van der Werf, G. R.: Biomass burning emissions estimated with a global fire assimilation system based on observed fire radiative power, Biogeosciences, 9, 527-554, doi:10.5194/bg-9-527-2012, 2012.

Massart, S., Flemming, J., Cariolle, D., Jones, L., High resolution CO tracer forecasts, MACC-III Deliverable D22.04, May 2015, available from http://www.gmes-atmosphere.eu/documents/macciii/deliverables/grg

Morcrette, J.-J., O. Boucher, L. Jones, D. Salmond, P. Bechtold, A. Beljaars, A. Benedetti, A. Bonet, J. W. Kaiser, M. Razinger, M. Schulz, S. Serrar, A. J. Simmons, M. Sofiev, M. Suttie, A. M. Tompkins, and A. Untch: Aerosol analysis and forecast in the ECMWF Integrated Forecast System. Part I: Forward modelling, J. Geophys. Res., 114, D06206, doi:10.1029/2008JD011235, 2009.

Rémy, S., Kipling, Z., Flemming, J., Boucher, O., Nabat, P., Michou, M., Bozzo, A., Ades, M., Huijnen, V., Benedetti, A., Engelen, R., Peuch, V.-H., and Morcrette, J.-J.: Description and evaluation of the tropospheric aerosol scheme in the European Centre for Medium-Range Weather Forecasts (ECMWF) Integrated Forecasting System (IFS-AER, cycle 45R1), Geosci. Model Dev., 12, 4627–4659, https://doi.org/10.5194/gmd-12-4627-2019, 2019.

Schulz, M., Y. Christophe, M. Ramonet, Wagner, A., H. J. Eskes, S. Basart, A. Benedictow, Y. Bennouna, A.-M. Blechschmidt, S. Chabrillat, E. Cuevas, A. El- Yazidi, H. Flentje, P. Fritzsche, K.M. Hansen, U. Im, J. Kapsomenakis, B. Langerock, A. Richter, N. Sudarchikova, V. Thouret, T. Warneke, C. Zerefos, Validation report of the CAMS near-real-time global atmospheric composition service: Period December 2019 – February 2020, Copernicus Atmosphere Monitoring Service (CAMS) report, CAMS84_2018SC2_D1.1.1_DJF2020.pdf, June 2020, doi:10.24380/322n-jn39.

Sindelarova, K., Granier, C., Bouarar, I., Guenther, A., Tilmes, S., Stavrakou, T., Müller, J.-F., Kuhn, U., Stefani, P., and Knorr, W.: Global data set of biogenic VOC emissions calculated by the MEGAN model over the last 30 years, Atmos. Chem. Phys., 14, 9317-9341, doi:10.5194/acp-14-9317-2014, 2014.

Williams, J. E., van Velthoven, P. F. J., and Brenninkmeijer, C. A. M.: Quantifying the uncertainty in simulating global tropo- spheric composition due to the variability in global emission es- timates of Biogenic Volatile Organic Compounds, Atmos. Chem. Phys., 13, 2857–2891, doi:10.5194/acp-13-2857-2013, 2013.

Annex 1: Acknowledgements for measurements used

We wish to acknowledge the provision of NRT GAW observational data by: Institute of Atmospheric Sciences and Climate (ISAC) of the Italian National Research Council (CNR), South African Weather Service, National Centre for Atmospheric Science (NCAS, Cape Verde), National Air Pollution Monitoring Network (NABEL) (Federal Office for the Environment FOEN and Swiss Federal Laboratories for Materials Testing and Research EMPA), Atmospheric Environment Division Global Environment and Marine Department Japan Meteorological Agency, Chinese Academy of Meteorological Sciences (CAMS), Alfred Wegener Institut, Umweltbundesamt (Austria), National Meteorological Service (Argentina), Umweltbundesamt (UBA, Germany)

We are grateful to the numerous operators of the Aeronet network and to the central data processing facility at NASA Goddard Space Flight Center for providing the NRT sun photometer data, especially Ilya Slutker and Brent Holben for sending the data.

The authors thank to all researchers, data providers and collaborators of the World Meteorological Organization's Sand and Dust Storm Warning Advisory and Assessment System (WMO SDS-WAS) for Northern Africa, Middle East and Europe (NAMEE) Regional Node. Also special thank to Canary Government as well as AERONET, MODIS, U.K. Met Office MSG, MSG Eumetsat and EOSDIS World Viewer principal investigators and scientists for establishing and maintaining data used in the activities of the WMO SDS-WAS NAMEE Regional Center (http://sds-was.aemet.es/).

We wish to acknowledge the provision of ozone sonde data by the World Ozone and Ultraviolet Radiation Data Centre established at EC in Toronto (http://woudc.org), by the Data Host Facility of the Network for the Detection of Atmospheric Composition Change established at NOAA (http://ndacc.org), by the Norwegian Institute for Air Research and by the National Aeronautics and Space Administration (NASA).

We wish to thank the NDACC investigators for the provision of observations at Ny Alesund, Bern, Jungfraujoch, Izaña, Xianghe, Harestua, Reunion Maido, Uccle, Hohenpeissen, Mauna Loa, Lauder and Haute Provence.

The authors acknowledge the NOAA Earth System Research Laboratory (ESRL) Global Monitoring Division (GMD) for the provision of ground-based ozone concentrations.

The MOPITT CO data were obtained from the NASA Langley Research Center ASDC. We acknowledge the LATMOS IASI group for providing IASI CO data.

SCIAMACHY lv1 radiances were provided to IUP-UB by ESA through DLR/DFD.

GOME-2 lv1 radiances were provided to IUP-UB by EUMETSAT.

The authors acknowledge Environment and Climate Change Canada for the provision of Alert ozone data and Sara Crepinsek – NOAA for the provision of Tiksi ozone data. Surface ozone data from the Zeppelin Mountain, Svalbard are from www.luftkvalitet.info. Surface ozone data from the Villum Research Station, Station Nord (VRS) were financially supported by "The Danish Environmental Protection Agency" with means from the MIKA/DANCEA funds for Environmental Support to the

Arctic Region. The Villum Foundation is acknowledged for the large grant making it possible to build VRS in North Greenland.

We acknowledge the National Aeronautics and Space Administration (NASA), USA for providing the OMPS limb sounder data (http://npp.gsfc.nasa.gov/omps.html) and the Aura-MLS offline data (http://mls.jpl.nasa.gov/index-eos-mls.php).

We thank the Canadian Space Agency and ACE science team for providing level 2 data retrieved from ACE-FTS on the Canadian satellite SCISAT-1.

The European Environment Information and Observation Network (Eionet) Air Quality portal provides details relevant for the reporting of air quality information from EU Member States and other EEA member and co-operating countries. This information is submitted according to Directives 2004/107/EC and 2008/50/EC of the European Parliament and of the Council.

We acknowledge the contribution of the ICOS Atmospheric Thematic Center (Lynn Hazan, Amara Abbaris, and Leonard Rivier) for the near real time data processing of surface CO_2 and CH_4 concentrations. The ICOS monitoring sites are maintained by the national networks: ICOS-Czech Rep. (Michal Marek, Katerina Komínková, Gabriela Vítková), ICOS-Finland (Olli Peltola, Janne Levula, Tuomas Laurila), ICOS-France (Michel Ramonet, Marc Delmotte, Sebastien Conil, Morgan Lopez, Victor Kazan, Aurélie Colomb, Jean Marc Pichon, Roxanne Jacob, Julie Helle, Olivier Laurent), ICOS-Germany (Matthias Lindauer, Dagmar Kubistin, Christian Plass-Duelmer, Dietmar Weyrauch, Marcus Schumacher), ICOS-Italy (Paolo Cristofanelli, Michela Maione, Francesco Apadula), ICOS-Norway (Cathrine Lund Myhre, Ove Hermansen), ICOS-Sweden (Jutta Holst, Michal Heliasz, Meelis Molder, Mikaell Ottosson Lofvenius, Anders Lindroth, Per Marklund), ICOS-Switzerland (Martin Steinbacher, Simon Wyss), European Commission, Joint Research Centre, Directorate for Energy, Transport and Climate (Peter Bergamaschi, Giovanni Manca).

The TCCON site at Orleans is operated by the University of Bremen and the RAMCES team at LSCE (Gif-sur-Yvette, France). The TCCON site at Bialystok is operated by the University of Bremen. Funding for the two sites was provided by the EU-project ICOS-INWIRE and the University of Bremen. The TCCON site at Réunion is operated by BIRA-IASB, in cooperation with UReunion and is funded by BELSPO in the framework of the Belgian ICOS program.

TCCON references:

Hazan, L., J. Tarniewicz, M. Ramonet, O. Laurent and A. Abbaris **(2016)**. *Automatic processing of atmospheric CO_2 and CH_4 mole fractions at the ICOS Atmosphere Thematic Centre*. Atmospheric Measurement Techniques 9(9): 4719-4736.

Blumenstock, T., F. Hase, M. Schneider, O. E. García, and E. Sepúlveda. 2017. "TCCON data from Izana (ES), Release GGG2014.R1." CaltechDATA. doi:10.14291/tccon.ggg2014.izana01.r1.

De Mazière, M., M. K. Sha, F. Desmet, C. Hermans, F. Scolas, N. Kumps, J.-M. Metzger, V. Duflot, and J.-P. Cammas. 2017. "TCCON data from Réunion Island (RE), Release GGG2014.R1." CaltechDATA. doi:10.14291/tccon.ggg2014.reunion01.r1.

Deutscher, N. M., J. Notholt, J. Messerschmidt, C. Weinzierl, T. Warneke, C. Petri, and P. Grupe. 2017. "TCCON data from Bialystok (PL), Release GGG2014.R1." CaltechDATA. doi:10.14291/tccon.ggg2014.bialystok01.r1/1183984.

Dubey, M. K., B. G. Henderson, D. Green, Z. T. Butterfield, G. Keppel-Aleks, N. T. Allen, J.-F. Blavier, C. M. Roehl, D. Wunch, and R. Lindenmaier. 2017. "TCCON data from Manaus (BR), Release GGG2014.R0." CaltechDATA. doi:10.14291/tccon.ggg2014.manaus01.r0/1149274.

Dubey, M. K., R. Lindenmaier, B. G. Henderson, D. Green, N. T. Allen, C. M. Roehl, J.-F. Blavier, et al. 2017. "TCCON data from Four Corners (US), Release GGG2014.R0." CaltechDATA. doi:10.14291/tccon.ggg2014.fourcorners01.r0/1149272.

Feist, D. G., S. G. Arnold, N. John, and M. C. Geibel. 2017. "TCCON data from Ascension Island (SH), Release GGG2014.R0." CaltechDATA. doi:10.14291/tccon.ggg2014.ascension01.r0/1149285.

Goo, T.-Y., Y.-S. Oh, and V. A. Velazco. 2017. "TCCON data from Anmeyondo (KR), Release GGG2014.R0." CaltechDATA. doi:10.14291/tccon.ggg2014.anmeyondo01.r0/1149284.

Griffith, D. W. T., N. M. Deutscher, V. A. Velazco, P. O. Wennberg, Y. Yavin, G. Keppel-Aleks, R. A. Washenfelder, et al. 2017. "TCCON data from Darwin (AU), Release GGG2014.R0." CaltechDATA. doi:10.14291/tccon.ggg2014.darwin01.r0/1149290.

Griffith, D. W. T., V. A. Velazco, N. M. Deutscher, C. Paton-Walsh, N. B. Jones, S. R. Wilson, R. C. Macatangay, G. C. Kettlewell, R. R. Buchholz, and M. O. Riggenbach. 2017. "TCCON data from Wollongong (AU), Release GGG2014.R0." CaltechDATA. doi:10.14291/tccon.ggg2014.wollongong01.r0/1149291.

Hase, F., T. Blumenstock, S. Dohe, J. Groß, and M.ä. Kiel. 2017. "TCCON data from Karlsruhe (DE), Release GGG2014.R1." CaltechDATA. doi:10.14291/tccon.ggg2014.karlsruhe01.r1/1182416.

Iraci, L. T., J. R. Podolske, P. W. Hillyard, C. Roehl, P. O. Wennberg, J.-F. Blavier, J. Landeros, et al. 2017. "TCCON data from Edwards (US), Release GGG2014.R1." CaltechDATA. doi:10.14291/tccon.ggg2014.edwards01.r1/1255068.

—. 2017. "TCCON data from Indianapolis (US), Release GGG2014.R1." CaltechDATA. doi:10.14291/tccon.ggg2014.indianapolis01.r1/1330094.

Kawakami, S., H. Ohyama, K. Arai, H. Okumura, C. Taura, T. Fukamachi, and M. Sakashita. 2017. "TCCON data from Saga (JP), Release GGG2014.R0." CaltechDATA. doi:10.14291/tccon.ggg2014.saga01.r0/1149283.

Kivi, R., P. Heikkinen, and E. Kyrö. 2017. "TCCON data from Sodankylä (FI), Release GGG2014.R0." CaltechDATA. doi:10.14291/tccon.ggg2014.sodankyla01.r0/1149280.

Liu, Cheng, Wei Wang, and Youwen Sun. 2018. "TCCON data from Hefei (PRC), Release GGG2014.R0." CaltechDATA. doi:10.14291/tccon.ggg2014.hefei01.r0.

Morino, I., N. Yokozeki, T. Matsuzaki, and M. Horikawa. 2017. "TCCON data from Rikubetsu (JP), Release GGG2014.R2." CaltechDATA. doi:10.14291/tccon.ggg2014.rikubetsu01.r2.

Morino, I., T. Matsuzaki, and M. Horikawa. 2017. "TCCON data from Tsukuba (JP), 125HR, Release GGG2014.R2." CaltechDATA. doi:10.14291/tccon.ggg2014.tsukuba02.r2.

Morino, Isamu, Voltaire A. Velazco, Akihiro Hori, Osamu Uchino, and David W. T. Griffith. 2018. "TCCON data from Burgos, Ilocos Norte (PH), Release GGG2014.R0." CaltechDATA. doi:10.14291/tccon.ggg2014.burgos01.r0.

Notholt, J., C. Petri, T. Warneke, N. M. Deutscher, M. Palm, M. Buschmann, C. Weinzierl, R. C. Macatangay, and P. Grupe. 2017. "TCCON data from Bremen (DE), Release GGG2014.R0." CaltechDATA. doi:10.14291/tccon.ggg2014.bremen01.r0/1149275.

Notholt, J., T. Warneke, C. Petri, N. M. Deutscher, C. Weinzierl, M. Palm, and M. Buschmann. 2017. "TCCON data from Ny Ålesund, Spitsbergen (NO), Release GGG2014.R0." CaltechDATA. doi:10.14291/tccon.ggg2014.nyalesund01.r0/1149278.

Pollard, David Frank, John Robinson, and Hisako Shiona. 2019. "TCCON data from Lauder (NZ), Release GGG2014.R0." CaltechDATA. doi:10.14291/tccon.ggg2014.lauder03.r0.

Sherlock, V., B. Connor, J. Robinson, H. Shiona, D. Smale, and D. F. Pollard. 2017. "TCCON data from Lauder (NZ), 120HR, Release GGG2014.R0." CaltechDATA. doi:10.14291/tccon.ggg2014.lauder01.r0/1149293.

—. 2017. "TCCON data from Lauder (NZ), 125HR, Release GGG2014.R0." CaltechDATA. doi:10.14291/tccon.ggg2014.lauder02.r0/1149298.

Strong, K., S. Roche, J. E. Franklin, J. Mendonca, E. Lutsch, D. Weaver, P. F. Fogal, J. R. Drummond, R. Batchelor, and R. Lindenmaier. 2018. "TCCON data from Eureka (CA), Release GGG2014.R3." CaltechDATA. doi:10.14291/tccon.ggg2014.eureka01.r3.

Sussmann, R., and M. Rettinger. 2017. "TCCON data from Garmisch (DE), Release GGG2014.R2." CaltechDATA. doi:10.14291/tccon.ggg2014.garmisch01.r2.

—. 2018. "TCCON data from Zugspitze (DE), Release GGG2014.R1." CaltechDATA. doi:10.14291/tccon.ggg2014.zugspitze01.r1.

Té, Y., P. Jeseck, and C. Janssen. 2017. "TCCON data from Paris (FR), Release GGG2014.R0." CaltechDATA. doi:10.14291/tccon.ggg2014.paris01.r0/1149279.

Warneke, T., J. Messerschmidt, J. Notholt, C. Weinzierl, N. M. Deutscher, C. Petri, and P. Grupe. 2017. "TCCON data from Orléans (FR), Release GGG2014.R0." CaltechDATA. doi:10.14291/tccon.ggg2014.orleans01.r0/1149276.

Wennberg, P. O., C. M. Roehl, D. Wunch, G. C. Toon, J.-F. Blavier, R. Washenfelder, G. Keppel-Aleks, N. T. Allen, and J. Ayers. 2017. "TCCON data from Park Falls (US), Release GGG2014.R1." CaltechDATA. doi:10.14291/tccon.ggg2014.parkfalls01.r1.

Wennberg, P. O., C. M. Roehl, J.-F. Blavier, D. Wunch, and N. T. Allen. 2017. "TCCON data from Jet Propulsion Laboratory (US), 2011, Release GGG2014.R1." CaltechDATA. doi:10.14291/tccon.ggg2014.jpl02.r1/1330096.

Wennberg, P. O., D. Wunch, C. M. Roehl, J.-F. Blavier, G. C. Toon, and N. T. Allen. 2017. "TCCON data from Caltech (US), Release GGG2014.R1." CaltechDATA. doi:10.14291/tccon.ggg2014.pasadena01.r1/1182415.

—. 2017. "TCCON data from Lamont (US), Release GGG2014.R1." CaltechDATA. doi:10.14291/tccon.ggg2014.lamont01.r1/1255070.

Wennberg, P. O., D. Wunch, Y. Yavin, G. C. Toon, J.-F. Blavier, N. T. Allen, and G. Keppel-Aleks. 2017. "TCCON data from Jet Propulsion Laboratory (US), 2007, Release GGG2014.R0." CaltechDATA. doi:10.14291/tccon.ggg2014.jpl01.r0/1149163.

Wunch, D., J. Mendonca, O. Colebatch, N. T. Allen, J.-F. Blavier, S. Roche, J. Hedelius, et al. 2017. "TCCON data from East Trout Lake, SK (CA), Release GGG2014.R1." CaltechDATA. doi:10.14291/tccon.ggg2014.easttroutlake01.r1.

Wunch, D., Toon, G. C., Sherlock, V., Deutscher, N. M., Liu, C., Feist, D. G., & Wennberg, P. O. (2015). The Total Carbon Column Observing Network's GGG2014 Data Version. Tech. rep., California Institute of Technology, Pasadena. doi:10.14291/tccon.ggg2014.documentation.R0/1221662

Copernicus Atmosphere Monitoring Service

ECMWF - Shinfield Park, Reading RG2 9AX, UK

Contact: info@copernicus-atmosphere.eu